1-1-1970

The high temperature creep behavior of polycrystalline strontium zirconate.

Joseph Nemeth
University of Windsor

THE HIGH TEMPERATURE CREEP BEHAVIOR OF POLYCRYSTALLINE STRONTIUM ZIRCONATE

A Thesis
Submitted to the Faculty of Graduate Studies through the Department of Engineering Materials in Partial Fulfillment of the Requirements for the Degree of
Doctor of Philosophy
at the University of Windsor

Faculty of Applied Science

by

Joseph Nemeth

Windsor, Ontario

1970

ProQuest Information and Learning Company
789 East Eisenhower Parkway
P.O. Box 1346
Ann Arbor, MI 48106-1346

APPROVED BY:

334069

ACKNOWLEDGEMENTS

The author expresses his sincere gratitude to Dr. J.G. Parr and Dr. W. V. Youdelis for the opportunity to undertake this research under their supervision. A special thanks is addressed to Dr. W. V. Youdelis for his many hours of helpful discussion, technical advice and aid in focusing the research effort. The author is indebted to many of the faculty and staff who gave willingly of their talents. In particular, to Professor R.G. Billinghurst for his helpful departmental supervision, to Dr. W. North for his technical advice, to Mr. L. Cory for his patience and generosity with his time, and to my colleague and friend Mr. R. T. Hamilton.

Acknowledgement is due to the National Research Council of Canada for financial support in the form of a scholarship and providing funds to accomplish the research endeavour (NRC Grant 650).

Finally, special mention is due to my patient wife, Janet.

CONTENTS

LIST OF FIGURES

LIST OF TABLES

ABSTRACT

The high temperature creep behavior of polycrystalline $SrZrO_3$ is investigated. Creep specimens were prepared from sintered powder compacts containing Fe_2O_3 additions of 0.85 wt.% and 1.35 wt.% to accelerate sintering and densification. A high temperature x-ray investigation showed no change in the structure of $SrZrO_3$ over the temperature range 25°C to 1300°C. Specimens varying in grain size from 0.45 μm to 2.04 μm were creep tested in air between 1160°C and 1350°C at stresses of 1000 psi to 4000 psi under four-point, dead load conditions. Only the specimens containing 1.35 wt.% Fe_2O_3 sintered to near theoretical density (99%) and exhibited a relatively stable creep behavior from which the various creep parameters were determined. An activation energy of 169 ± 10 kcal/mole, and a dependence of creep rate upon the stress cubed and reciprocal of the grain size, i.e., $\dot{\epsilon} \propto \sigma^3/d$, was determined for the creep process in $SrZrO_3$. This is consistent with the nonviscous creep model developed by Weertman and modified by Garofalo for grain size effects, in which the controlling mechanism is dislocation generation and climb. It is proposed that deformation occurs in $SrZrO_3$ principally through mechanical twinning, which Cottrell and Bilby show to be a dislocation mechanism.

I INTRODUCTION

The principal limiting factor in the more widespread use of ceramics as an engineering material is susceptibility to brittle fracture. Although all ceramics will show a finite plasticity at sufficiently elevated temperatures, they are known as a class of materials that displays no plasticity at normal temperatures. In examining matrix materials for metal fiber reinforced ceramics, Tinklepaugh et. al.[1] observed that hot pressed and sintered polycrystalline strontium zirconate ($SrZrO_3$) displayed a measurable yield when stressed at room temperature. Figure 1 shows the typical room temperature stress-strain curve exhibited by $SrZrO_3$. The curve shows a non-linear behavior, a remnant strain upon removal of stress, and an increase in the stress level results in an increased remnant yield up to the fracture stress. Although this cannot be viewed as ductility in the classical sense, because of the small extent of the plastic strain ($\sim 8 \times 10^{-5}$ in/in at fracture), and the lack of a measurable yield point, the plastic deformation phenomenon in a ceramic oxide must be considered very significant. An intrinsic yield offers increased thermal shock resistance, and in many

high temperature applications spalling and abrasion problems would be accordingly alleviated. For applications in metal-ceramic composites, mechanical compatibility with a wider range of materials and over a larger temperature range would be enhanced because unequal thermal expansion coefficients would no longer be the limiting factor.

In view of the advantages associated with the yield characteristic of $SrZrO_3$, and the various possibilities this ceramic may offer as a high temperature engineering material (melting point, 2850°C [2,3]), it was decided to undertake an investigation of the high temperature creep behavior of sintered powder compacts for the purpose of characterizing its properties and determining the probable deformation mechanism. Creep rate information is obtained using the four-point transverse bending test. In this investigation the effect of microstructure (grain size), stress, and temperature on the creep rate is determined, and the results obtained are examined in the light of the several creep mechanisms proposed for ceramic oxides.

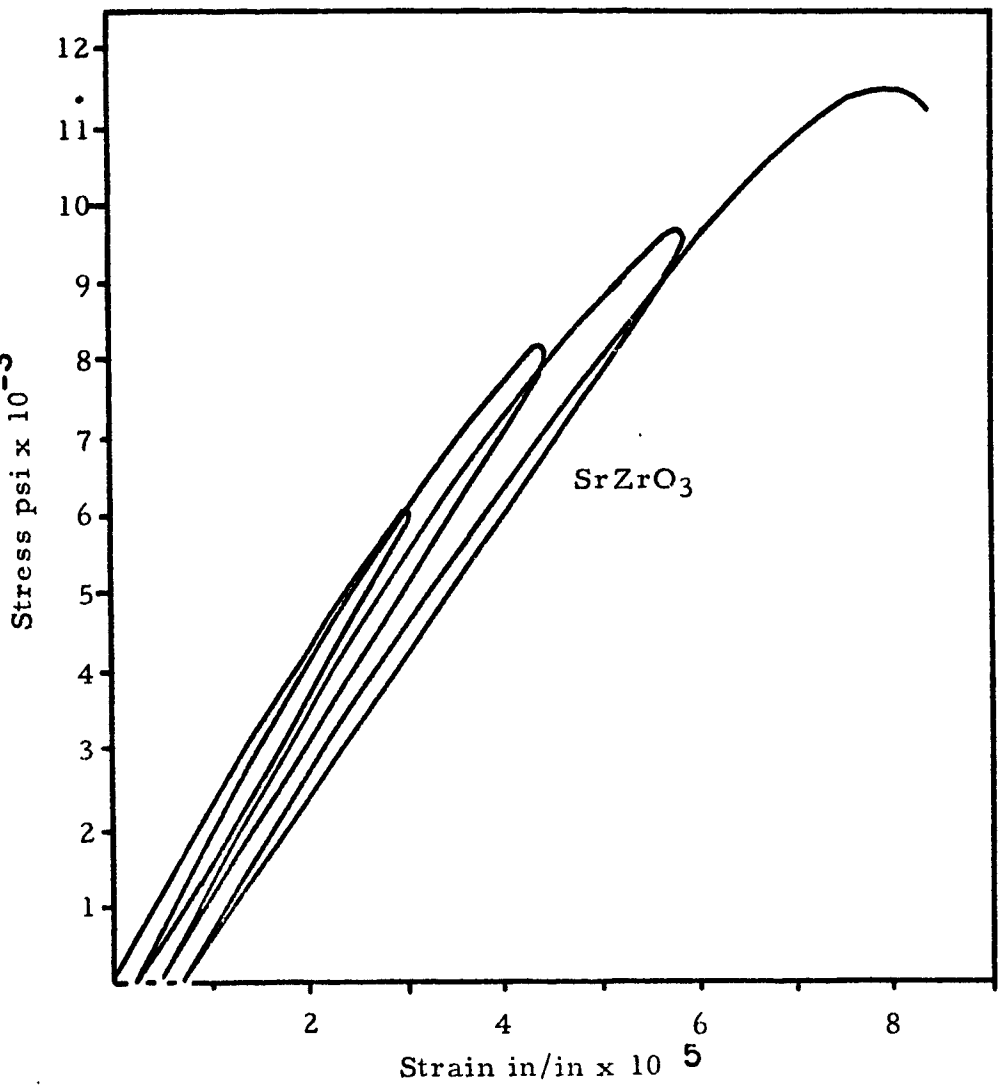

Figure 1

Room Temperature Stress Strain Behavior

of Hot Pressed Commercial $SrZrO_3$

II LITERATURE REVIEW

DEFINITION OF CREEP

Creep is defined as the time-dependent inelastic deformation of materials. Typical isothermal creep curves are shown in Figure 2. It is observed that both temperature and stress similarly affect the shape of the curve, which is generally divided into four stages. Stage I is the instantaneous elastic strain that occurs upon loading. Stage II is referred to as the primary or transient creep because of its decreasing creep rate. Stage III, termed the secondary or steady state creep, describes the region of relatively constant creep rate, and Stage IV refers to the increasing creep rate leading to fracture known as tertiary creep.

The steady state creep region is of particular interest because (at low creep rates) the largest creep occurs in this region , and also, because the steady state characteristics facilitate the development of definite, quantitative models. Most of the literature on creep is directed to the investigation and formulation of the steady state creep process.

EMPIRICAL TREATMENT OF CREEP

The first attempts to understand the creep

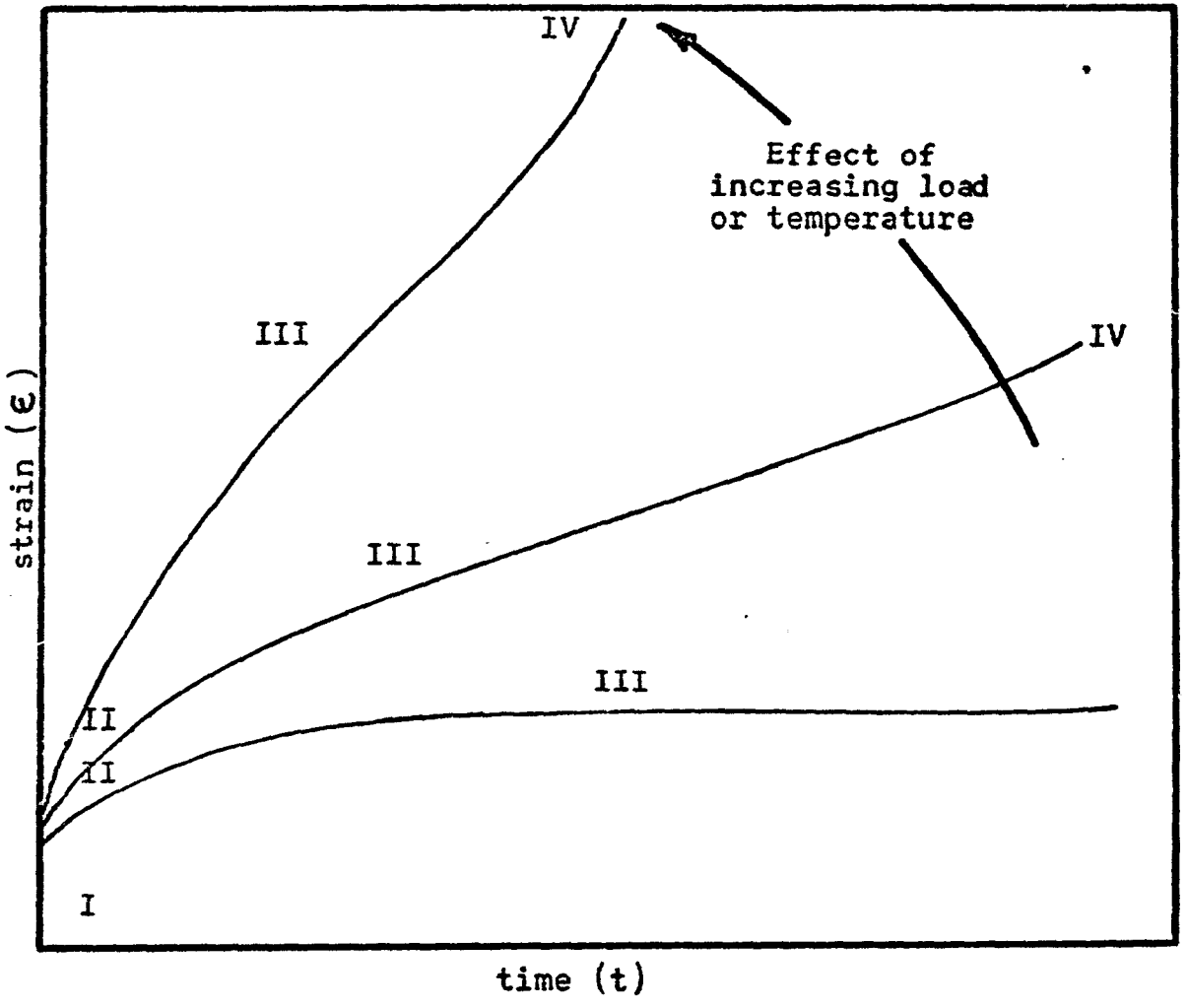

Figure 2
Typical creep curves for polycrystalline ceramics

process began by determining time functions for the primary and secondary stages. Mathematical functions were empirically obtained relating strain (ϵ) and time (t), and usually took the form

$$\epsilon = \epsilon_o + \beta t^m + K_s t, \qquad (1)$$

where ϵ_o is the instantaneous elastic strain, β and m are time-independent, empirically determined constants, and K_s is the steady state creep rate. Equation (1) provided the logical first step in developing an understanding of plastic deformation phenomenon at elevated temperatures.

A more profound understanding of the creep process can be arrived at only by the development of a phenomenological theory of creep rate and atomistic models for the creep mechanisms consistent with the phenomenological description. It is generally assumed that if several (say n) mechanisms contribute tc the creep rate, $\dot{\epsilon}$, it can be expressed by the general relation

$$\dot{\epsilon} = \sum_1^n F_i(\sigma, T, S), \qquad (2)$$

where F_i represents the functional relationship between the stress (σ), temperature (T), and structure factor (S) for a specific (ith) creep mechanism. The structure factor is a function of grain size, porosity, dislocation density, and other physical and geometrical characteristics affecting the mechanical behavior of the aggregate.

Porosity and substructure are generally assumed constant however, so that (S) is essentially expressed by the effect of grain size (d). If it may be assumed that the effects of stress, temperature, and structure are mutually independent, then the creep rate can be described by an equation of the form

$$\dot{\epsilon} = f_1(\sigma) f_2(T) f_3(d), \qquad (3)$$

where $f_1(\sigma)$ is a function of stress, $f_2(T)$ a function of temperature, and $f_3(d)$ a function of structure (grain size). Thus, if Equation (3) is valid the effects of stress, temperature and structure may be separated from the creep rate data. The temperature effect is most easily determined, for all creep stages exhibit thermally activated processes, expressed through the exponential factor $e^{-\Delta H_i/kT}$, where ΔH_i is the activation energy for the controlling mechanism and k is Boltsmann's constant. The activation energy obtained from the usual Arrhenius treatment of the creep rate data is generally compared to known activation energies for vacancy or ion diffusion, grain boundary motion, etc. to construct a creep model and specify the controlling mechanism for the creep process. The various theories to account for the stress and grain size dependency of creep rate will now be reviewed briefly.

SPECIFIC CREEP MODELS AND THEORIES

A. VISCOUS CREEP

(1) Reaction Rate Theory

The theoretical work on creep was influenced by the work of Glasstone, Laidler, and Eyring[4] on the phenomena of viscosity, plasticity, and diffusion in viscous fluids. The Reaction Rate Theory assumes that rate processes (including flow) can be characterized by an initial configuration passing through some intermediate configuration, known as an activated complex, to arrive at the final configuration. Activated complexes are assumed to be in thermodynamic equilibrium with the initial reactants and that they behave as ordinary molecules with the exception that one classical degree of freedom (e.g. vibrational) is substituted for by a translational degree of freedom along the "reaction coordinate" path. The rate of the reaction is determined by the rate at which the activated complexes move across the top of the energy barrier.

Kausman[5] used the Reaction Rate Theory in an attempt to describe the steady state creep process. Kausman assumed that "units of flow", which are vaguely defined as elementary structures within a solid, move past one another constituting the shear process. This

movement can be accomplished only by activating the units of flow over an energy barrier ($\Delta H^{\ddagger}$). The shear rate is then expressed as

$$\dot{\epsilon} = \lambda\nu/l, \tag{4}$$

where ν is the "jump" frequency for the flow units separated by the distance l, and λ is the jump distance. Kausman assumed that the activation energy for motion in the direction of shear was lowered by an amount proportional to the applied shear stress (σ) and derives for the creep rate

$$\dot{\epsilon} = \frac{\lambda}{hl}\sigma(\lambda\lambda_2\lambda_3)e^{-\Delta H^{\ddagger}/RT}, \tag{5}$$

where $\lambda_2\lambda_3$ is the projected cross-sectional area of each unit of flow in the shear plane, λ is the average distance moved in one jump by the flow unit, and h is Planck's constant. The term $\sigma(\lambda\lambda_2\lambda_3)$ represents the work accomplished in carrying the flow unit from the initial to the final state. As the strain rate is proportional to the applied stress it is referred to as viscous or Newtonian flow.

The principal advantage of the Reaction Rate Theory as applied to the phenomenon of creep is in its elegance; however, the Kausman model of creep has the limitations that neither the activated volume ($\lambda\lambda_2\lambda_3$) nor the specific activation process (measured as $\Delta H^{\ddagger}$) can be clearly defined.

(2) Nabarro-Herring Theory

A creep mechanism resulting from the stress-directed diffusion of vacancies was originally proposed by Nabarro [6], and subsequently developed in more detail by Herring.[7] The Nabarro-Herring model is applicable to polycrystalline systems, and differs from most other creep processes in that no dislocation motion is involved. Thus the model may be applied to polycrystalline systems in which the grains contain no dislocations, or where dislocation motion is effectively blocked.

Grain boundaries are regarded as regions of discontinuity and serve as sources and sinks for vacancies. An individual grain is considered to be acted upon by a system of normal stresses as shown in Figure 3. It is noted that application of a tensile stress will decrease the energy required to form a vacancy, and accordingly a compressive stress will increase that energy. Faces AB and DC will have a vacancy concentration proportional to $e^{+\sigma\Omega/kT}$, where Ω is the vacancy volume, and the faces AD and BC will have a vacancy concentration proportional to $e^{-\sigma\Omega/kT}$. Thus a vacancy concentration gradient is established in a direction colinear with the applied tensile stress, and a flow of vacancies will occur to relieve the inequality of

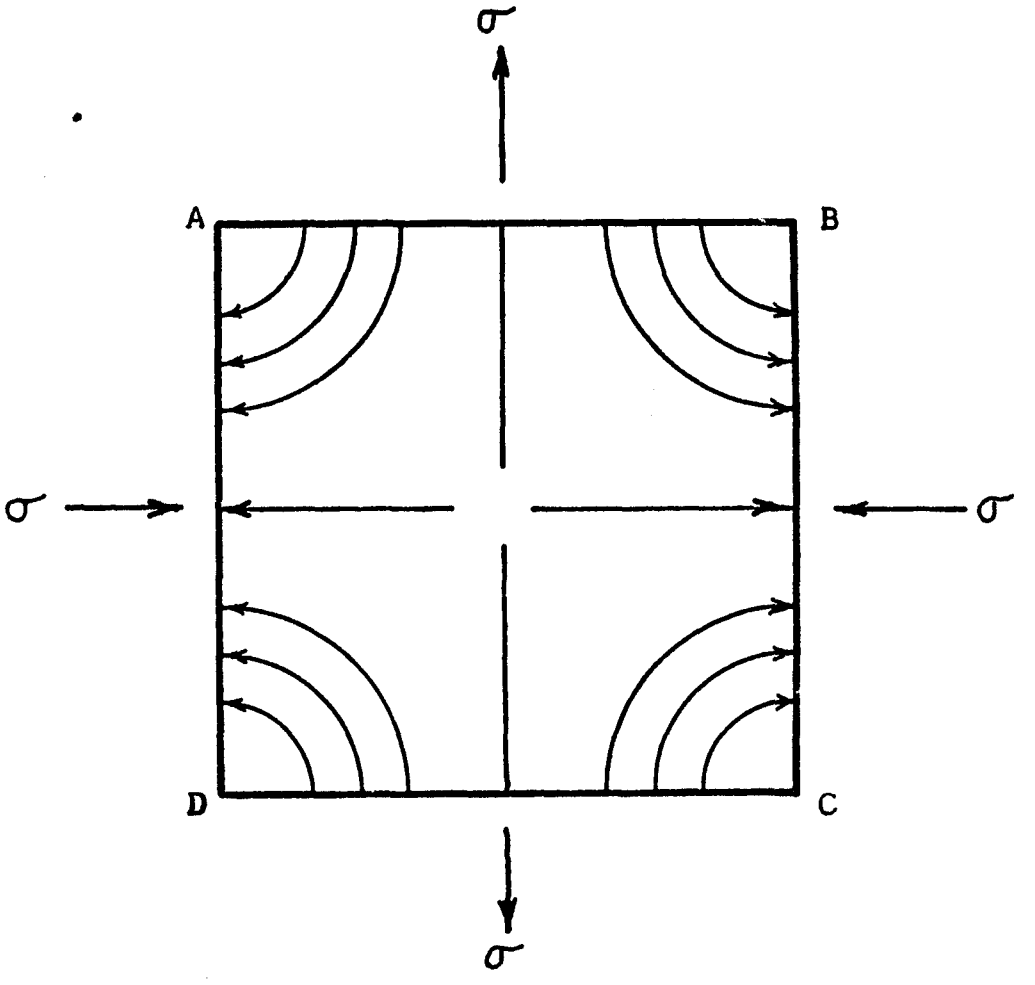

Figure 3

Schematic diagram showing
vacancy flux imposed by
tensile and compressive stresses

pressure as shown (curved arrows, Figure 3), leading to a grain elongation in the direction of the tensile stress. Three stages are involved in the stress directed diffusion model for creep; the formation of a vacancy in the grain volume near the grain boundary under the positive stress, its migration to a boundary where the stress is negative, and the annihilation of the vacancy at the boundary. The assumption is made that the generation and annihilation of vacancies is rapid compared to their diffusion rate through the lattice. Due to the material transport tangential stresses develop at the grain boundaries which are relaxed by a diffusional process. Herring has shown that $\dot{\epsilon}$ (relaxed) = 5/2 $\dot{\epsilon}$ (unrelaxed), and gives for the relaxed creep rate

$$\dot{\epsilon} = \frac{32\alpha\sigma D_s \Omega}{\pi d^2 kT} \quad , \tag{6}$$

where Ds is the coefficient of volume self-diffusion, d is the grain diameter, and α is a constant which corrects for the difference in vacancy concentration from equilibrium (approximately unity).

The significant features of the Nabarro-Herring theory may be summarized as follows:

(1) there is no consideration of transient phenomena

(2) the activation energy for creep is equal to that for volume self-diffusion

(3) the creep rate is proportional to stress (i.e. viscous creep).

(4) the creep rate varies inversely with the square of the grain diameter.

(5) a grain elongation occurs in the direction of the tensile stress.

(3) Coble Theory

Coble[8] noted that in oxides the diffusion coefficients for the small cations can be apparently less than the diffusion coefficient for the larger oxygen ion by several orders of magnitude when calculated from creep data. For creep dependent upon a vacancy diffusion mechanism, it would be expected that the creep rate would be determined by the diffusion rate of the least mobile (larger) species, i.e. O^{-2}. Paladino and Coble[9] proposed that the creep deformation process in alumina and other ionic type materials consists of cation diffusion through the lattice, in agreement with Nabarro and Herring, but that oxygen ion diffusion occurs largely along grain boundaries where its diffusion coefficient is enhanced.

In the creep model proposed by Coble, spherical grains are assumed for simplification; and as in the Nabarro-Herring Model, a stress induced vacancy flow is assumed for the transport process, with the difference that boundary diffusion rather than volume

diffusion predominates. Coble gives for the creep rate

$$\dot{\epsilon} = \frac{150\sigma D_b w \Omega}{d^3 kT}, \qquad (7)$$

where w is the width of the grain boundary and D_b is the diffusion coefficient for atoms in the boundary. The enhancement of the creep rate by shear stress relaxation at the grain boundaries is included in Equation (7) which Coble assumes (in agreement with Herring) is 5/2 times the unrelaxed creep rate.

Note that the creep rate is a viscous process (Proportional to σ) and requires elongation of the grain in the direction of tensile stress as in the Nabarro-Herring model, but may be differentiated from the former by dependence on the reciprocal of the cube of the grain diameter.

The boundary width (w) introduces a degree of arbitrariness to Cobles Model, because only the product D_bW has been separable from diffusion measurements. Early measurements in metals indicated that w was three to five Å, but recent measurements of diffusion coefficients of (O^{-2}) in alumina[10] and (Cl^-) in polycrystalline NaCl[11] have shown that the thickness of the region in which the diffusion coefficient is enhanced may be of the order 100 to 1000 Å. Thus for small grains an enhanced "volume" diffusion model (equation 6) may describe the creep

process more accurately, while for larger grains the creep process may be described by the grain boundary diffusion model, i.e., Equation (7).

(4) Gifkins Theory

The Gifkins[12-14] theories are also based on a diffusion model, where creep extension occurs by a grain boundary sliding mechanism controlled by diffusion. The Nabarro-Herring and Coble models depend on an elongation of individual grains and ignores any contribution to total strain due to a true grain boundary sliding mechanism (not to be confused with the tangential stress relaxation phenomenon of the Nabarro-Herring and Coble models), which Gifkins and Snowden[12] note is frequently observed in metals. Earlier theories considered grain boundary sliding and changes in grain shape as separate phenomena when, in fact, they may occur simultaneously. Such readjustments could lead to grain rotation, local slip, diffusion and grain boundary migration.

Protrusions or double ledges such as AB and CD are assumed to exist as shown in Figure 4. When the boundary XY is subjected to an applied shear stress, AB is placed in compression and CD in tension. This leads to a variation in vacancy concentration as described in the Nabarro-Herring theory, and a localized diffusional creep occurs which moves the protrusion forward to A'C'. Thus grain boundary sliding occurs at the rate of movement of

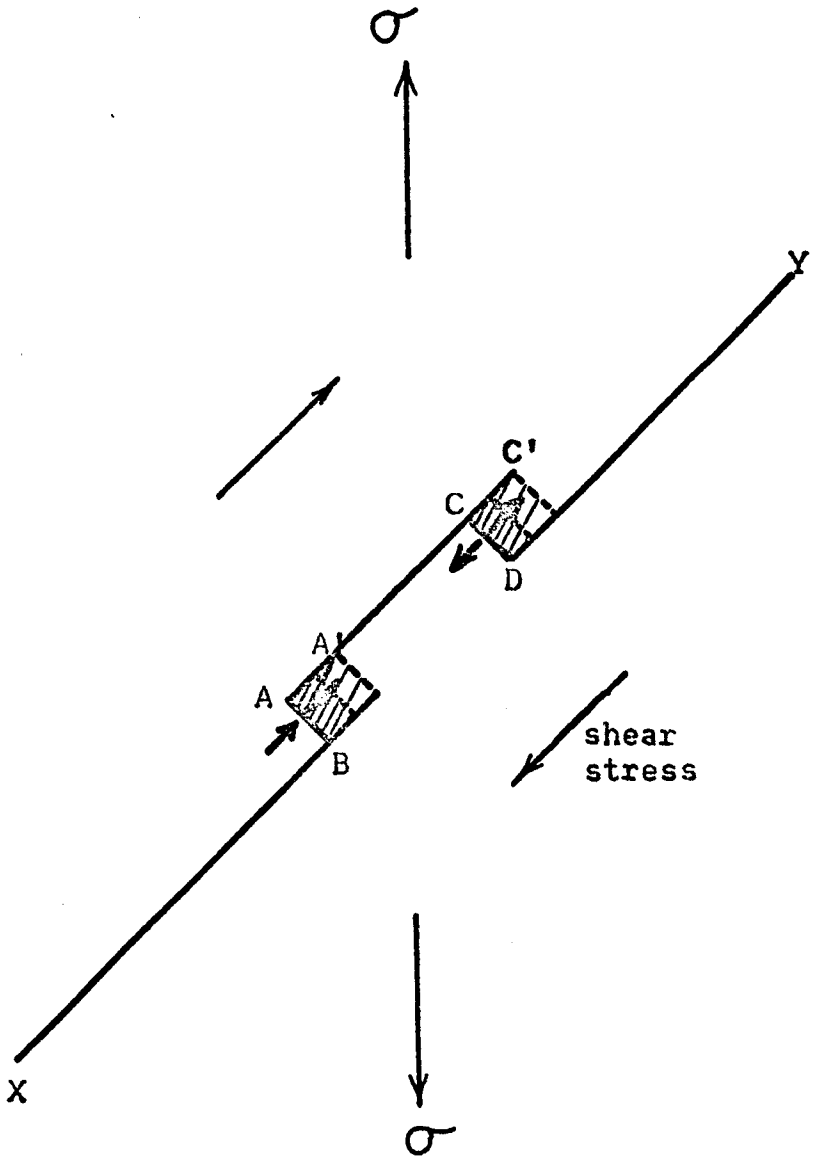

Figure 4

Grain boundary sliding
controlled by diffusional movement
of a "protrusion".

the protrusions. It is assumed that the stress concentrations that develop at the ledges due to the sliding can be relaxed by slip or twinning.

Gifkins related the creep parameters to a local vacancy flux through the grain boundary, and gives for the strain rate

$$\dot{\epsilon} \simeq \frac{K\sigma D_b \Omega}{LRTd} , \qquad (8)$$

where L is the length of the protrusion, and the proportionality constant (K) is close to 2. Thus creep rate can be related to a (1/d) dependency if L is independent of grain size; however, Gifkins notes that L may also be proportional to the grain size so that the creep rate may go as $(1/d^2)$

In another paper, Gifkins[13,14] proposed that when grain boundary sliding occurs, the rate of accommodation at triple points (see Figure 5) may be slower than the sliding process and thus be the rate controlling mechanism. Sliding along AB due to a shear stress causes compression stresses along BC and tensile stresses along BD. The conditions for diffusional creep as required by the Nabarro-Herring theory are thus developed and a local flux of vacancies will occur from BD to BC. For a boundary at 45^o to the applied stress, the creep rate controlled by triple-point accomodation is given as:

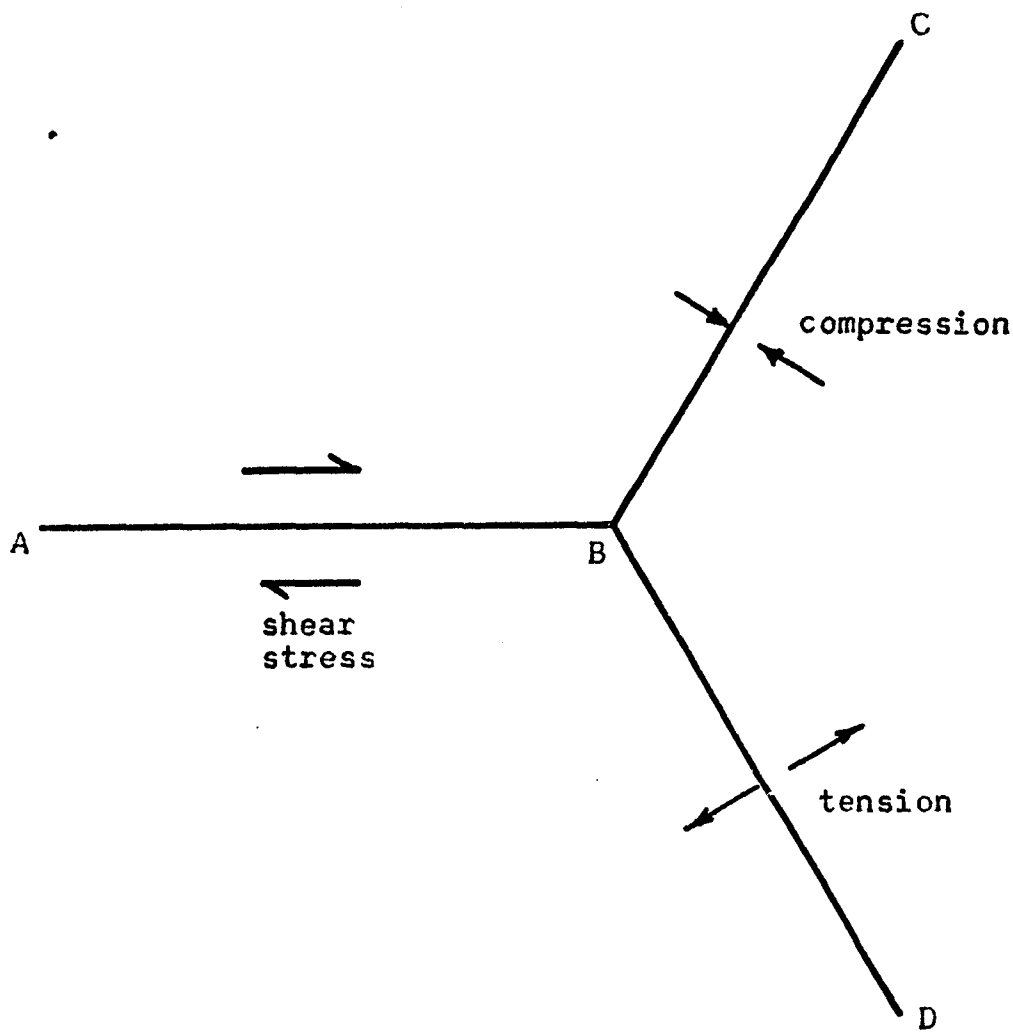

Figure 5

Accomodation
of grain boundary sliding
along AB by diffusion between BD and BC

$$\dot{\epsilon} \simeq \frac{40\,\sigma(D_b w)\Omega}{d^3 kT}, \qquad (9)$$

which is very similar to the equation Coble derived for creep controlled by grain-boundary diffusion. Thus, depending on the particular mechanism of grain boundary sliding, strain rate may be proportional to $(1/d)$, $(1/d^2)$, or $(1/d^3)$, indicating the difficulty in defining the specific creep mechanism on the basis of grain size dependence alone.

B. NON-VISCOUS CREEP (DISLOCATION MOVEMENT)

(1) Mott Theory

Mott[15] discussed a low temperature, fine slip (slip lines spaced at 50 Å or less) mechanism which permits the formation of sub-grain boundaries (or dislocation cells) by the alignment of dislocations which are dispersed over a large number of planes. In comparison the formation of boundaries after coarse slip (slip lines spaced approximately 2000 Å apart) is possible only if dislocations can climb out of a piled-up group. Mott notes that fine slip is frequently associated with deformation at elevated temperatures (for which dislocation climb is relatively easy), and extends his fine slip model to include dislocation climb in developing a high temperature creep theory.

The slip modes are characterized further as involving continuous "dynamic" or discontinuous "non-dynamic" motion. Non-dynamic motion occurs if the slip plane contains small obstacles, extending only a few atom distances, which impede dislocation motion. A stress (σ_0) is defined as that necessary to force a dislocation through the obstacle. If the applied stress σ, is greater than σ_0, dislocation movement is rapid and dynamic motion results. If σ is less than σ_0, dislocations will be frequently held up, released by thermal excitation, held up, etc., resulting in so-called "non-dynamic" motion.

The stress necessary to operate a dislocation source (e.g. Frank Read source) is represented by σ_F. If for a given source $\sigma \geq \sigma_F > \sigma_0$, the momentum of the rapidly moving dislocation allows the source to continue and dynamic generation of dislocations is expected. Once a source has started to generate dislocations, it will continue to do so until the stress at the source due to them is about σ_F. Normally, about 1000 dislocation rings are formed before the source stops, resulting in coarse slip. If however, sources exist for which $\sigma \leq \sigma_F < \sigma_0$, the dislocation exerts a stress at the source, which will stop acting, and result in other sources becoming active on nearby planes, thus resulting in fine slip. Low stresses are generally used in creep testing and thus non-dynamic fine slip is expected.

The obstacles in creep are assumed to be sessile dislocations (cannot move by glide), which are not expected to lie in a long dislocation line but extend over smaller

distances, moving into other planes. The barriers against which non-dynamic dislocations pile up will thus have gaps in them (say, length l). Climb occurs at these pile-ups, enabling dislocations to escape the barriers. The escape rate is assumed to be the rate controlling mechanism in creep which is given as:

$$\dot{\epsilon} \simeq A/\theta \; e^{-(\Delta H_s - lb^2\sigma)/kT} \qquad (10)$$

where θ is the stress-strain curve gradient, A is a constant, b is the Burgers vector, and ΔH_s the activation energy for self-diffusion. The relationship denotes that the apparent activation energy be stress dependent, and this has not been verified experimentally.

In a later modification of the theory, Mott[16] retained non-dynamic fine slip as the basis for the creep model, but noted that slip at elevated temperatures probably occurs on more than one plane in many polycrystalline materials. Slip itself is considered rate controlling, and in each cell not more than one dislocation moves on each slip line. The dislocations, envisioned as dispersed on numerous parallel planes in the previous model, now are viewed as having to cross a "forest" of dislocations intersecting the slip plane of the mobile dislocation. When a screw dislocation cuts another screw dislocation, a jog or double ledge in the slip plane is formed. In addition intersecting screw dislocations leave a trail of vacancies behind so that the resistance to screw dislocation motion increases proportionally to the

distance moved. Mott relates the stress necessary to operate the dislocation source to the lattice constant by the equation $\sigma = Kb/a$, where K contains the shear modulus and a is the distance between slip planes. If the distance between jogs on a screw dislocation is λ, the work done by the stress in moving the dislocation through one atomic distance in the vicinity of a jog is $\lambda b^2/\sigma$, and against this work one vacancy must be created. The activation energy is the energy necessary to form and move the vacancies formed by the intersecting screw dislocation process, which is the energy for vacancy diffusion. For slip occurring on intersecting planes Mott gives for the creep rate

$$\dot{\epsilon} \simeq \nu(b/a)e^{-(\Delta H_s - \lambda b^2\sigma/kT)} \qquad (11)$$

where ν is the atomic vibrational frequency. As indicated above, σ is proportional to 1/a so that to the first order, a linear dependence upon stress results. The exponential dependence of activation energy upon stress, which again has not been experimentally substantiated, is a second order effect and modifies the linear dependence of $\dot{\epsilon}$ on σ only slightly.

(2) Weertman Theory

Weertman Theory

Weertman[12] has also proposed a steady state creep theory based on the climb of dislocations over

obstacles. Frank-Read sources are assumed for the dislocation which, under stress, moves in the form of loops until a natural obstacle such as a grain boundary is encountered. Stresses are produced by the piled-up groups and activate other dislocation sources on different slip systems. The dislocations generated combine with those already existing in the piled up group to form a new dislocation of pure edge character (Lomer-Cottrell dislocation[18]). This new dislocation is sessile because its Burgers vector does not lie in either of the interacting slip planes. Dislocations between a Frank-Read source and a Lomer-Cottrell dislocation disperse through climb, but are continually replaced by newly created dislocations.

The creep rate in Weertmans theory is proportional to the rate of escape of dislocations (past the Lomer-Cottrell barriers) and the reciprocal of the height the dislocations must climb. Weertman shows that climb height is proportional to $1/\sigma^2$ and that the rate of climb is related to the vacancy concentration gradient between dislocations; the latter is in turn proportional to σ^2. Thus the creep rate expression becomes proportional to σ^4, and is given by

$$\dot{\epsilon} = \frac{30 C_1 \sigma^4 \nu b^2}{\mu^2 kT} \; e^{S/k} \; e^{-\Delta H_s/kT} \qquad (12)$$

where S is the entropy of activation for self-diffusion,

and μ is the shear modulus. $C_1 = MLL'\dot{\mathcal{L}}$, where M is the number of active Frank-Read sources per unit volume, L is the distance the edge portion of the dislocation moves after breaking away from the barrier, L' is the same distance for the screw portion of the dislocation, and $\dot{\mathcal{L}}$ is the width of the piled up dislocation group. Weertman empirically determined that for single crystals $C_1\sigma^4 \sim \sigma^4$ and for polycrystalline materials $C_1\sigma^4 \sim \sigma^3$ so that equation (12) can be expressed for polycrystalline ceramics (where dislocation climb occurs) as

$$\dot{\epsilon} \simeq \frac{K\sigma^3}{kT} e^{-\Delta H_s/kT} \qquad (13)$$

The dependence of creep rate upon the 3rd or 4th power of stress is the characteristic feature of the dislocation climb mechanism. An obvious limitation is that the effect of grain size does not appear in the creep expression.

Garofalo[19] proposed that the mobile dislocation theories could be refined to include grain size effects. Steady state creep may be defined by the relation

$$\dot{\epsilon} = bN_s\bar{V} \qquad (14)$$

where N_s is the mobile dislocation length per unit volume, and $\bar{V}$ is the average velocity of mobile dislocations. Both grain boundaries and sub-grain boundaries are known to act as sources and sinks for

vacancies and N_s should depend on generation at both locations, so that $N_s = (N_b + N_{sb})$. N_b is the contribution of grain boundary generation to Ns and Nsb is the sub-grain boundary generation contribution. Nb is shown to be proportional to D_l/d where D_l is the density of ledges generating dislocations per unit area of grain boundary. At low temperatures D_l is small and contributes negligibly to steady state creep. Above a minimum temperature boundaries become mobile, ledges reform, and D_l increases and is maintained at a steady state value. The N_{sb} factor is shown to be proportional to d^2. Thus Equation (14) becomes

$$\dot{\epsilon} \simeq (k_1 D_l/d + k_2 d^2) b\bar{V} \qquad (15)$$

where k_1 and k_2 are constants with appropriate units to give the correct dimensions for strain rate. Although stress dependence is not explicitly shown, stress is known to be related to dislocation density and velocity. Friedel[20] showed that for many single crystal and polycrystalline materials, σ (as related to hardness tests) is related to dislocation density ρ (cm^{-2}, which corresponds to Ns) by

$$\sigma = (\mu b/4)\rho^{1/2}, \qquad (16)$$

thus suggesting $\rho \propto \sigma^2$. Cottrell[21] reports that under a force F an atom (or vacancy) migrating by thermal agitation acquires a steady drift velocity of

$$\bar{V} = (D/kT)F \qquad (17)$$

which is also the rate of climb (diffusion process) of the dislocation. The force in the slip plane of a dislocation is $F = \sigma b$, and a dependence of $\bar{V} \propto \sigma$ results. At constant stress Equation (15) has been found to agree with experimental results for low, intermediate and high temperatures[19]. At low temperatures where D_L is small, Equation (15) predicts a dependence of $\dot{\epsilon} \propto d^2$. At high temperatures a dependence of $\dot{\epsilon} \propto 1/d$ is indicated. When Equations (16) and (17) are combined with (14) a dependence upon stress of $\dot{\epsilon} \propto \sigma^3$, similar to Weertman's Theory, is suggested. Thus when dislocation climb is the rate controlling mechanism in creep, Garofalo's refinement may be combined with Weertman's Equation to give a creep rate dependence which goes as $\dot{\epsilon} \propto \sigma^3/d$.

CREEP EXPERIMENTS

In the following, a review of the more recent investigations on ceramic systems will be considered in relation to the creep theories presented above. Most of the work has been concentrated on magnesium oxide (MgO), the "classical" ceramic aluminum oxide (Al_2O_3), and beryllium oxide (BeO).

(1) MgO

The development of refractory materials capable of withstanding loads at elevated temperatures led to interest in MgO which has a melting point of 2800°C. Single crystal MgO has also received attention because of its ductility at low temperatures, which has been attributed to slip[22]. Polycrystalline MgO acts in a brittle manner at low temperatures, and Pask[23] has suggested that this is due to grain boundaries which strongly inhibit dislocation movement.

Numerous investigations involving constant load creep experiments on MgO have been reported, and most of the work is on polycrystalline samples. In the earlier work on polycrystalline MgO, Wygant[24] reported an activation energy for creep of 47 kcal/mol for specimens of very fine grain size ($<<$ 1μm) and 95% of theoretical density. The samples were tested in

torsion and a rate dependence on stress, $\dot{\epsilon} \propto \sigma^{3.5}$ was reported.

Vasilos et. al.[25] tested polycrystalline samples (99.5% of theoretical density) varying in grain size from 1-3μm. The creep rates were obtained at 1180-1260°C using a four point loading technique. An activation energy of 74 kcal/mol and a linear dependence of creep rate upon stress was reported. Although Vasilos et. al. make no attempt to determine the effect of grain size, the Nabarro-Herring model was proposed for the creep mechanism because $\dot{\epsilon} \propto \sigma$.

Cummerow[26] using a three point loading technique, studied creep in single crystals of MgO over the temperature range 1450-1700°C. A range of activation energies from 80-160 kcal/mol was reported on test samples cut from a single master specimen. The variation was attributed to small deviations from the stoichiometric composition, resulting in transitions from cation to anion self-diffusion processes. The stress dependence of the creep rate varied from $\dot{\epsilon} \propto \sigma^4$ to $\epsilon \propto \sigma^7$ with the higher exponent occurring at lower temperatures. Cummerow suggested Weertman's dislocation climb model for the creep process but noted that a diffusion mechanism was also contributing to the creep.

Passmore et. al.[27], using a four-point transverse bending technique, investigated creep in polycrystalline MgO (99.5% of theoretical density) over the range 1100-1500°C. The activation energy was observed to decrease as the grain size increased; 96 kcal/mole for the 2 μm grain size samples to 54 kcal/mole for the 5.5 μm grain size samples. For the samples ranging in grain size from 5.5-20 μm, the activation energy remained constant at 54 kcal/mole. For grain sizes 2-5.5 μm, $\dot{\epsilon} \propto \sigma^{1.5}$, and for grain sizes 5.5-20 μm, $\dot{\epsilon} \propto \sigma$. The dependence of creep rate upon grain size per se. was determined as $\dot{\epsilon} \propto 1/d^{2.5}$. Passmore et. al. suggested that the high activation energy for creep obtained by Cummerow was related to a vacancy generation process resulting from the applied tensile stress. This mechanism would operate in addition to the stress-directed self diffusion proposed by the Nabarro-Herring model for viscous creep. Lattice vacancy creation was also used to explain the continual decrease in $\dot{\epsilon}$ with ϵ in the secondary creep stage. Passmore et. al. suggested that three creep mechanisms were operative in the high temperature deformation of polycrystalline MgO, viz. the Nabarro-Herring lattice diffusion mechanism, the Coble grain boundary diffusion (σ^{-2}) mechanism, and a lattice vacancy forming mechanism. The first two mechanisms were suggested

to be responsible for the dependence of creep rate on $d^{-2.5}$.

Tagai and Zisner[28] studied creep in polycrystalline MgO (99.9% of theoretical density) in the temperature range 1200-1500°C. A four point loading technique was used. An activation energy of 104 kcal/mole and a stress dependence of $\dot{\epsilon} \propto \sigma^n$ (where n is in excess of unity) was reported. The phenomenon of decreasing $\dot{\epsilon}$ with increasing ϵ was also noted and proposed to be an inherent quality of dense refractory oxides explainable by grain growth. In another investigation,[29] Zisner and Tagai investigated the effects of porosity and additives (eg. Fe) on the creep rate for MgO. Additives decreased the tendency for grain growth and significantly affected mechanical properties at levels of contamination (ppm range) well below those usually considered significant in oxide ceramics. The additives promoted a linear dependence of $\dot{\epsilon}$ upon σ; suggesting that nonviscous dislocation mechanisms were being inhibited and replaced by a viscous diffusion mechanism. Previous investigators assumed that the effect of porosity on creep was independent of temperature, and that a given pore content should produce a fixed stress amplification factor over a wide temperature range. Zisner and Tagai showed that the effect of porosity per se. is related

to a thermally activated process, which increases the overall apparent activation energy of creep and produces a variable amplification factor. A concentration of pores could enhance creep by processes such as grain boundary sliding. It was observed that for up to 6% porosity, the creep rate was not significantly affected if the pores were fine, well distributed, and cracking was absent. The authors proposed that several processes contributed to creep. The Nabarro-Herring mechanism was assumed to be the principal process occurring (although no dependence of $\dot{\epsilon} \propto 1/d^2$ is reported). The stress dependency (σ^n) was accounted for by using Weertman's theory, implying that both diffusion and dislocation mechanisms were simultaneously operative.

Hensler and Cullen[30] investigated creep in polycrystalline MgO (97-98.9% of theoretical density) under compression. The grain size of the samples varied from 13-68 μm. An activation energy of approximately 110 kcal/mol was reported. The authors proposed that the large discrepancies in the reported activation energies for creep in MgO makes the stress dependency a more reliable quantity in determining creep mechanisms. A stress dependence $\dot{\epsilon} \propto \sigma^n$ ($n = 2.3\text{-}3.1$) was obtained, but the grain size effect was not considered. It was

observed that no change in grain size or specimen shape occurred during testing. Despite the fact that the stress dependence factor (n = 2-3) suggests a nonviscous dislocation mechanism, the authors concluded that no existing theories were applicable to their data, and that Gifkins diffusion induced grain boundary sliding mechanism represented the best choice of creep model.

Terwilliger et. al.[31] investigated creep in polycrystalline MgO and MgO-Fe_2O_3 solid solutions (all samples were approximately 99.5% of theoretical density). The grain size of specimens varied from 4-68 μm. A four point flexure loading method was used to produce creep over the temperature range 1000-1400°C. Characterization of the creep process involved the determination of the dependence of creep on stress, grain size, and the diffusion constant for the system. In samples containing no Fe_2O_3 additive, creep by a nonviscous dislocation mechanism was proposed to account for $\epsilon \propto \sigma^n$ (n = 2.4-3.6). The authors note that Langdon and Pask[32] found a similar stress correlation (n = 3.3) in polycrystalline MgO at 1200°C for creep tested in compression. The results of Terwilliger et. al. were interpreted in terms of dislocation climb controlled creep. For the pure MgO

specimen no grain size effect was reported. Addition of small percentages of Fe_2O_3 (0.10-3.0%) inhibited the nonviscous creep mechanisms and promoted diffusional, viscous ($\dot{\epsilon} \propto \sigma$) creep. Similar effects for Fe_2O_3 additions were observed by Hensler and Cullen[30]. Groves and Fine[33] have postulated that Fe^{+3} ions in solid solution inhibit dislocation motion during deformation of MgO single crystals. Terwilliger et. al. also noted that creep rate increased with increasing Fe_2O_3, and in all cases was higher than for pure MgO. The creep rate in the Fe_2O_3 doped specimens changed from a $1/d^3$ to $1/d^2$ dependency as grain size increased. These results suggested a transition in the creep mechanism from grain boundary anion diffusion (Coble) to lattice diffusion (Nabarro-Herring). A decrease in $\dot{\epsilon}$ with ϵ was also observed. The decay was too great to be explained in terms of grain growth as was suggested by Tagai and Zisner, and was described as an inherent, nonviscous, time-hardening mechanism.

(2) $\underline{Al_2O_3}$

Alumina has found widespread use in the field of ceramics because of its availability, chemical stability and relatively high strength. Its high melting point (2040°C) has led to extensive application in refractories.

Warshaw and Norton[34] did extensive creep testing on polycrystalline Al_2O_3 (97-100% of theoretical density) over the grain size range from 3-100 μm. Four point loading was used to produce creep at temperatures ranging from 1600-1800°C. Fine grained creep specimens (3-13 μm) displayed a vicous behavior ($\dot{\epsilon} \propto \sigma$) with an activation energy of 130 kcal/mole and a dependence on grain size of $\dot{\epsilon} \propto 1/d^2$. In coarse grained samples (50-100 μm) the activation energy increased to 185-kcal/mole and $\epsilon \propto \sigma^4$ suggesting a dislocation mechanism. Creep in the fine grained material was attributed to the lattice diffusion of cations, according to the classical description of viscous flow by Nabarro-Herring. For the coarse grained material, creep was assumed to occur by a dislocation climb mechanism (Weertman theory).

Al_2O_3 possesses a hexagonal crystal structure and in single crystals only one active slip system has been observed at low temperatures. Scheuplein ang Gibbs[35] suggested additional systems would be activated at high temperatures. Wachtman and Maxwell[36] observed such slip systems operating at elevated temperatures, adding weight to the conclusion that Weertman's dislocation theory applies in

Al_2O_3 in the temperature range studies by Warshaw and Norton (1600-1800°C). Wachtman and Maxwell also noted a strain hardening effect during creep.

(3) BeO

The interest in BeO (m.p. 2550°C) lies in its demonstrated stability in air at high temperatures, and also in its low neutron capture x-section and hence potential as a structural material in nuclear reactors. BeO has an hexagonal structure, and the basal slip system is the only one expected to be active at low temperatures.

Barmore and Vandervoort[37] performed creep tests on polycrystalline BeO (99% of theoretical density) samples varying in grain size from 10-30 μm. A four-point loading technique was used to produce creep over the temperature range 1400-1700°C. An activation energy of 100 kcal/mole was reported with $\dot{\epsilon} \propto \sigma/d^2$, suggesting the classical viscous creep process of stress induced vacancy diffusion (Nabarro-Herring theory). Based on the calculation of the diffusion constants from the creep rate data, the authors proposed that the diffusion of the (O^{-2}) ion was the rate controlling mechanism. This is in agreement with the work of Newkirk and Cline[38], who showed (by

electrical conductivity measurements) that the cation moves faster than the oxygen ion in the BeO lattice. The results obtained by Barmore and Vandervoort agree very well with earlier work by the same authors[39] on compressive creep in BeO. Porosity up to 4% was found to have negligible effect on the creep rate if it was well distributed and remained constant during testing.

Fryxell and Chandler[40] studied compressive creep of polycrystalline BeO at 1200°C with a porosity range of 1-15%. The grain size varied from 5-100 μm. The results essentially agree with those of Barmore and Vandervoort[37, 39]. There was too little control over impurity and porosity content to establish trends, except that in fine-grained samples abnormally high creep rates were observed when porosity was concentrated between grains. The phenomenon of decreasing $\dot{\epsilon}$ with ϵ in the secondary region of creep was reported for BeO.

In summary, it is difficult to compare the creep data, and it can only be assumed that the differences in test design, grain size, purity, and porosity are responsible for the large discrepancies in creep results reported by different observers for the same ceramic systems. However, several inferences regarding creep in ceramics may be drawn from the investigations

discussed above:

(1) In ceramics for which crystal structure is prohibitive to several slip systems operating, or when impurity additions effectively block dislocation glide or climb, creep is characterized by viscous, diffusion mechanisms. Frequently a transition from a volume diffusion mechanism ($\dot{\epsilon} \propto \sigma/d^2$) to a grain boundary diffusion mechanism ($\dot{\epsilon} \propto \sigma/d^3$) will occur in creep when the grain size is decreased.

(2) Ceramic materials in which slip systems are known to operate will often exhibit a nonviscous creep behavior at elevated temperatures where grain boundaries do not act as barriers to dislocation motion. Ceramics that do not normally exhibit multiple slip at low temperatures will exhibit nonviscous creep at temperatures approaching the melting point, where new slip systems become operative.

(3) Strain hardening during creep is frequently observed in dense ceramic oxides, which is manifested as a progressive decrease of $\dot{\epsilon}$ with increasing ϵ. In some cases the strain hardening has been associated with grain growth.

(4) Increasing concentration of Fe_2O_3 additives

increase the creep rate in MgO. This has been attributed to a promotion of viscous creep, as the impurity in solid solution inhibits dislocation movement and hence nonviscous creep. The implication is that the increase in viscous creep rate exceeds the decrease in creep rate due to dislocation mechanisms.

(5) The general effect of porosity seems to be to increase creep rate and appears to be related to a thermally activated process. Thus over a temperature range, porosity may drastically affect all creep parameters, including activation energy.

(6) The effect of grain size over wide ranges is not consistent. The sensitivity of the activation energy and the stress dependency of creep rate to grain size for some ceramics suggests a transition in the creep mechanism.

(7) The effect of stress and grain size on creep rate in generally more indicative of the rate controlling mechanism in creep than the activation energy.

STRONTIUM ZIRCONATE ($SrZrO_3$)

A search of the literature disclosed that with the exception of the work of Tinklepaugh et. al.[1], Funk et. al.[41-43], and Nemeth[44], there have been no investigations on the mechanical properties of $SrZrO_3$. The above investigators attributed the "ductile" stress-strain behavior of $SrZrO_3$ to the domain structure which occurs in some members of the perovskite type family (ABO_3 structure, e.g. $BaTiO_3$, $SrZrO_3$, etc). A domain may be described as a zone in a crystal (or grain) where the axes of the primitive cells are coincident. Adjacent to this zone are other domains containing primitive cells of a different orientation. It has been demonstrated[45-49] that the domain structure in the perovskites is associated with twinning, and the line of crystallographic mismatch between adjacent domains is referred to as a twin plane.

The idealized structure for the perovskite-type structure is cubic, and is shown in Figure 6. The $SrZrO_3$ structure is obtained by a slight distortion of this perfect cube as shown in Figure 7. The distortion consists of an elongation of one of the face diagonals of the cube to become the orthorhombic a-axis, a compression of the other face diagonal to become the orthorhombic c-axis and b' is doubled to

form the orthorhombic b-axis. Roth[50] reported that the orthorhombic cell of $SrZrO_3$ possesses the dimensions a=5.814 Å, b=8.196 Å and c=5.792 Å. From Figure 7 it is evident there are four primitive pseudocells per orthorhombic unit cell, and each pseudocell is monoclinic with a'=c'=4.096 Å, b'=4.098 Å, with the angle between a' and c' being 90° 14'.

The twinning (associated with the domain structure) is generally defined as a shear operation in which the atoms are displaced parallel to a mirror plane, with the displacement being a fraction of the lattice translation vector. All atoms in the displaced region move through distances proportional to their distance from the mirror (twin) plane. The slight deviation of the primitive structure (0° 14') from a cube allows twinning to occur by shear as depicted schematically in Figure 8a. The effect of mechanical twinning upon the orthorhombic cell is shown in Figure 8b, viz. a 90° rotation of the a and c axes about the b-axis, which remains unchanged. Adjacent domains across a twin boundary are shown in Figure 9. Twinning may be affected by a slip process, i.e. dislocation movement (c.f. section V, Creep Mechanism), however, Cottrell[21] notes that mechanical

twinning phenomenon differs from slip, with its main features being:

1) A lamella (domain) in the stressed crystal deforms into a new orientation, related symmetrically about some simple crystal plane (mirror plane) or axis (rotation) to the orientation of the undeformed parts of the crystal.

2) Macroscopically, the twinned lamella is formed by a simple shear on the twinning plane in the twinning direction. In contrast to slip, this shear is homogeneous throughout the entire twinned region and is fixed by the geometry of the crystal structure.

3) On the atomic scale, successive lattice planes parallel to the twinning plane slide over one another in the twinning direction, each plane moving over those below it by a fraction of the lattice spacing.

Mechanical twinning has been shown to be compatible with the orthorhombic perovskite structure[46-48]. Nemeth[44] has grown single crystals of $SrZrO_3$ and observed the domain structure using a petrographic microscope. Domains were observed to move through the crystals under the influence of a directional force. Hayden[51] noted that the shear deformation

associated with mechanical twinning can cause local stresses when the twin ends within the crystal (or grain) of a polycrystalline material. The deformation accompanying twinning can then cause the twinning to continue in neighboring grains. It was suggested that the above mechanism is responsible for the unique "ductility" of $SrZrO_3$.

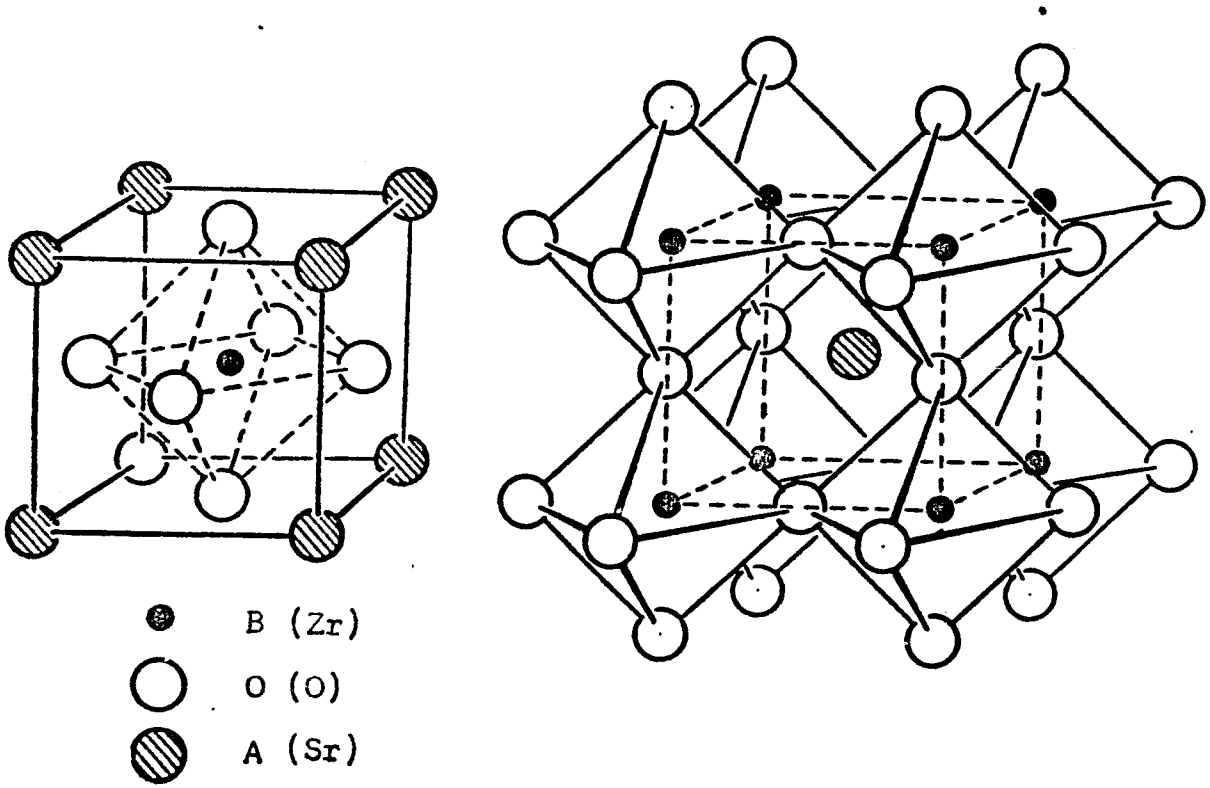

Figure 6

The Idealized Perovskite Structure

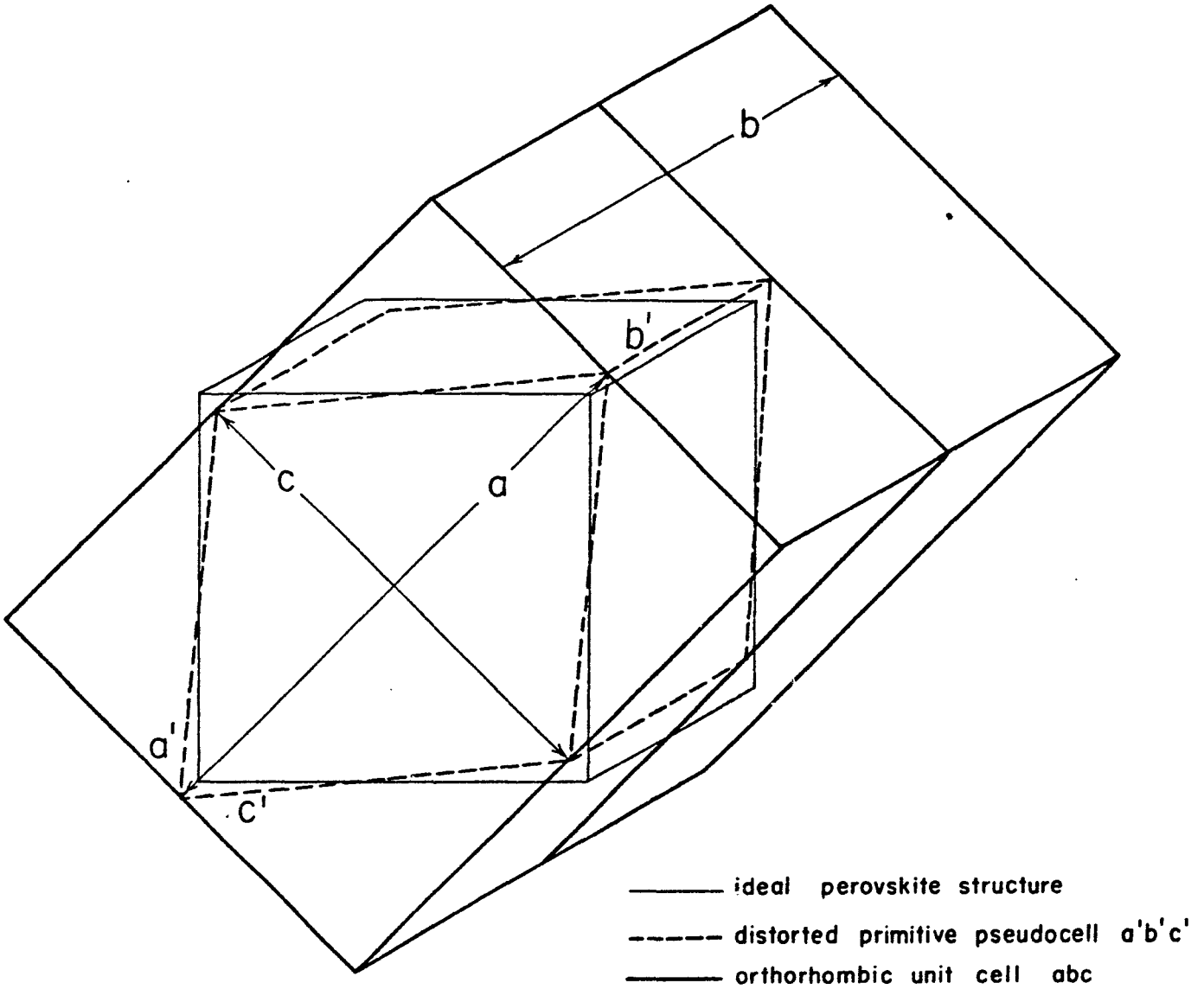

Figure 7

Relationship of Primitive Pseudocell and Orthorhombic Unit Cell of $SrZrO_3$

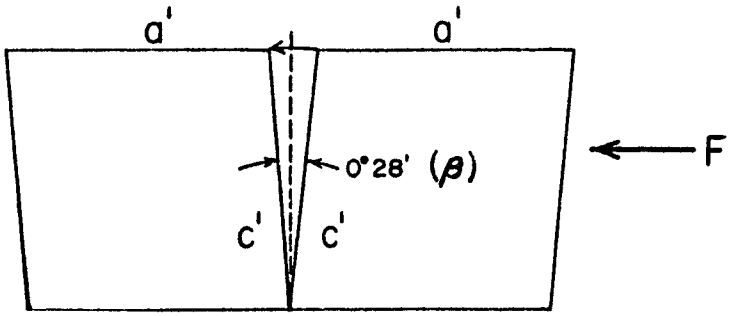

(a) 8a (b)

after force F is applied — pseudocubic cells — before force F is applied

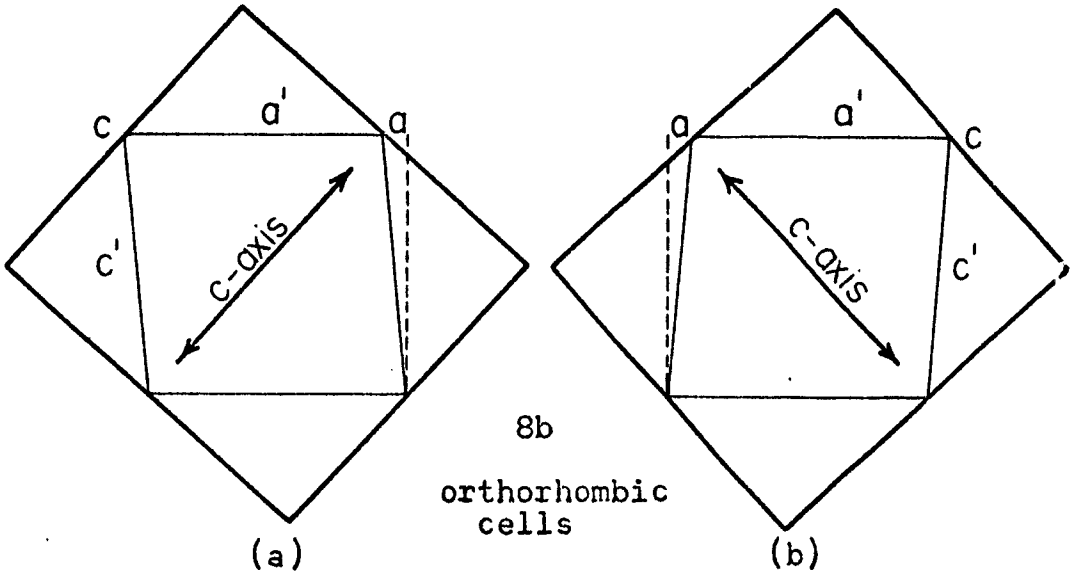

8b

orthorhombic cells

(a) (b)

Figure 8

Effect of an applied force (F) on the pseudocell a'b'c' and the orthorhombic cell of $SrZrO_3$ (b' and b are perpendicular to the page).

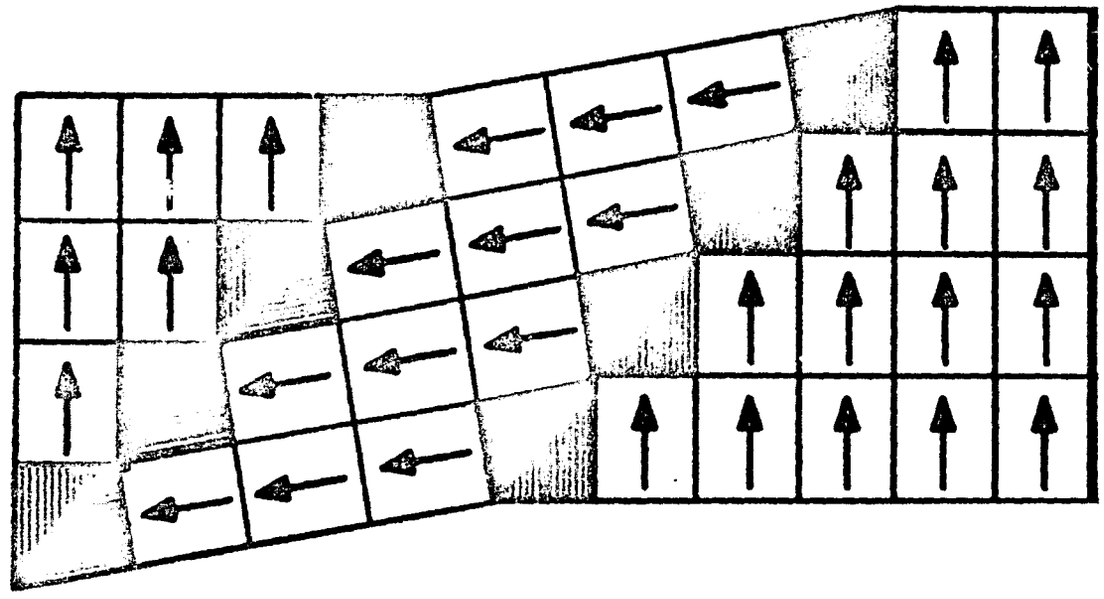

Figure 9

Adjacent twin domains across a twin boundary. The arrows indicate the a direction of the orthorhombic cell.

III EXPERIMENTAL

A. SAMPLE PREPARATION

The problem of sintering consistently dense, homogeneous specimens of $SrZrO_3$ has been the object of considerable research.[41-43] The control of atmosphere and temperature for sintering is difficult with gas fired kilns, and consequently an electric furnace utilizing super kanthal elements was constructed. These elements are capable of achieving a maximum operating temperature of 1700°C in air. The use of an electric furnace for sintering eliminated the problems associated with the inconsistent oxidizing-reducing atmosphere conditions due to variable gas-air mixtures.

Chemically pure $SrZrO_3$ was obtained from TAM Division of the National Lead Co. (Niagara Falls, N. Y.). A spectrographic analysis of impurities occurring in this material is shown in Table I. All test specimens were prepared from the same lot of $SrZrO_3$ powder to eliminate or minimize variations in the test results arising from differences in specimen composition.

The high melting temperature of $SrZrO_3$ necessitates addition of mineralizers to lower the sintering temperature. In their attempts to sinter $SrZrO_3$, Keler and Kusnetsov[52] achieved only 66% of theoretical density by firing to 1500°C with no additives. They obtained up

to 90% theoretical density by adding strontium borate ($3SrO.B_2O_3$) in excess of 5 wt.%. The addition of the mineralizer ($3SrO.B_2O_3$) cannot be considered a satisfactory means of densification; firstly because almost theoretical densification is required, and secondly too high concentrations of the mineralizer will alter those characteristic properties of $SrZrO_3$ which result in its unique behavior.

Funk, Nemeth, and Tinklepaugh[43] conducted extensive sintering tests on C.P. $SrZrO_3$ in which B_2O_3, Fe_2O_3, $FeCl_3$, $AlCl_3$, H_3PO_4, $(NaPO_3)_6$, LiF, LiCl, and KCl were added in amounts up to 1 wt.%. In these tests only the iron compounds were effective in obtaining sintered densities in excess of 90% of theoretical. A slow scan X-ray pattern of the high angle $2\theta = 146.32^{\circ}$ peak of $SrZrO_3$ showed that such small additions cause no measurable shift, indicating that there is no disruption of the crystal structure, and thus the twinning phenomenon in $SrZrO_3$.

Sintering and the resultant densification of oxides is believed to occur by a diffusion process whereby vacancies diffuse from pores to grain boundaries where they are annihilated. Conversely, the mechanism can be viewed as the migration of ions into the voids from nearby grain boundaries. The Nabarro-Herring model described earlier, again serves to describe the densification process.

Jorgenson and Anderson[53] discussed the sintering of relatively pure oxide powders and noted that "discontinuous grain growth", i.e., grain boundaries breaking away from pores and leaving them entrapped within the grains, makes it increasingly difficult to achieve high densities. Inhibiting grain boundary migration (retarding grain growth) so that the distance between pores and grain boundaries remains small allows a high vacancy diffusion flux to the grain boundaries to eliminate voids. They suggested accomplishing this by adding to the oxide small amounts of ThO_2 which segregates at the grain boundary and thus exert a drag on grain boundary motion. Jorgenson and Anderson found, however, that additions of 10 wt.% ThO_2 were necessary to achieve the desired results.

Kingery[54] indicated that small additions of a low surface tension component to an oxide powder would segregate at the surface of a grain and decrease the surface energy, a driving force for grain growth. This too may provide a means of retarding grain growth.

Accordingly, a series of sintering experiments were performed using mixtures of $SrZrO_3$ with an as received grain size of < 0.3 μm and ThO_2 to give fine particles segregated at boundaries, and another series with Fe_2O_3 to give a low surface tension liquid (above 1565°C) at the grain boundary. A series of tests was

also conducted using both ThO_2 and Fe_2O_3 additions. Hydrated thorium nitrate ($Th(NO_3)_4.4H_2O$), which is soluble in alchohol, was mixed with alchohol and $SrZrO_3$ to form a slurry. NH_4OH was added to the slurry while it was vigorously mixed, resulting in gelatinous $Th(OH)_4$ precipitating on the grains of the $SrZrO_3$ powder, which on ignition results in the formation of ThO_2.

Iron was added as ferric chloride, which is also soluble in alchohol, and the same treatment described above for $Th(NO_3)_4.4H_2O$ results in ferric oxide (Fe_2O_3) coating the $SrZrO_3$ grains.

The slurries were agitated during drying to promote intimate mixing. After drying all batches were dry-mixed in a V-shell blender for 24 hours and then milled for one hour in a vertical reciprocating mill to further promote mixing and reduction in particle size. Fine particle size aids sintering by increasing the surface free energy. The milling medium was high density burundum (Al_2O_3 composition) cylinders, ½" diameter, by ½" in length (obtained from Canadian Laboratory Supplies Ltd., Toronto, Ont.). The grinding cylinders and powder were placed in a one to one volume ratio to form a charge which occupied 30-40% of the volume of the grinding mill.

Lewis and Lindley[55,56] have demonstrated that the strains introduced in refractory oxide particles by ball milling contribute to the sintering process more than the increased surface area due to reduced grain size. It has also been shown[57,58] that a reciprocating action is more effective in developing this lattice strain that the conventional tumbling technique. A vertical reciprocating ball mill was constructed which oscillated the charge in a straight up and down motion over a 0.75 in. throw distance at 700 cycles per minute.

The effects of increased lattice strain can usually be measured by x-ray line broadening.[55,56] However, the small grain size of the as received $SrZrO_3$ (<0.3 μm) itself resulted in line broadening, and the twinning mechanism active in $SrZrO_3$ would act as an accomodation process to inhibit lattice strain buildup. These effects masked any contribution to lattice strain resulting from the milling procedure.

Two inch long rectangular bars, 0.5" x 0.15" in cross-section,were double compacted at 15,000 psi from powder slightly dampened by alchohol. The samples were then loaded in the kiln and sintered. Table II shows the density and fracture strengths of the compacts.

Densities were measured by the water displacement technique[59] which is reported to have a precision of

$\pm 0.05\%$.[37] This method has the advantage that it does not depend on the specimen shape, and also permits the determination of pore volume. To obtain the results the sample is weighed dry (W_1), vacuum impregnated with water and again weighed (W_2), and finally weighed suspended in water (W_3).

The density properties to be measured are related to three volumes which are represented by :

V_m = volume of solid material (cm^3)

V_o = volume of open pores (cm^3)

V_c = volume of closed pores (cm^3).

From the measured weights, (W_1), (W_2), and (W_3), the bulk volume (V_t) and open pore volume (V_o) are computed as follows (for water as the immersion liquid):

$$V_t = V_m + V_o + V_c = W_2 - W_3 \qquad (18)$$

$$V_o = W_2 - W_1. \qquad (19)$$

Also the bulk density (ρ_b), apparent porosity (P_a), true porosity (P_t), and closed porosity (P_c) are given by:

$$\rho_b = \frac{W_1}{V_t} = \frac{W_1}{W_2 - W_3} \quad (gm/cm^3) \qquad (20)$$

$$P_a = \frac{V_o}{V_t} = \frac{W_2 - W_1}{W_2 - W_3} \times 100 \qquad (21)$$

$$P_t = 1 - \frac{\rho_b}{\rho_{theoretical}} \qquad (22)$$

$$P_c = P_t - P_a. \qquad (23)$$

The closed porosity is a measure of the amount of vitrification occurring due to pores being sealed

off in grain boundaries, and of discontinuous grain growth which entraps pores within the grains themselves.

Besides density, strength was also used as a criterion for selection of the system to examine because this determines the materials usefulness. Funk, et. al.[41-43] reported fracture strengths of 10,000-13,000 psi for $SrZrO_3$ in flexure. The values reported in Table II are for room temperature and were obtained using an Instron Tensile Testing machine. The samples were loaded by pure bending and strained at 0.002 in./min.

It was decided that F_2O_3 was the most desirable mineralizer because of the high densification obtained for the relatively small additions. The fracture strength of 24,000 psi for the 1.35 wt. % F_2O_3 addition is twice as high as results previously reported.[41-43]

The samples for the high temperature deformation tests were prepared as described above. After sintering, all samples were surface ground with a diamond wheel and finished with silicon carbide paper to a uniform cross section of 0.135" x 0.325". The specimens to be tested are described in Table III.

Transmission electron micrographs of typical specimens were obtained for each composition and grain size. The grain size was too small (0.4 - 2.0 μm) to be resolved by the optical microscope, and grain

size measurements were made by the intercept method from the electron micrographs.

Fracture surfaces were etched with a 1.5% solution of 40% HF acid. Replicas were obtained by the two step technique using 60 % Au- 40% Pd metal shadow and a carbon substrate. The replicas were examined on an RCA electron microscope, and the photographs of the replicated surfaces are shown in Figures A-1 to A-6 of Appendix A. Scanning Electron micrographs (SEM) of the unetched fracture surfaces were obtained on a Joelco SEM and are also shown in Figures A-1 to A-6.

TABLE I

Spectrographic Analysis of Principal Impurities in Chemically Pure $SrZrO_3$

Silicon	< 0.1%
Iron	< 0.1%
Aluminum	0.1%
Magnesium	< 0.1%
Copper, Titanium, Hafnium	ppm range

TABLE II

Summary of Data for Sintering Experiments

Composition Wt %		Firing Temp.	Firing Time	Density (% theoretical)	Fracture Strength psi
$SrZrO_3$ (no additives)	100.0	1580-1600°C	2 hrs	75	------
$SrZrO_3$	97.0	1580-1600°C	2 hrs	78.10	7,500
ThO_2	0.7				
$SrZrO_3$	98.0	1580-1630°C	20 hrs	94.58	17,000
ThO_2	1.3				
Fe_2O_3	0.7				
$SrZrO_3$	97.0	1580-1630°C	20 hrs	91.42	15,500
ThO_2	2.3				
Fe_2O_3	0.7				
$SrZrO_3$	99.15	1580-1600°C	2 hrs	84.33	9,100
Fe_2O_3	0.85				
$SrZrO_3$	99.15	1580-1630°C	20 hrs	93.20	16,200
Fe_2O_3	0.85				
$SrZrO_3$	98.65	1580-1630°C	20 hrs	98.64	24,000
Fe_2O_3	1.35				

TABLE III

Summary of Sintering Characteristic

Data for Samples to be Creep Tested

Composition Wt %		Firing Temp.	Firing Time	ρ_b % Theoretical	% Open Pores	% Closed Pores	Grain Size
$SrZrO_3$	99.15	1600°C	2 hrs	87.90	9.84	2.26	0.45 µm
Fe_2O_3	0.85						
$SrZrO_3$	99.15	1577-1620°C	10 hrs	97.01	0.75	2.42	1.03 µm
Fe_2O_3	0.85						
$SrZrO_3$	99.15	1575 1597°C	20 hrs	92.46	6.02	1.52	1.83 µm
Fe_2O_3	0.85						
$SrZrO_3$	98.65	1600°C	2 hrs	99.04	0.01	0.95	0.45 µm
Fe_2O_3	1.35						
$SrZrO_3$	98.65	1577-1620°C	10 hrs	99.07	0.03	0.90	1.06 µm
Fe_2O_3	1.35						
$SrZrO_3$	98.65	1575 1597°C	20 hrs	98.87	0.01	1.12	2.04 µm
Fe_2O_3	1.35						

B. HIGH TEMPERATURE X-RAY DIFFRACTION

The literature review indicated the importance of the crystallography of $SrZrO_3$ in relation to its mechanical properties. Bush and Hummel obtained stress-strain curves in flexure for magnesium dititanate[60] ($MgO.2TiO_2$) and β-eucryptite[61] ($Li_2O.Al_2O_3.2SiO_2$) similar to those displayed by $SrZrO_3$ (see Figure 1), and they attributed the nonlinear behavior (hysteresis) of these materials to internal stresses arising from anisotropy. Differential thermal contraction during cooling causes microcracks to develop after the material has been sintered. Repeated application of stress causes continual growth of internal fractures, resulting in increasing strain.

To insure that thermal expansion anisotropy is not a contributing factor to the stress-strain and creep behavior of $SrZrO_3$, its thermal expansion was measured by x-ray diffraction over the temperature range 25°C-1300°C. A Phillips generator, type 12215 was used with a Materials Research Corporation, Model X-86N-II, high temperature attachment. The temperature was maintained at $\pm$ 2°C using a Materials Research Corporation automatic proportional controller.

C. CREEP APPARATUS

Creep specimens were deformed in four-point pure bending. The load was applied by weights acting through a lever system and transmitted to the specimen by hot pressed silicon carbide knife edges (see Figure 10) The sample was supported by 1/8 in. sapphire rods. The tensile stress (σ_t) in the outer fiber of the creep specimen under a total load (F) is calculated using the equation:

$$\sigma_t = \frac{3Fa}{wh^2} \qquad (24)$$

where a is the moment arm (0.25 in), w is the specimen width (0.325 in.), and h is the specimen thickness (0.135 in.). The creep tests in this investigation measured plastic deformation under constant load. Although Equation (24) is extensively used in the study of plastic deformation, its normal use is to relate bending moment to elastic stress, and there is some question whether the actual stress is represented by this expression. Regions of high stress would undergo stress relaxation during plastic deformation and could cause the outer fiber stress to be less than Equation (24) indicates. Timoshenko[62] has shown that for plastic deformation of a rectangular beam the maximum outer fiber stress is given by:

$$\sigma_t = \frac{3Fa}{wh^2} \cdot \frac{2n+1}{3n} \qquad (25)$$

where n is the stress exponent in the general creep equation given in Equation (32). Unity is the usual value given to n (at least for the purpose of calculating applied load) and thus Equation (24) is obtained.

Strain (ϵ) was obtained from the deflection (δ) within the region of pure bending. Deflection was measured by placing three linear variable differential transformers (LVDT), model 24 DCDT-250 (Hewlett Packard), coupled directly to sapphire rods which contacted the tension side of the specimen (cf. Figure 10). The rods were placed slightly inside of the region of pure bending (e) to avoid irregularities in deflection due to the adjoining region of decreasing bending moment. The LVDT's were powered by a DC power supply (Hewlett Packard). The configuration of sapphire rods allows measurement of displacement due to sample bending alone and eliminates the contributions due to deformation of knife edges at elevated temperatures, thermal expansion of the sample support column, and thermal expansion of the contact rods. The transformers in conjunction with a three channel potentiometric recorder (Rickadenki Kogyo, Model B-31) provided a continuous deflection-time plot. A strain sensitivity of 10^{-5} is reported for similar apparatus[37]. The outer fiber strain in the region of pure bending is determined from the expression:

$$\epsilon = \frac{4h\delta}{g^2 + 4\delta^2} \qquad (26)$$

If $\delta \ll g$ (g = 1 in.), Equation (26) can be simplified to $\epsilon = 4h\delta$.

The creep chamber was heated by four silicon carbide globar elements (Carborundum Co.). Temperature was measured at the center of the gage section (g) using a Pt-Pt 10 Rh thermocouple and was controlled to $\pm 3^{\circ}$C (maximum), with a probable error of $\pm 2^{\circ}$C.

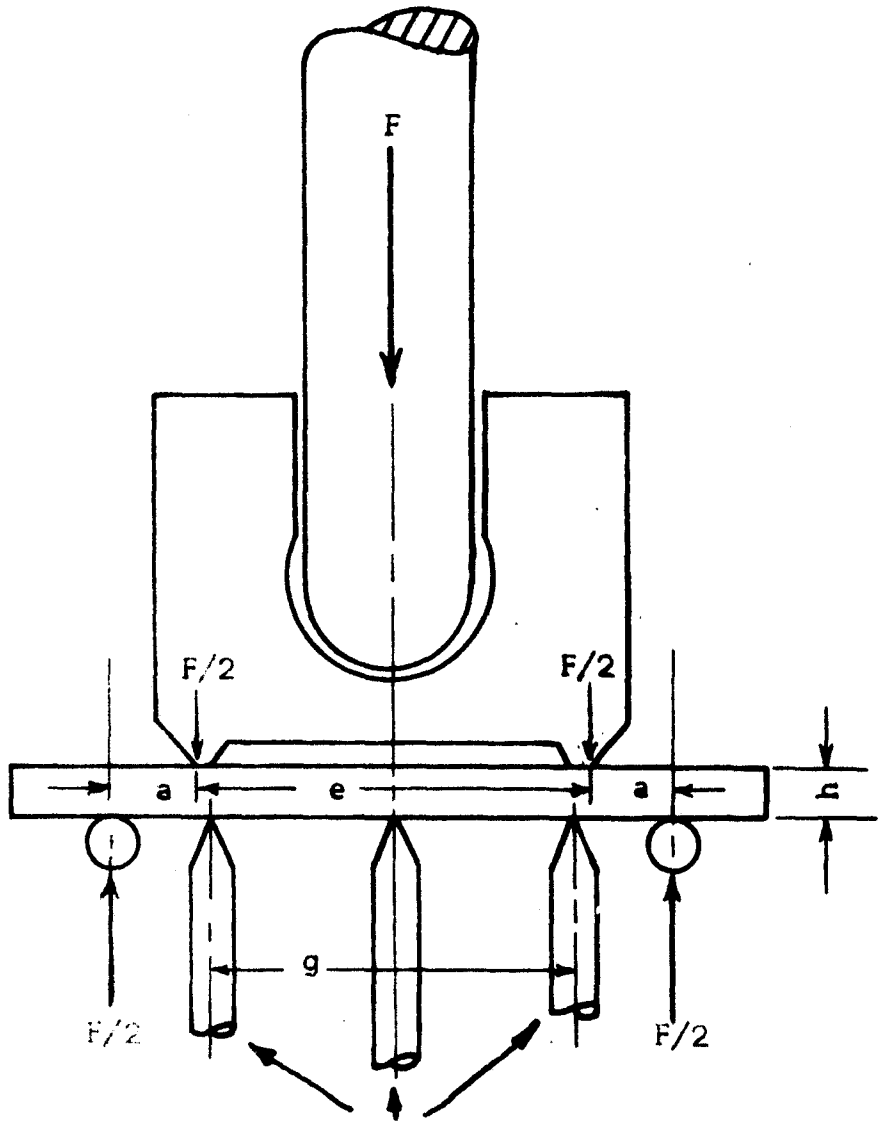

Figure 10

Flexure specimen
in
four point loading

IV RESULTS

A. X-RAY DIFFRACTION

An x-ray pattern was obtained for various temperatures by scanning at 2^{o}/min. for a 2θ value from 25^{o} to 80^{o} to determine if peaks appeared or disappeared. Such variations, if present, would indicate a change in crystal structure with temperature. The structure was found constant over the temperature range measured. Subsequently, the (204), (163), and (610) peaks were slow scanned at 0.25^{o}/min at each temperature. Lattice spacing (d_1) for each of the three planes was calculated using the Bragg equation. The (d_1) and corresponding (hkl) values were substituted in the equation relating the lattice spacing to the unit cell dimensions for the orthorhombic system. The shear angle (β, cf. Figure 8a) at each temperature was relatively constant averaging at 34' over the temperature range 25°C to 1300°C. This suggests that the twinning mechanism, which presumably results in the stress-strain behavior of $SrZrO_3$, is active over the entire temperature range. Figures 11 to 13 show the average linear thermal expansion for $SrZrO_3$ and the thermal expansion for a, b, and c axes upon heating and cooling. These figures show that anisotropy is

negligible and is not a factor in the stress-strain or creep behavior of $SrZrO_3$. Table IV summarizes the results, giving the average linear thermal expansion and thermal expansion for the a, b, and c axes of $SrZrO_3$.

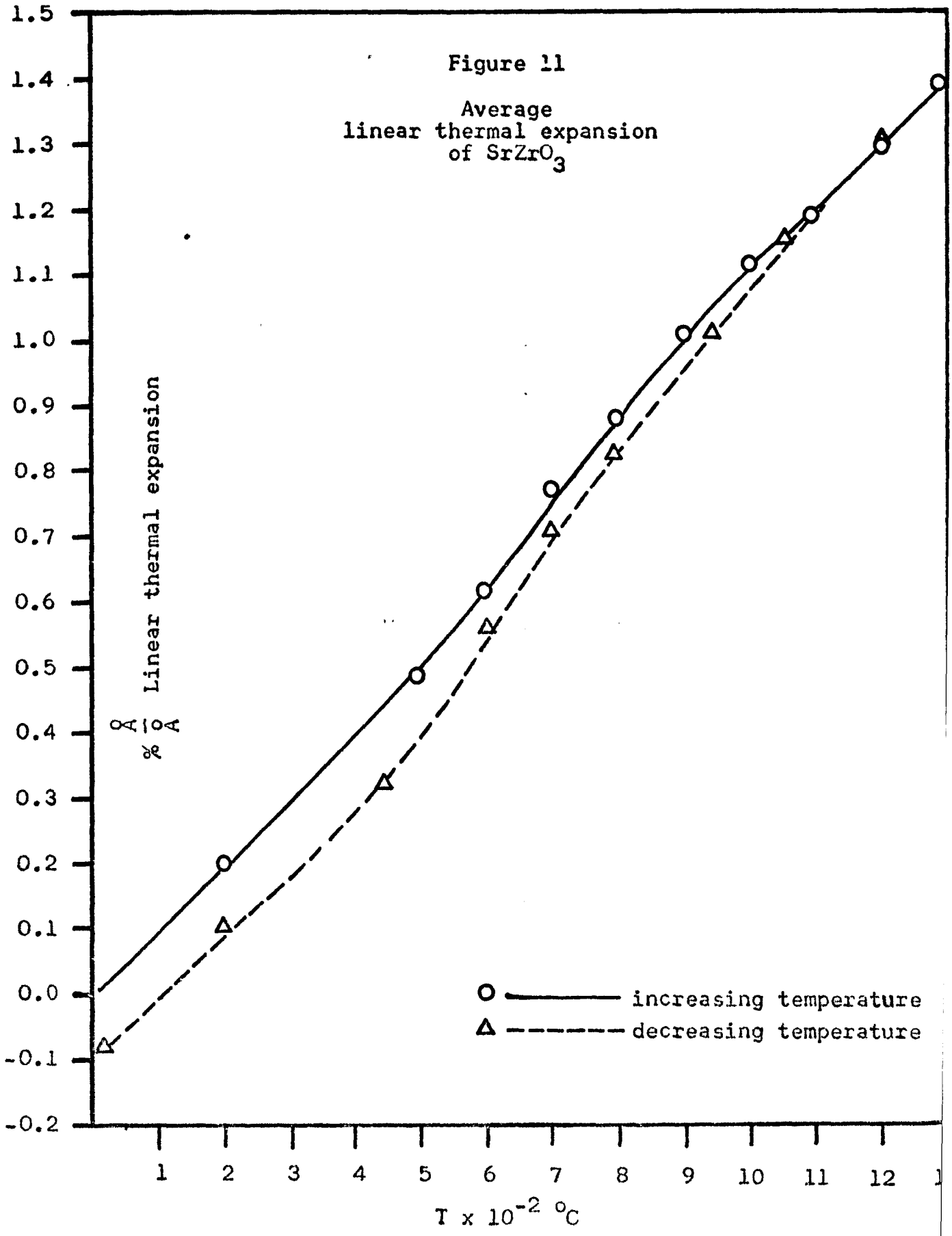

Figure 11

Average
linear thermal expansion
of $SrZrO_3$

Figure 12

Linear Thermal Expansion
of $SrZrO_3$
for a, b and c axes
(increasing temperature)

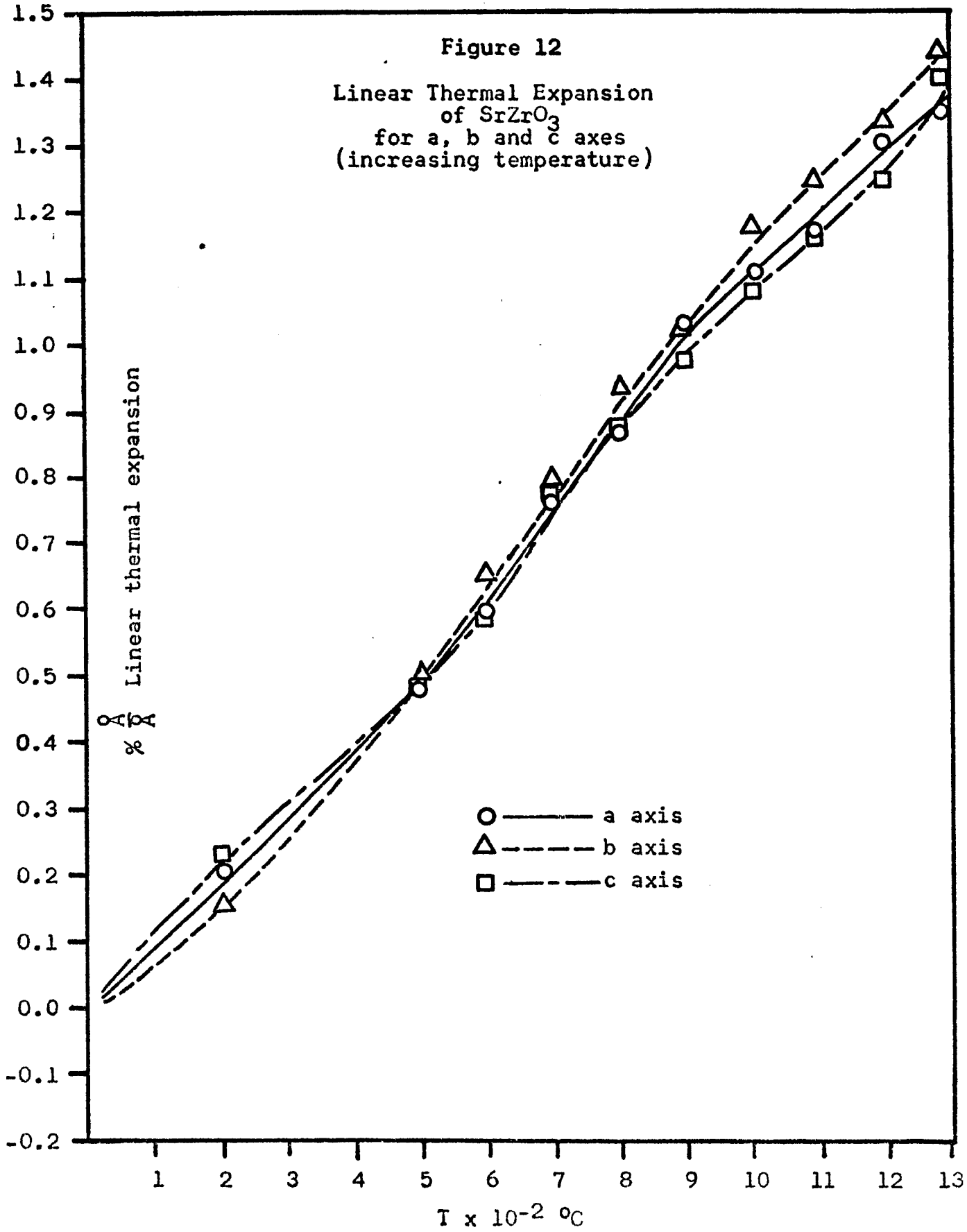

Figure 13

Linear Thermal Expansion
of $SrZrO_3$
for a,b and c axes
(decreasing temperature)

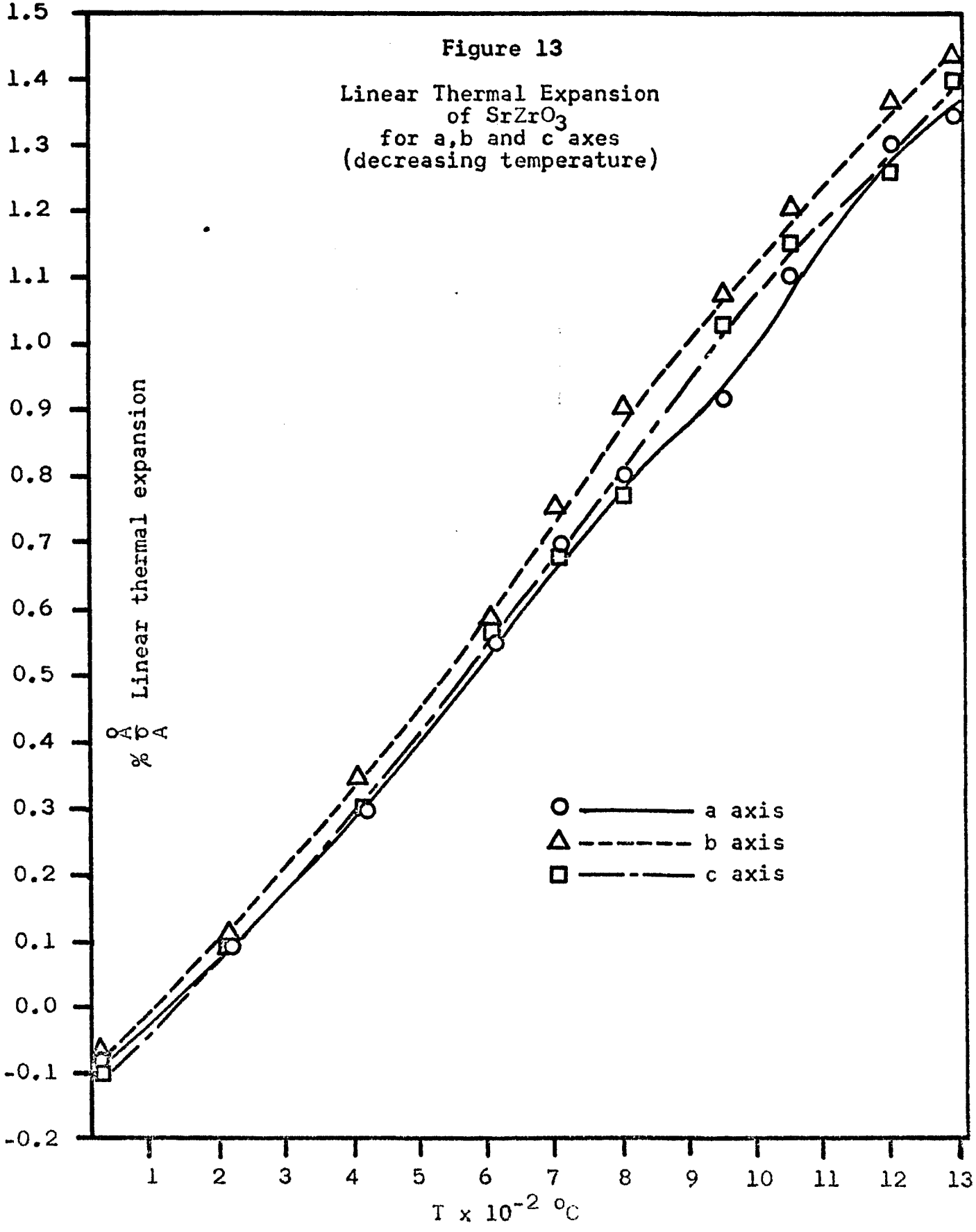

TABLE IV

Thermal Expansion of $SrZrO_3$

	Thermal Expansion %/°C
Average	10.74×10^{-4}
a-axis	10.34×10^{-4}
b-axis	11.08×10^{-4}
c-axis	10.76×10^{-4}

B. CREEP RATE

(1) Effect of Temperature (Activation Energy)

Most of the creep rate results in this investigation were obtained using the differential method (see Dorn[63]). If creep is assumed to be a thermally activated process, the effect of temperature upon rate may be expressed as:

$$\dot{\epsilon} = Ae^{\Delta S/R} e^{-\Delta H/RT}, \qquad (27)$$

where A is the pre-exponential factor (strain/second/activation) and ΔS and ΔH are respectively the entropy and activation energy (enthalpy) for the process. The effect of temperature upon creep rate is determined by abruptly changing the temperature during creep under constant load conditions. Figure 14 shows a typical strain vs time plot for $SrZrO_3$ when the temperature is varied in a step-wise manner between (T_1) and (T_2). The creep rate is obtained from the slope of the (ϵ) vs (t) curve in Figure 14. The logarithm of the creep rate is then plotted against the strain as shown in Figure 15. Since it may be assumed that there is no change in substructure when the temperature is abruptly varied, the change in creep rate must be attributed solely to the temperature change. The creep rates ($\dot{\epsilon}_1$) and ($\dot{\epsilon}_2$) immediately preceeding and following

the temperature change (T_1) and (T_2) are related by:

$$\frac{\dot{\epsilon}_1}{\dot{\epsilon}_2} = \frac{e^{-\Delta H/RT_1}}{e^{-\Delta H/RT_2}} , \qquad (28)$$

when the enthalpy and entropy of activation are assumed to be invarient. From Equation (28) it follows that:

$$\Delta H_i = \frac{R \ln(\dot{\epsilon}_1/\dot{\epsilon}_2)}{(1/T_2 - 1/T_1)} . \qquad (29)$$

Thus the activation energy for the creep process, at constant load and substructure, is readily determined from creep data plots as shown in Figure 15. Tables B - I and B-II in Appendix B contain all the data required for the log ($\dot{\epsilon}$) vs (ϵ) plots. Table B-1 gives the results for $SrZrO_3$ with 1.35 wt. % Fe_2O_3 addition (these samples henceforth designated SZ-1.35-Fe), and Table B-II gives the results for $SrZrO_3$ with 0.85 wt. % Fe_2O_3 addition (designated SZ-0.85-Fe). The activation energies obtained for a 2000 psi stress level for three grain sizes are given in Tables V and VI for the SZ-1.35-Fe and SZ-0.85-Fe samples respectively.

Creep rate is clearly dependent upon temperature, stress and grain size, and is also related to the amount of strain as evident from Figure 15 . In order to determine the effect of a particular variable on creep therefore, it is necessary to normalize the creep results against those variables not specifically studied. This

was effectively done in determining the activation energies given in Tables V and VI, for the creep load and grain size of the specimens were kept constant.

It is useful to recast the creep rate data in the form:

$$Z = \dot{\epsilon} e^{\Delta H/RT} \qquad (30)$$

where Z (Zener-Hollomon parameter[64]) is independent of the temperature effect on the creep rate. If creep results from a single process which has a unique activation energy, then a plot of log (Z) vs (ϵ) (at a constant stress level and grain size) should give a curve which is common to all points irrespective of the test temperature. This method is frequently used to determine if a singular creep mechanism is operating. The log (Z) vs (ϵ) curves for a 2000 psi dead load are shown for the SZ-1.35-Fe and SZ-0.85-Fe samples in Figures 16 and 17 respectively.

Furthermore, when the creep rate data from different samples are to be used in the determination of the activation energy, the log ($\dot{\epsilon}$) vs (1/T) curves for constant grain size must be normalized to the same strain level (the substructure variable also appears to be dependent on the strain level). If log Z (or $\dot{\epsilon}$) vs. (ϵ) plots approximately as a straight line, then it is easily shown that the creep rate for a specific strain

level (for comparative studies the creep rates in this investigation were normalized to 0.004 strain) is related to an arbitrary strain level (ϵ_x) by

$$\log \dot{\epsilon}_{0.004} = \log \dot{\epsilon}_x - (\text{slope})(\epsilon_x - 0.004) \quad (31)$$

The normalized creep rates obtained from Equation (31) are summarized in Tables B-III and B-IV of Appendix B for the SZ-1.35-Fe and SZ-0.85-Fe samples respectively. The creep rate data for all grain sizes, normalized for a strain level of 0.004, were then recast as Arrhenius plots to obtain the activation energies for the creep process. These results were then compared to the activation energies obtained directly by the differential method and are also given in Tables V and VI. Figures 18 and 19, shows the strain normalized Arrhenius plots for all grain sizes of SZ-1.35-Fe and SZ-0.85-Fe respectively.

(2) Effect of Stress

The effect of stress upon creep rate was determined by a differential technique similar to the temperature effect measurements. Creep rate at constant temperature was measured for a given stress. The stress was then abruptly changed and the resultant rate measured. This procedure assumes no significant substructural changes occur due to the abrupt change in stress. In comparing

Equations (3) and (30), if $f_1(\sigma) \propto \sigma^n$ and $f_3(d)$ may be represented by s, then it is evident that

$$Z = S\sigma^n \qquad (32)$$

so that the slope of log (Z) or log $(\dot{\epsilon})_T$ vs log (σ) for a constant grain size and strain will give the stress factor (n). The log $(\dot{\epsilon}_{0.004})_T$ vs log (σ) plots are shown in Figures 20 and 21 for the SZ-1.35-Fe specimens and in Figures 22 and 23 for SZ-0.85-Fe specimens.

The SZ-1.35-Fe specimens displayed a creep rate dependence upon stress with $n \backsimeq 3$, where n decreased slightly with increasing grain size, i.e., n=3.3 for the 0.45 μm and n=3.1 for 2.04 μm specimens. The n factor varied from 1.9 to 3.4 with increasing temperature for the 0.45 μm specimens of SZ-0.85-Fe. The n value for the 1.83 μm specimens of SZ-0.85-Fe increased from 0.55 at 1200°C to 1.88 at 1300°C.

Creep rate data for the 1.83 μm grain size specimens of SZ-0.85-Fe at the stress levels of 850 psi and 3000 psi were obtained by conventional long-term creep tests rather than the differential method. Figures C-1 and C-2 in Appendix C show the constant temperature-constant load, (ϵ) vs (t) curves for σ=850 psi and

σ = 3000 psi respectively. These were preliminary tests to determine that no irregularities were present over the temperature and stress range studied.

The $(\dot{\epsilon}^{o})$ - (σ) data for various temperatures was replotted to determine if the activation energy is stress dependent. The curves showing the effect of stress upon the Arrhenius plots for the 0.45 μm and 2.04 μm grain size specimens of SZ-1.35-Fe are shown in Figures 24 and 25. Figure 26 is a similar plot for the 1.83 μm specimen of SZ-0.85-Fe. Since the 0.45 μm and 1.03 μm grain size specimens of SZ-0.85-Fe display an activation energy variation with temperature (see Figure 19), Equations (27) and (29) do not apply and the stress dependency was therefore not determined. The complexities observed in Figures 22, 23 , and 26 for the behavior of SZ-0.85-Fe, which is related to the high porosity in these specimens (see Table III , preclude attempts to describe the effects of (T), (σ), and (d) upon activation energy and creep rate.

(3) Effect of Grain Size

The effect of grain size upon creep rate for the SZ-1.35-Fe specimens was determined by plotting all the strain normalized creep rate data obtained by the differential technique (Equation 31) at 2000 psi as log $(\dot{\epsilon}^{o}_{0.004})$

vs. log (d), and is shown in Figure 27. A consistent slope of (-1) was obtained which indicates that $\dot{\epsilon} \propto 1/d$. This was confirmed for all stress levels by examining the (Z) parameter. Warshaw and Norton[34] noted this could be determined by considering Equation (32). If ΔH is relatively independent of stress, the creep rate may be normalized for (σ^n) as well as for (T). All data for SZ-1.35-Fe were included in a log (d) vs. log (Z/σ^3) plot as shown in Figure 28. Average values for each stress, temperature, and all data are shown for three grain sizes. The slope indicates a (1/d) dependence upon grain size.

A relationship of the form $\dot{\epsilon} \propto \sigma^3/d$ is thus indicated. If this is so, all data for SZ-1.35-Fe should fall on a straight line of slope = 1 when log (σ^3/d) is plotted vs. log (Z). The curve in Figure 29 shows this relationship.

Figure 14

Creep Strain vs Time

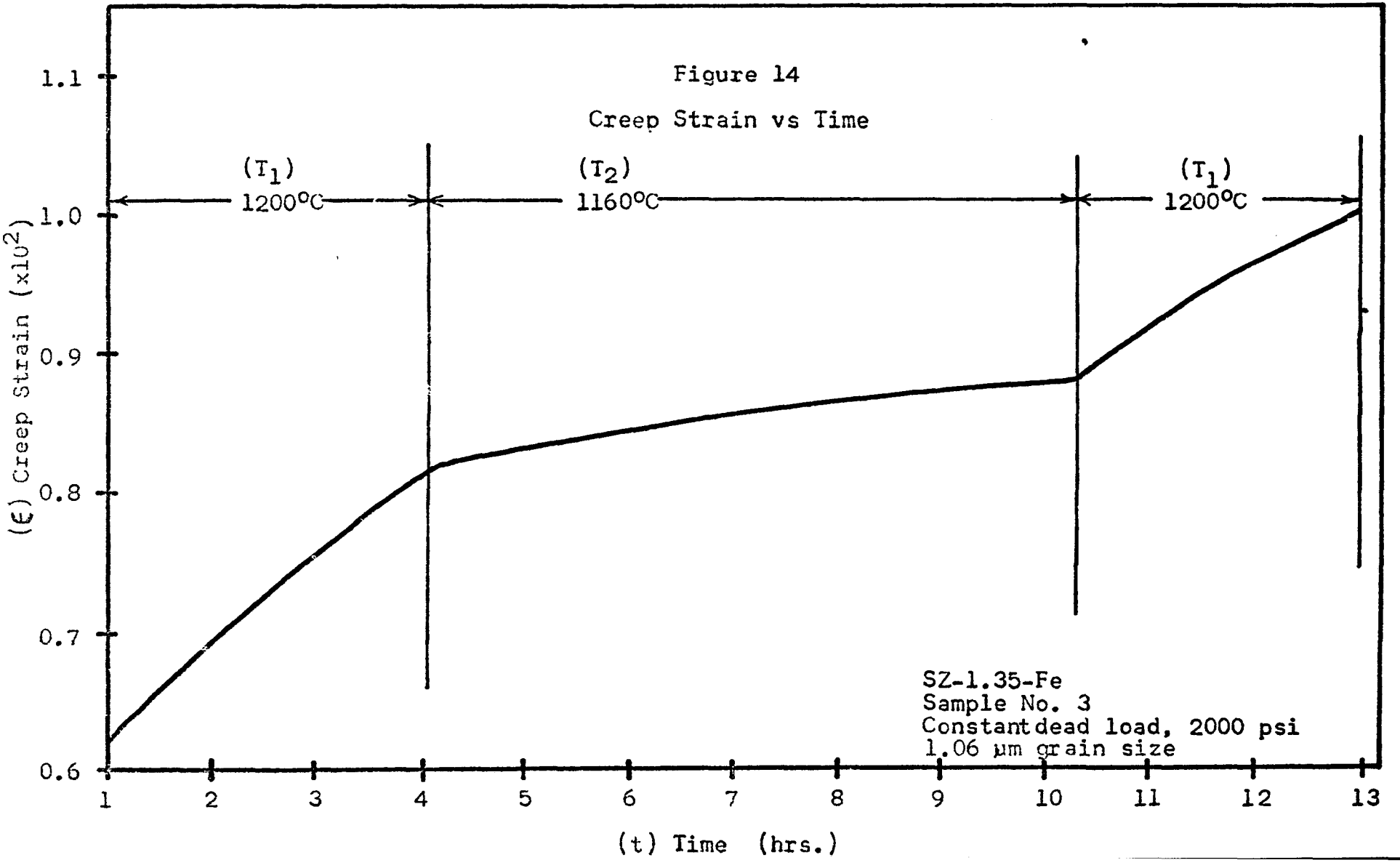

Figure 15

Log Creep Rate vs Creep Strain

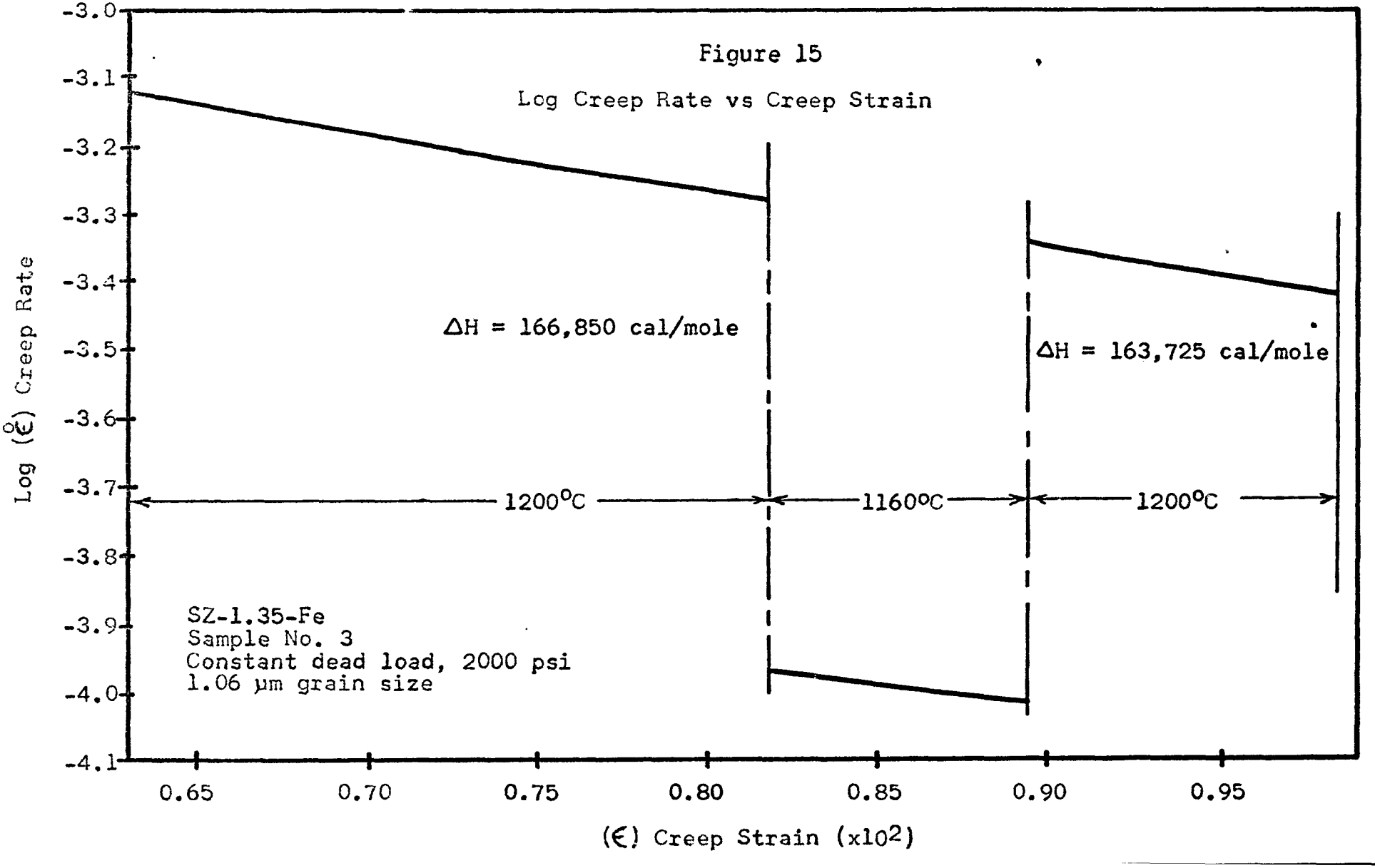

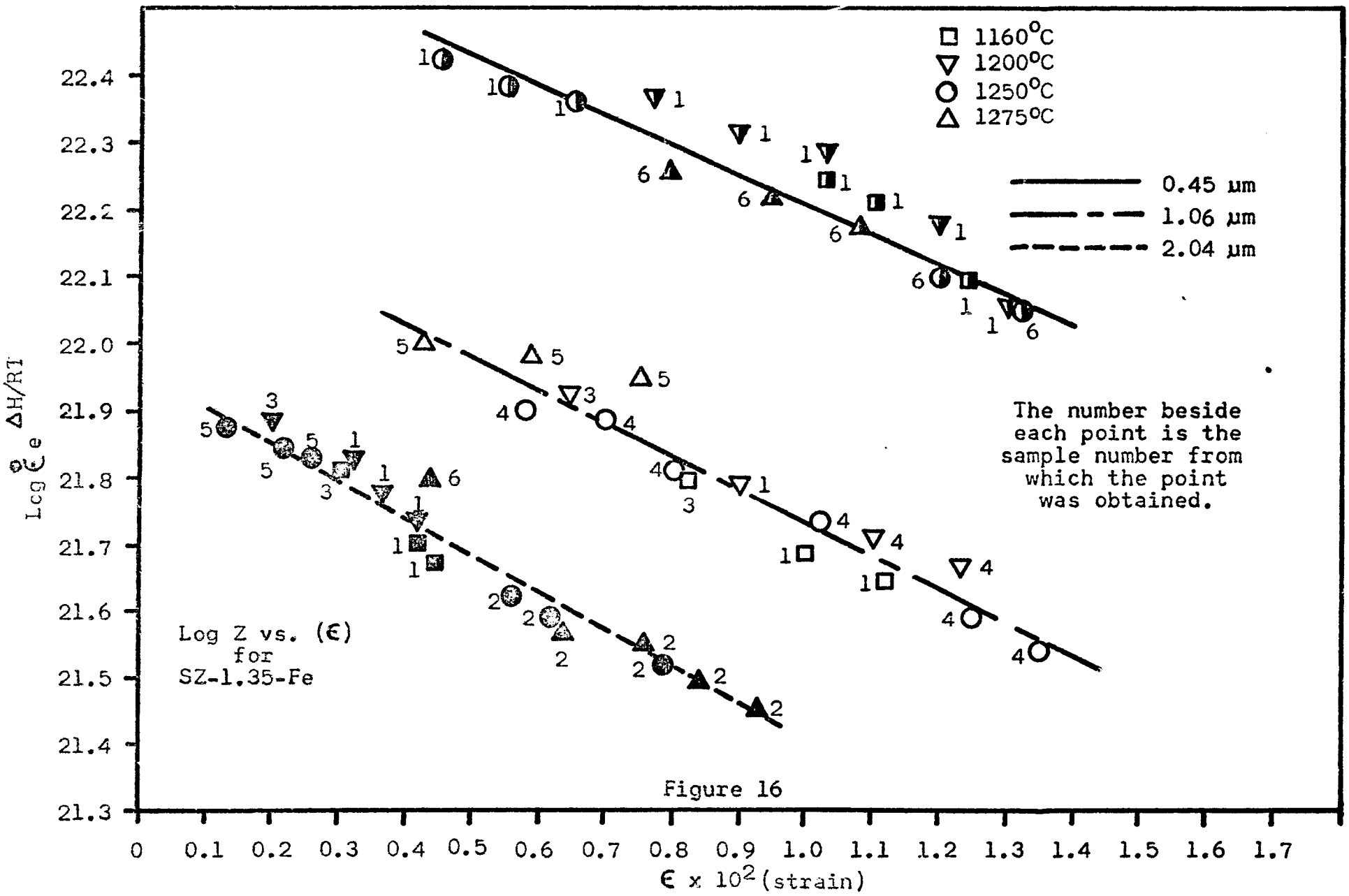
□ 1160°C
▽ 1200°C
○ 1250°C
△ 1275°C
0.45 μm
1.06 μm
2.04 μm
The number beside each point is the sample number from which the point was obtained.
Log Z vs. (ϵ) for SZ-1.35-Fe
Log ϵ²e ΔH/RT
ϵ x 10² (strain)
22.4
22.3
22.2
22.1
22.0
21.9
21.8
21.7
21.6
21.5
21.4
21.3
0
0.1
0.2
0.3
0.4
0.5
0.6
0.7
0.8
0.9
1.0
1.1
1.2
1.3
1.4
1.5
1.6
1.7

Figure 16

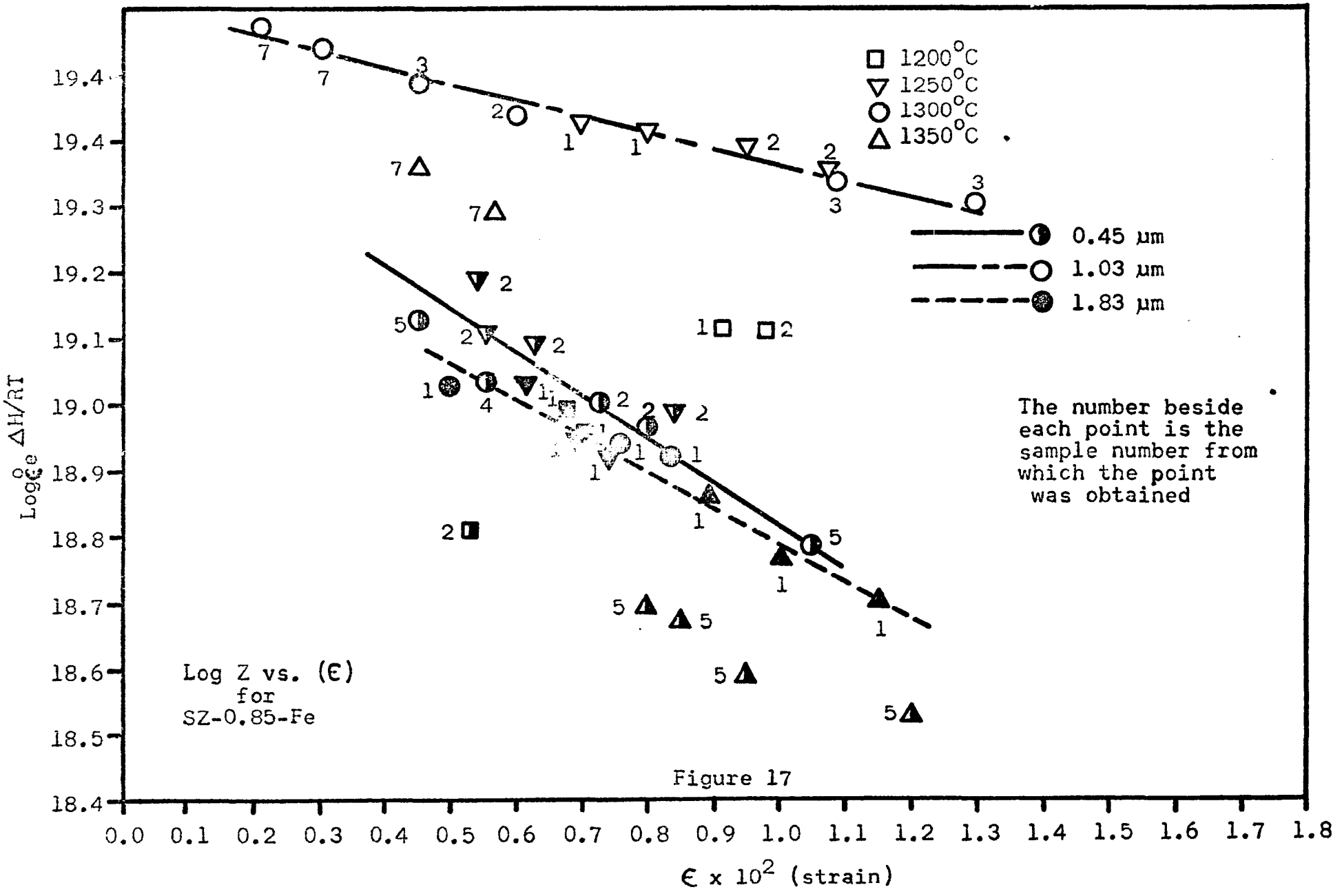
1200°C
1250°C
1300°C
1350°C
0.45 μm
1.03 μm
1.83 μm
The number beside each point is the sample number from which the point was obtained
Log Z vs. (ϵ) for SZ-0.85-Fe
Log$_e^0$ ΔH/RT
ϵ x 10^2 (strain)
19.4
19.4
19.3
19.2
19.1
19.0
18.9
18.8
18.7
18.6
18.5
18.4
0.0 0.1 0.2 0.3 0.4 0.5 0.6 0.7 0.8 0.9 1.0 1.1 1.2 1.3 1.4 1.5 1.6 1.7 1.8

Figure 17

Figure 18

$\text{Log } \dot{\epsilon}$ vs. 1/T

(average for all samples tested at 2000 psi.)

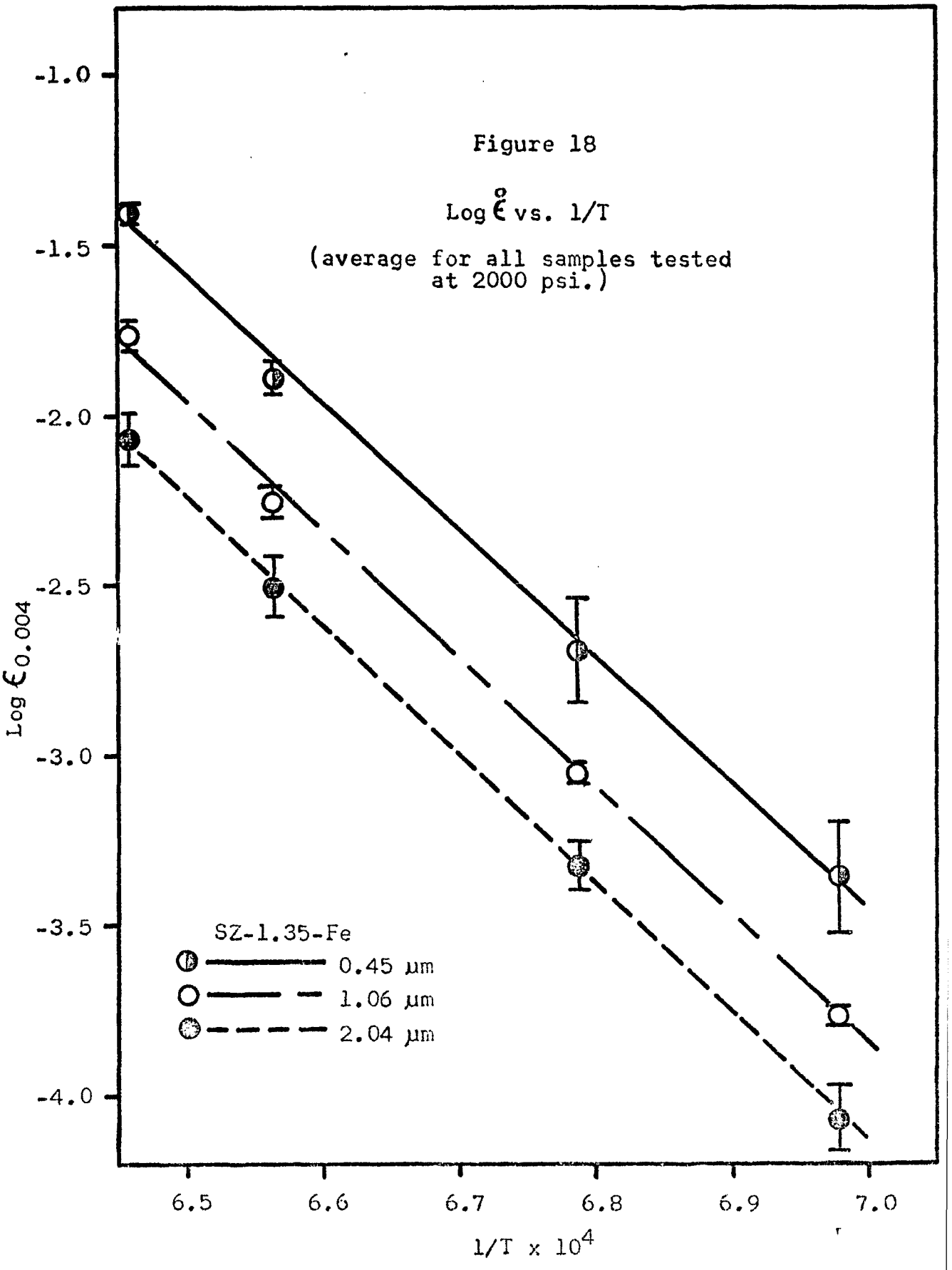

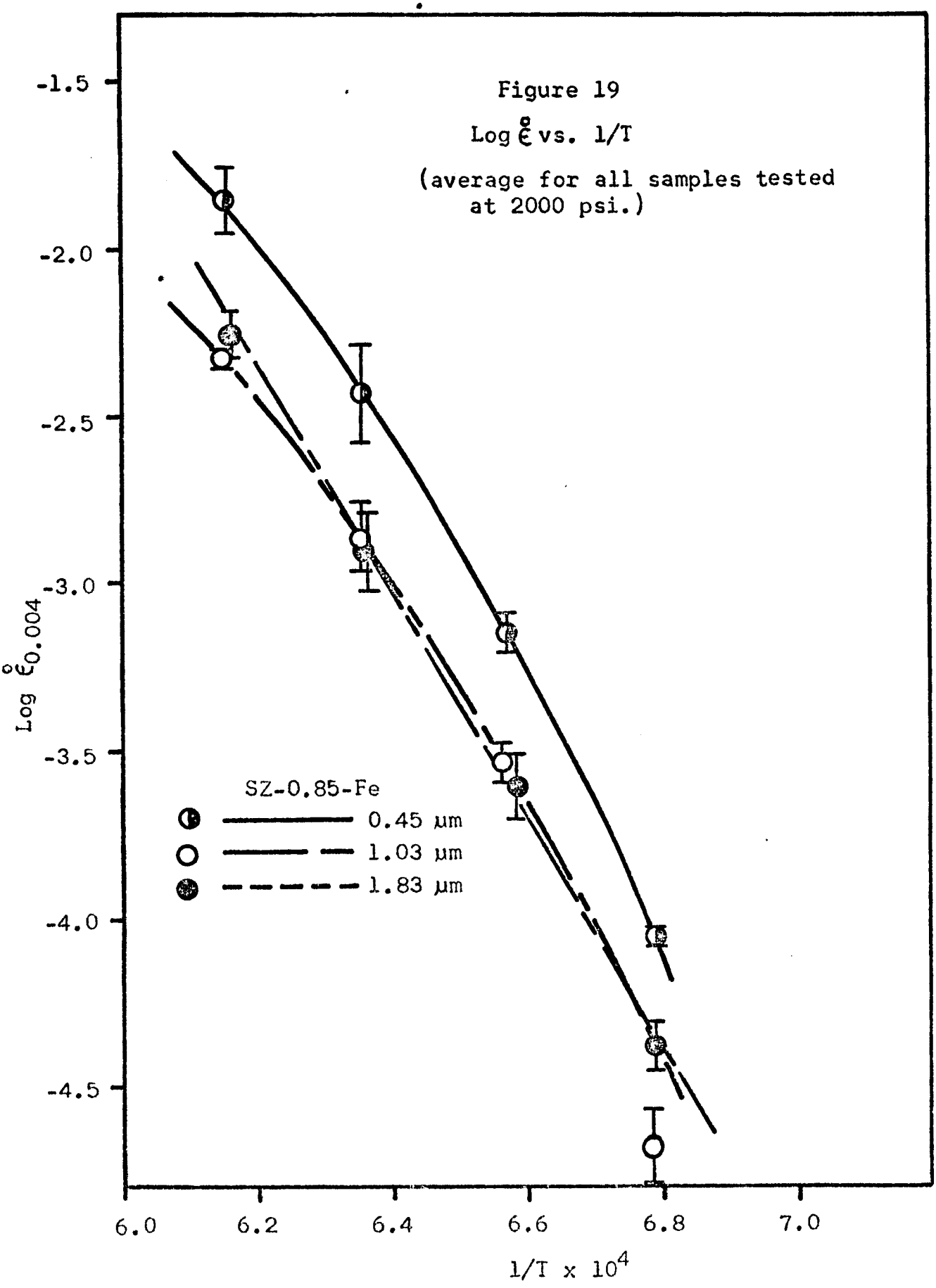

Figure 19

Log $\dot{\epsilon}$ vs. 1/T

(average for all samples tested at 2000 psi.)

Figure 20

Log ($\dot{\epsilon}_{0.004}$) vs. Log (σ)

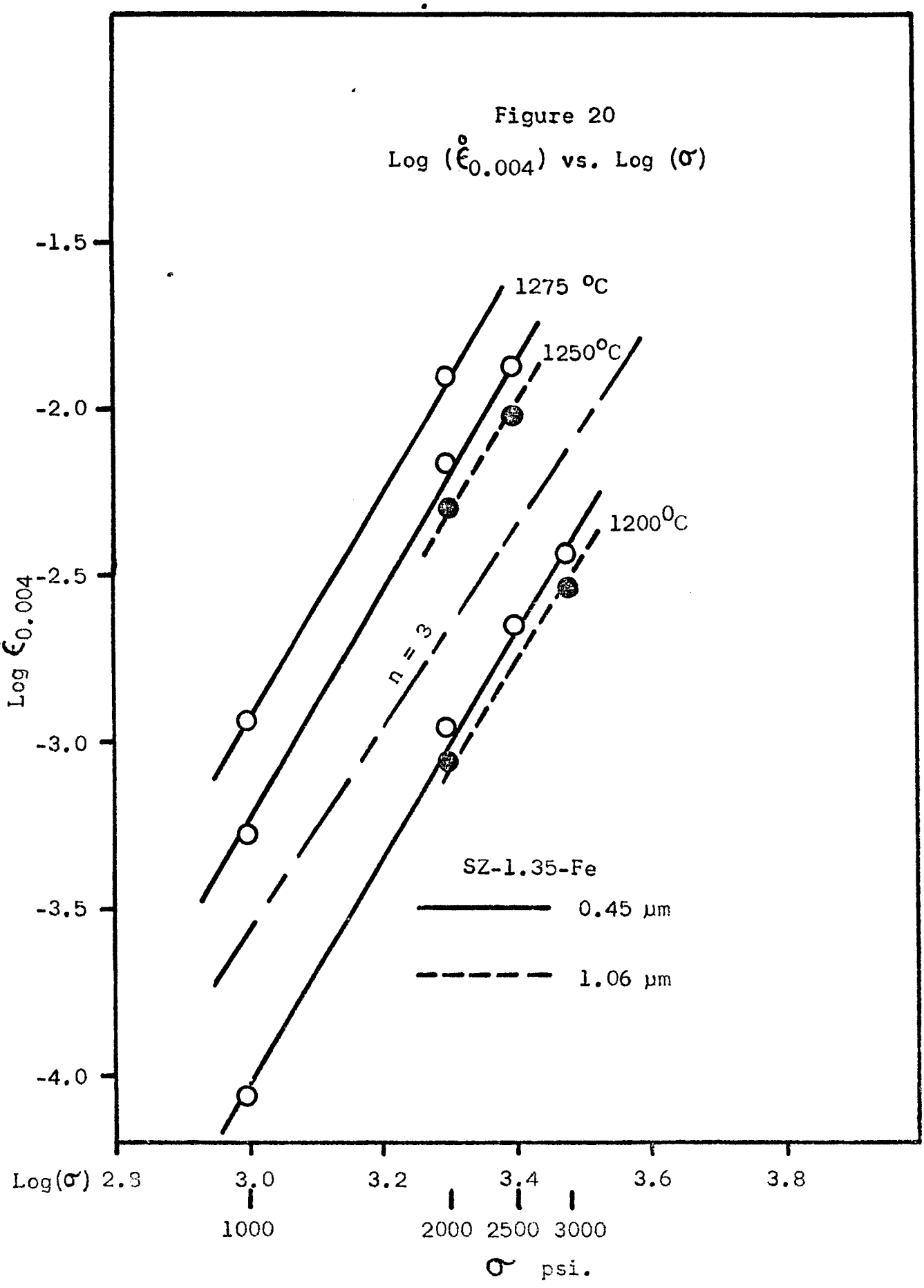

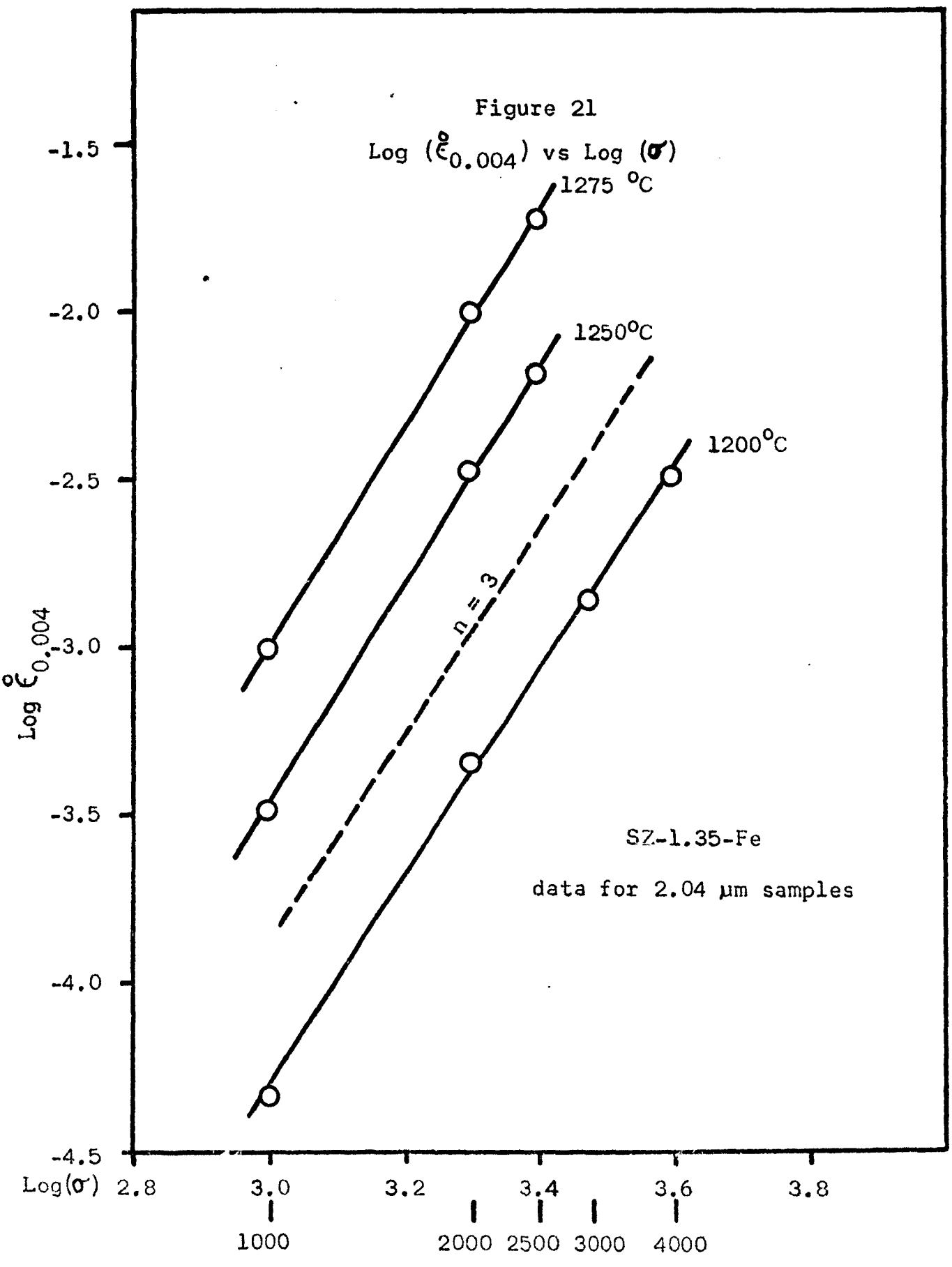
Figure 21
Log ($\dot{\epsilon}_{0.004}$) vs Log (σ)
1275 °C
1250°C
1200°C
n = 3
SZ-1.35-Fe
data for 2.04 μm samples
Log $\dot{\epsilon}_{0.004}$
-1.5
-2.0
-2.5
-3.0
-3.5
-4.0
-4.5
Log(σ) 2.8 3.0 3.2 3.4 3.6 3.8
1000 2000 2500 3000 4000
σ psi.

Figure 22

Log ($\dot{\epsilon}^{\circ}_{0.004}$) vs. Log ($\sigma$)

SZ-0.85-Fe

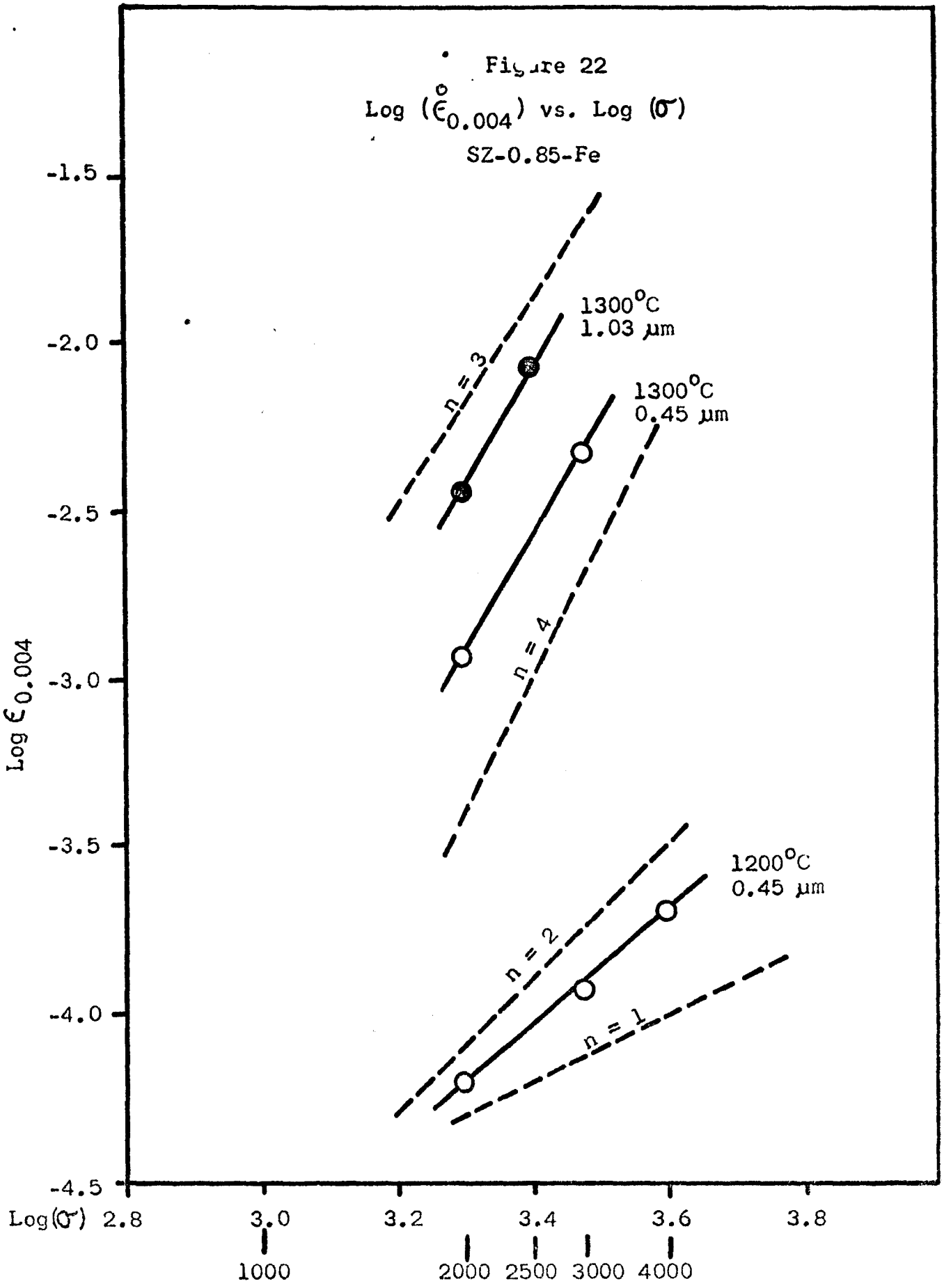

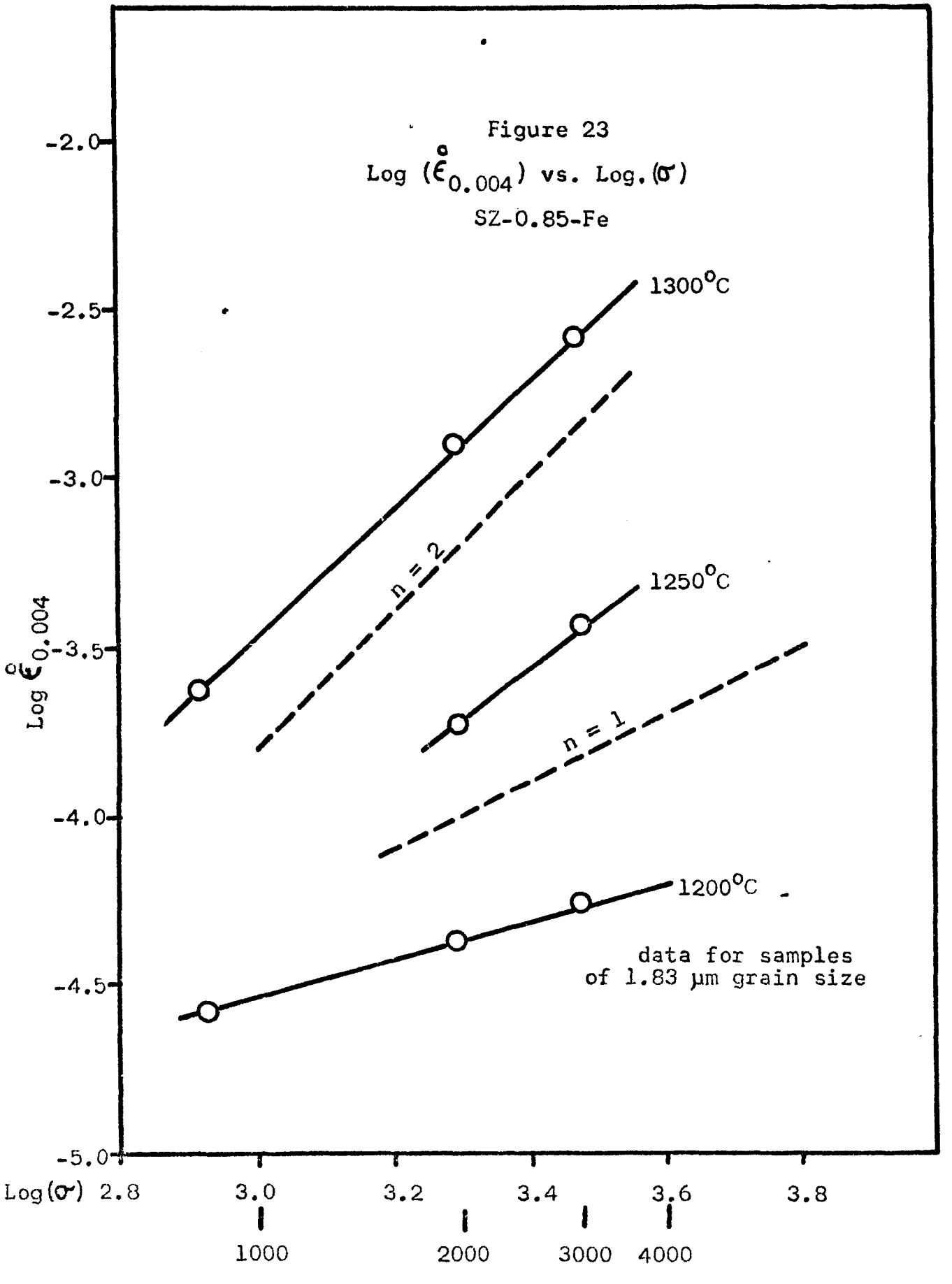

Figure 23

Log ($\dot{\epsilon}_{0.004}$) vs. Log.(σ)

SZ-0.85-Fe

Figure 24

$\text{Log}(\dot{\epsilon}_{0.004})$ vs. 1/T

SZ-1.35-Fe

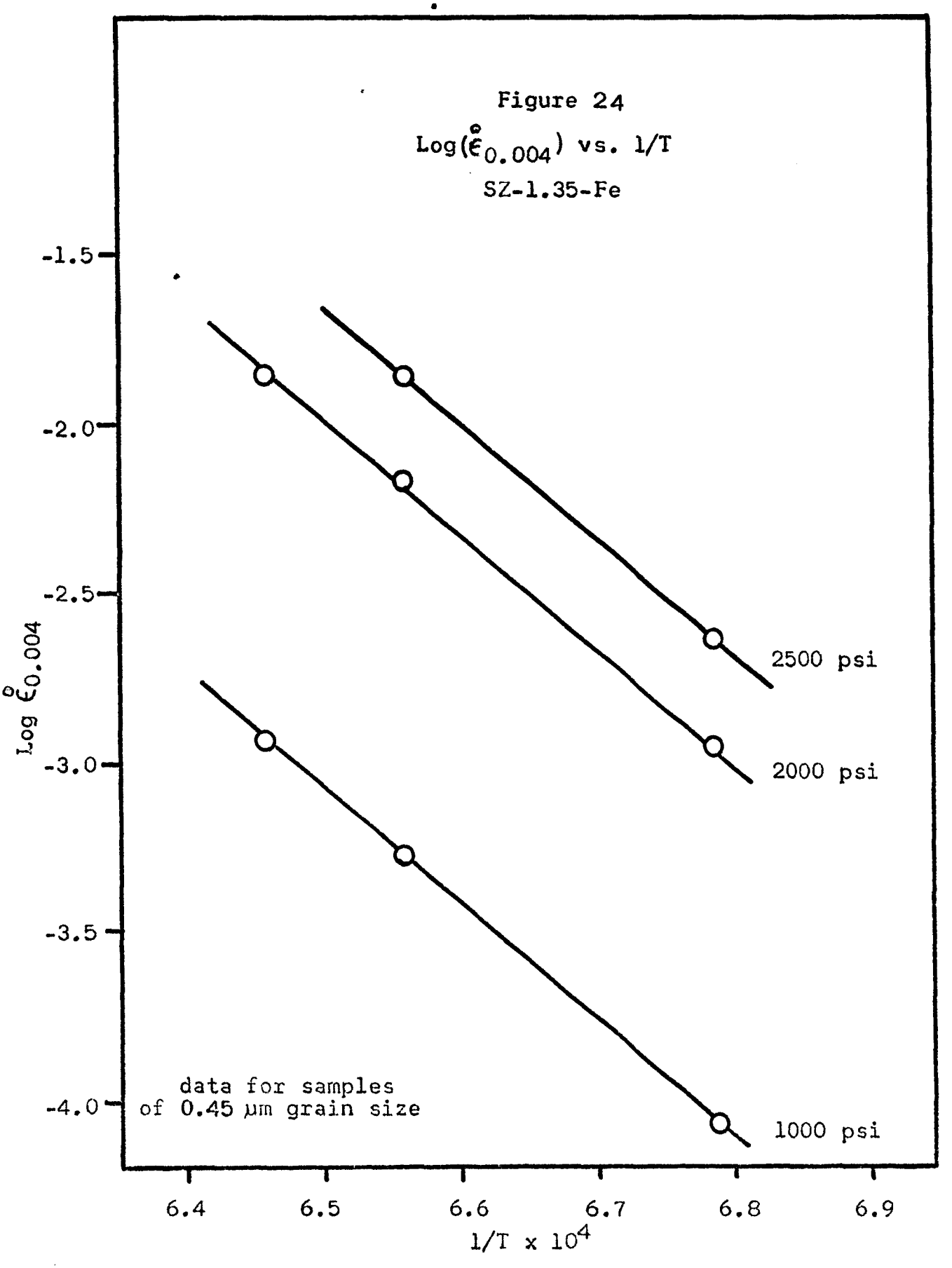

Figure 25

Log ($\dot{\epsilon}_{0.004}$) vs. 1/T

SZ-1.35-Fe

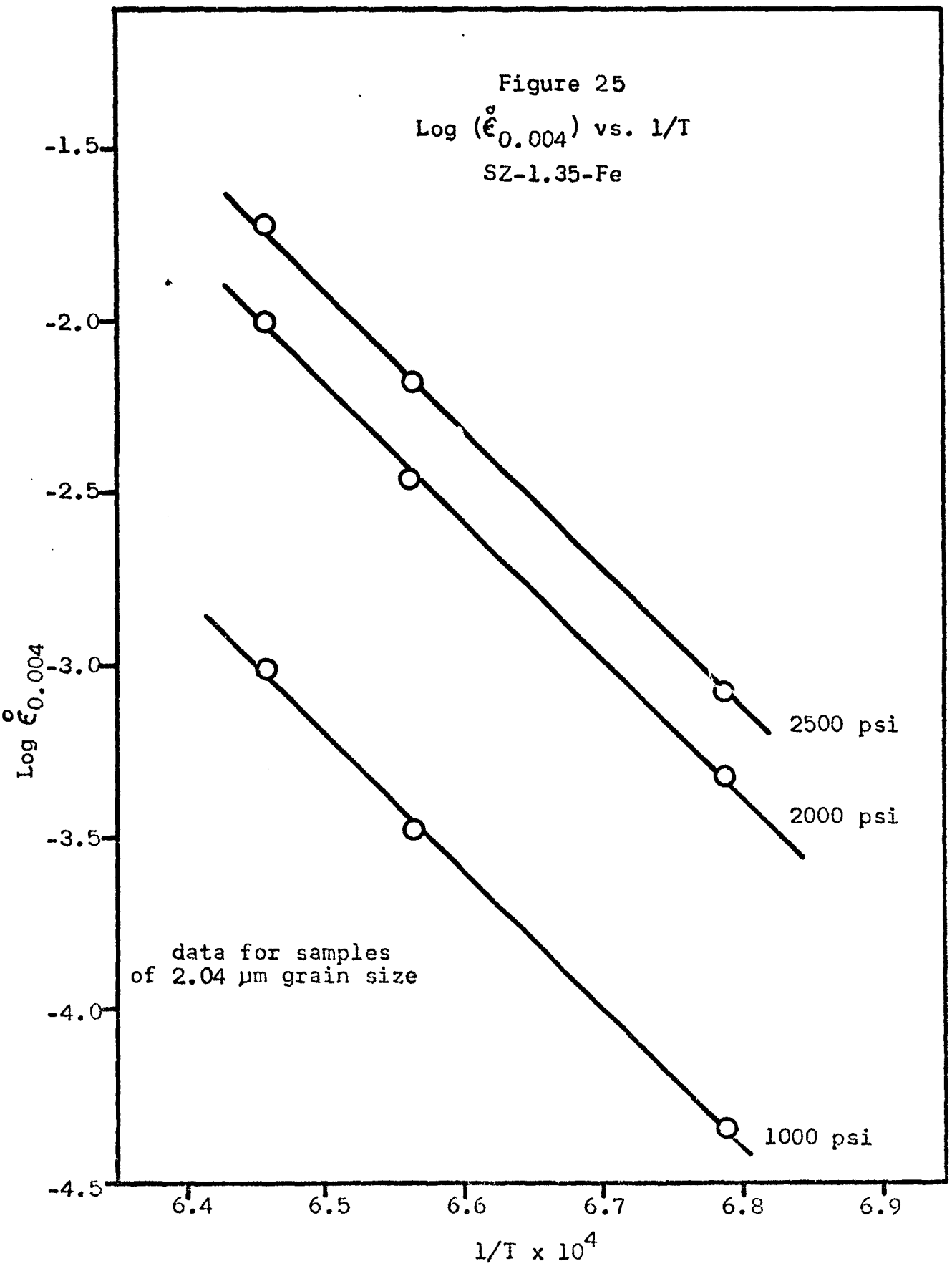

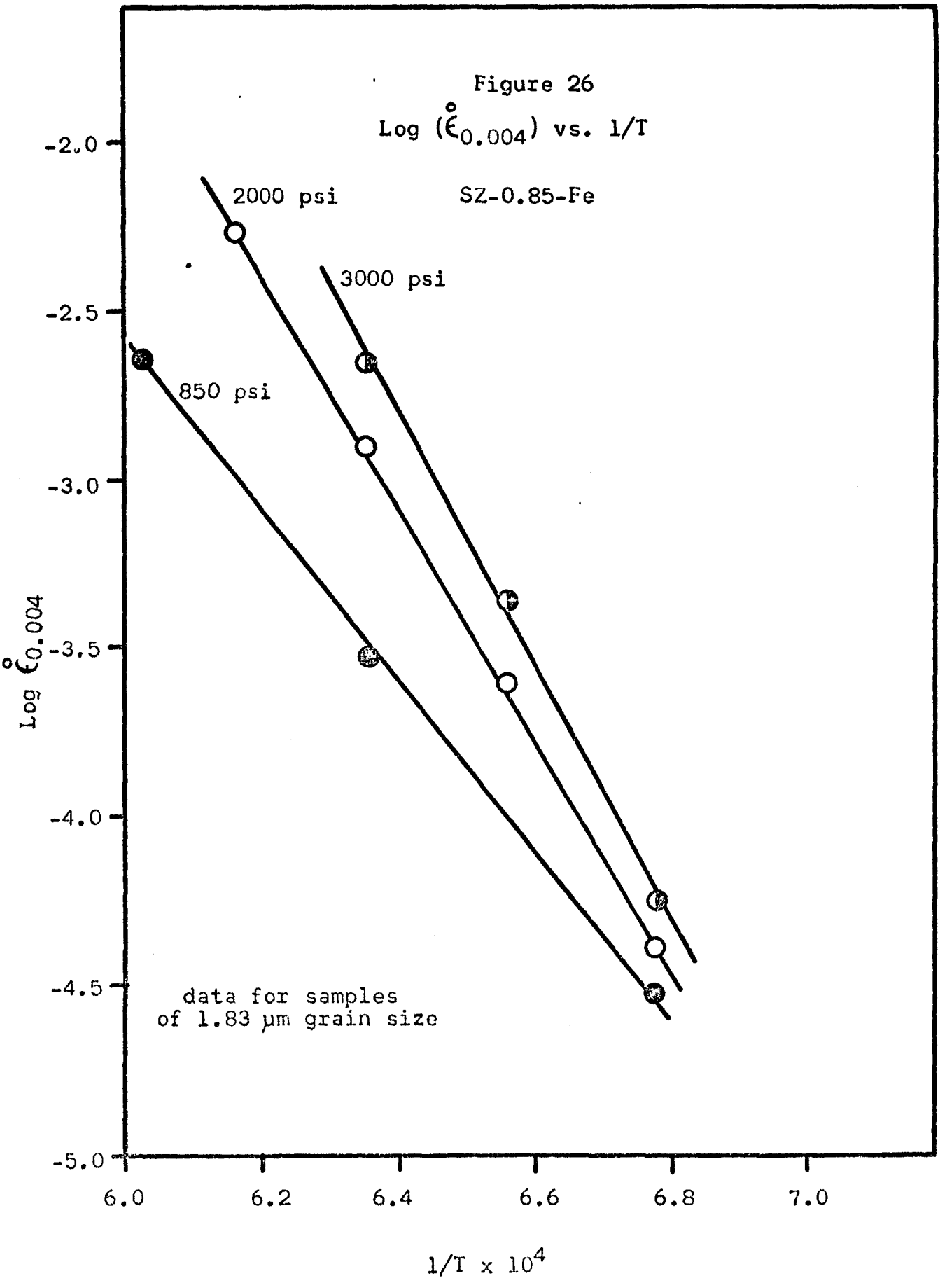
Figure 26
Log ($\dot{\epsilon}_{0.004}$) vs. 1/T
SZ-0.85-Fe
2000 psi
3000 psi
850 psi
data for samples
of 1.83 μm grain size
Log $\dot{\epsilon}_{0.004}$
-2.0
-2.5
-3.0
-3.5
-4.0
-4.5
-5.0
6.0
6.2
6.4
6.6
6.8
7.0
1/T x 10^4

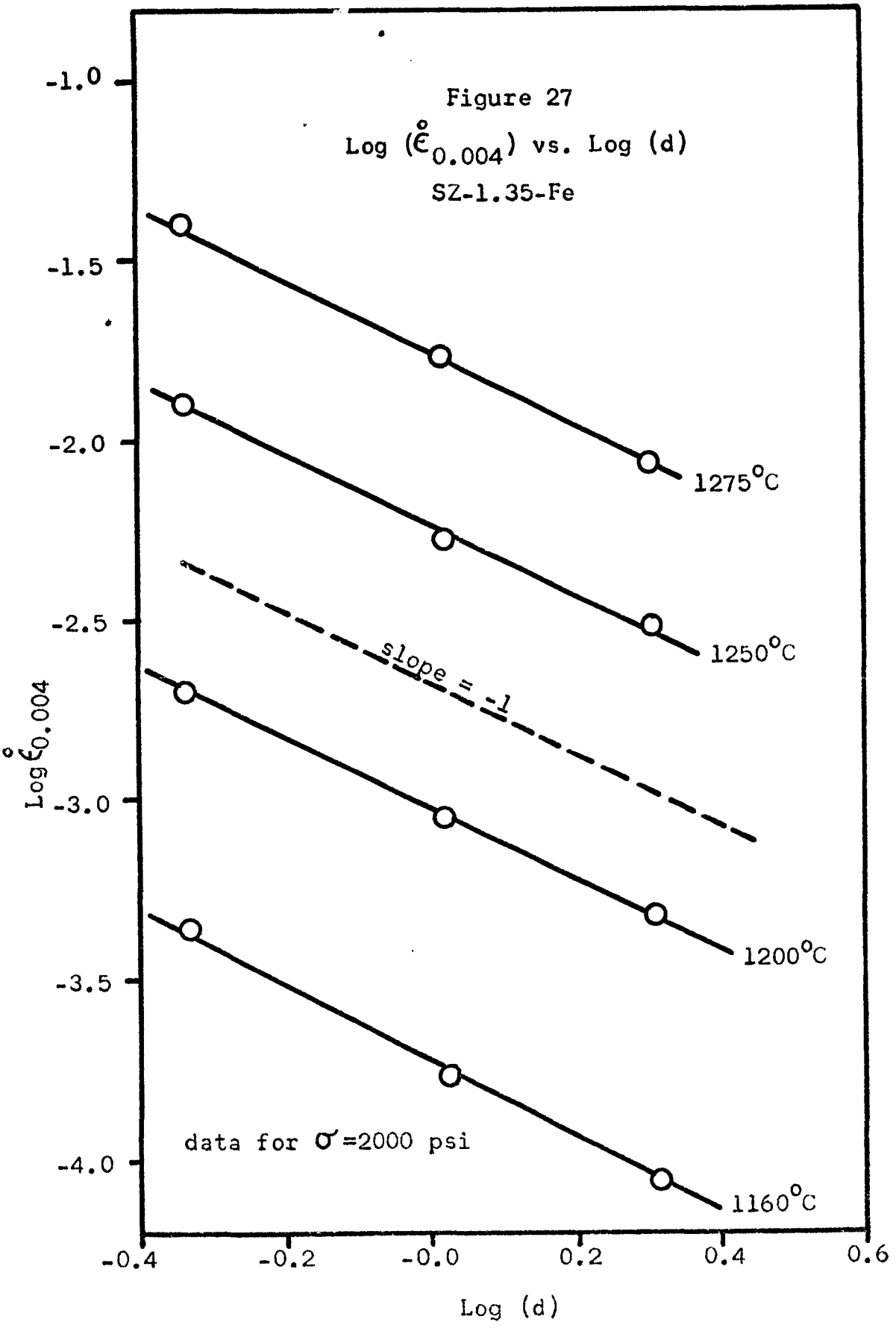
Figure 27
Log ($\dot{\epsilon}_{0.004}$) vs. Log (d)
SZ-1.35-Fe
-1.0
-1.5
-2.0
-2.5
-3.0
-3.5
-4.0
Log $\dot{\epsilon}_{0.004}$
1275°C
1250°C
slope = -1
1200°C
1160°C
data for σ=2000 psi
-0.4
-0.2
-0.0
0.2
0.4
0.6
Log (d)

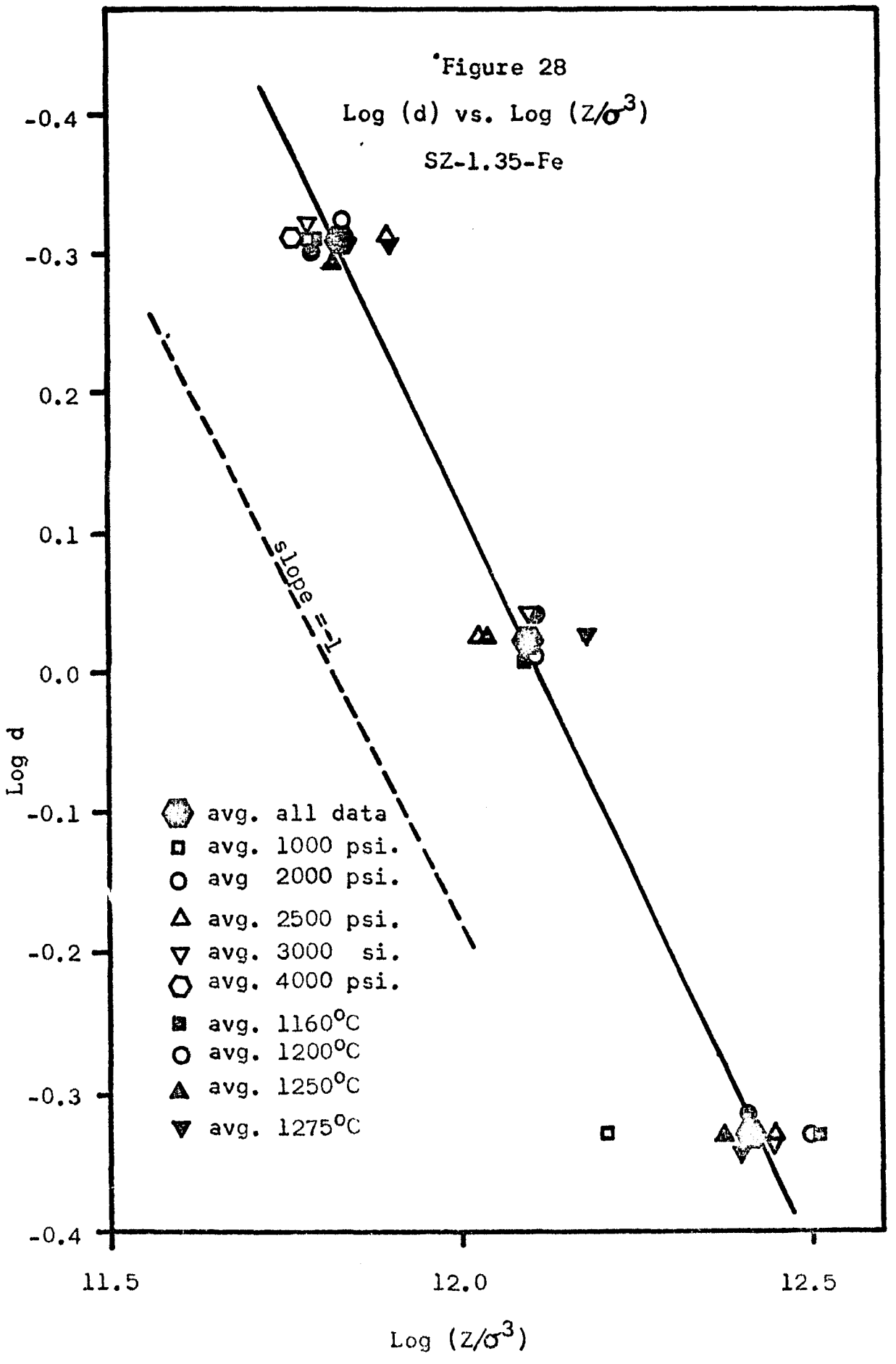
Figure 28
Log (d) vs. Log (Z/σ^3)
SZ-1.35-Fe
slope = -1
avg. all data
avg. 1000 psi.
avg 2000 psi.
avg. 2500 psi.
avg. 3000 si.
avg. 4000 psi.
avg. 1160°C
avg. 1200°C
avg. 1250°C
avg. 1275°C
Log d
-0.4
-0.3
0.2
0.1
0.0
-0.1
-0.2
-0.3
-0.4
11.5
12.0
12.5
Log (Z/σ^3)

Figure 29

Log (σ^3/d) vs. Log (Z)

SZ-1.35-Fe

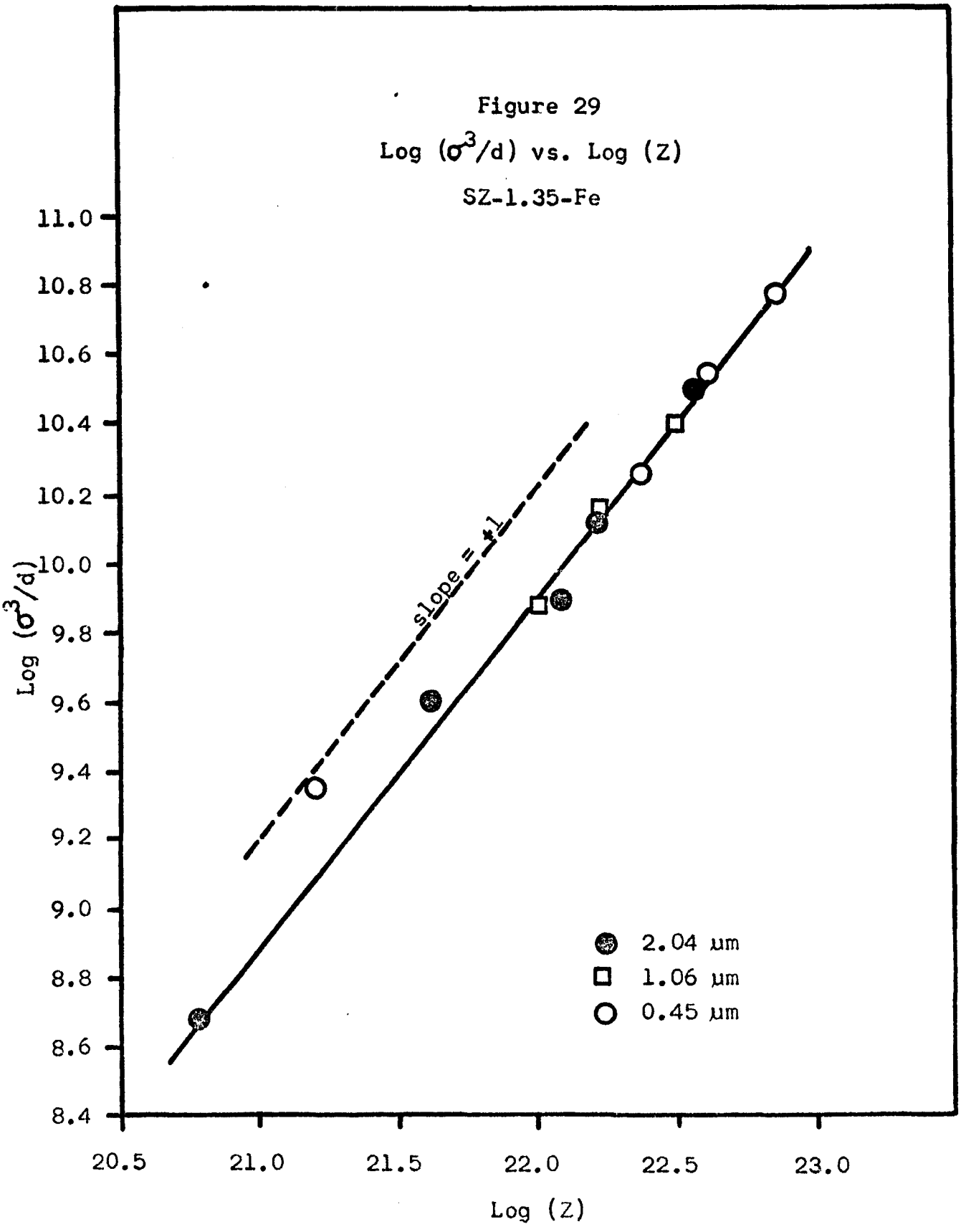

TABLE V

Activation Energies

for SZ-1.35-Fe

Grain Size of Sample	Temp. Range °C	Differential Method cal/mole	Standard Deviation cal/mole	Temp. Range °C	Arrhenius Method cal/mole
0.45 μm	1160-1200	178,900 (5)*	6,300	1160-1275	169,700
	1200-1250	171,000 (4)	6,050		
	1250-1275	169,300 (3)	3,675		
1.06 μm	1160-1200	169,850 (6)	3,675	1160-1275	169,700
	1200-1250	168,875 (6)	11,500		
	1250-1275	160,525 (5)	12,300		
2.04 μm	1160-1200	169,950 (6)	4,600	1160-1275	169,700
	1200-1250	169,300 (6)	6,175		
	1250-1275	161,650 (5)	2,360		

* The number in the ( ) indicates the number of determinations which were averaged to obtain the value for ΔH, shown.

TABLE VI

Activation Energies

for SZ-0.85-Fe

Grain Size of Sample	Temp. Range °C	Differential Method cal/mole	Standard Deviation cal/mole	Temp. Range °C	Arrhenius Method cal/mole
0.45 μm	1200-1250	213,200 (4)*	16,500	1200-1350	not a straight line
	1250-1300	159,200 (5)	8,500		
	1300-1350	113,500 (4)	9,800		
1.03 μm	1200-1250	214,675 (4)	5,500	1200-1350	not a straight line
	1250-1300	153,000 (5)	3,550		
	1300-1350	118,725 (4)	5,800		
1.83 μm	1200-1250	161,025 (3)	2,850	1200-1350	156,100
	1250-1300	159,675 (4)	9,160		
	1300-1350	155,900 (4)	7,640		

* The number in the ( ) indicates the number of determinations which were averaged to obtain the value for ΔH shown.

(4) Estimation of Errors

In the following the probable errors in the experimental measurements are considered and used in the determination of the probable errors in the calculated values of stress, strain, strain rate, activation energy, stress factor (n), and structure factor exponent. The calculated probable errors are then compared, where possible, to the standard deviations obtained in the statistical analysis of the results (i.e. for ΔH).

(a) Stress (σ_t)

The maximum tensile stress on the outer fibers of the creep specimen is given by Equation (24), viz,

$$\sigma_t = \frac{3Fa}{wh^2} ,$$

from which it follows,

$$\frac{d\sigma_t}{\sigma_t} = \pm\left(\frac{dF}{F} + \frac{da}{a} + \frac{2dh}{h} + \frac{dw}{w}\right).$$

It is estimated that the probable errors in measuring the load F, and the specimen dimensions a, , and w are in each case $\pm$0.5%, which gives $d\sigma_t/\sigma_t$=2.5%. The actual error in stress is undoubtedly considerably larger, due to the uncertainty in the validity of Equation (24) for stress in systems involving plastic deformation. The 2.5% is a measurement in precision and is assumed reasonable.

(b) Strain (ϵ)

Strain is related to the deflection (δ) using the simplified equation,

$$\epsilon = 4h\delta,$$

from which it follows that,

$$\frac{d\epsilon}{\epsilon} = \frac{dh}{h} + \frac{d\delta}{\delta} .$$

It is estimated that the probable error in determining δ is $\pm 0.5\%$, so that the probable error in strain determination is 1.0%.

(c) Strain Rate ($\dot{\epsilon}$)

Strain rated are calculated from the slopes of the ϵ vs t curves (e.g. Figure 14). The measurement of time is essentially exact and all of the uncertainty is in the determination of ϵ. Thus

$$\dot{\epsilon} = \Delta\epsilon/\Delta t ,$$

and

$$d\dot{\epsilon}/\dot{\epsilon} = 2d\epsilon/\Delta\epsilon .$$

The probable error is thus very sensitive to the strain increment used in the determination of $\dot{\epsilon}$, which varied from 0.03×10^{-2} in/in to 0.4×10^{-2} in/in depending on the temperature. Since $d\epsilon = 1.0\%\epsilon$ (Section b), the probable error in the strain rate determination varied approximately from 2% (high temperatures) to 30% (low temperatures), with the mean probable error at approximately 15%. It is noted that the actual error in determining strain (due to the measurement of δ) is probably better than the 1% indicated, for there is a continuous

trace to follow. The author believes the trace of the strain-time curve can be interpolated to obtain a deflection accuracy greater than that assumed.

(d) Activation Energy (ΔH)

The activation energy is determined by the Dorn technique using the equation

$$\Delta H = \frac{R \ln (\dot{\epsilon}_1/\dot{\epsilon}_2)}{(1/T_2 - 1/T_1)} ,$$

from which it follows that

$$\frac{d(\Delta H)}{\Delta H} = \frac{2d\epsilon}{\epsilon} \frac{1}{\ln \dot{\epsilon}_1/\dot{\epsilon}_2} + \frac{2dT}{\Delta T} ,$$

where $\Delta T = T_2 - T_1$, and $(T + \Delta T)/(T\Delta T) \sim 1/\Delta T$. The probable error in ΔH is thus very sensitive to the error in temperature measurement and in particular to the temperature interval ΔT. For most creep runs $\Delta T \sim 40^{\circ}C$ and $\ln (\dot{\epsilon}_1/\dot{\epsilon}_2) \sim 2.0$ (See Figure 15), which gives a probable error of $\pm 12\%$ for ΔH (precision in T is taken as $\pm 2^{\circ}C$). The standard deviation based on a statistical analysis of the activation energy results varied from approximately $\pm 2\%$ to $\pm 7\%$ (See Table V), so that the temperature measurement was probably somewhat better than $\pm 2^{\circ}C$ (assuming all errors are random). A probable error of $\pm 7\%$ or less is also consistent with the standard deviation for the activation energies obtained from the Arrhenius treatment of the rate data shown in Figure 18.

Thus the standard deviation of ±10,000 calories/mole seems to represent a reasonable estimate for the error in activation energy.

(e) Stress Factor (n)

The values of n were determined from the plots of $\log \dot{\epsilon}_{0.004}$ vs $\log \sigma$ for various temperatures. Thus

$$n = \frac{\Delta \ln \dot{\epsilon}}{\Delta \ln \sigma} ,$$

from which it follows that,

$$\frac{dn}{n} = \frac{2d\dot{\epsilon}}{\dot{\epsilon}} \cdot \frac{1}{\Delta \ln \dot{\epsilon}} + \frac{2d\sigma}{\sigma} \cdot \frac{1}{\Delta \ln \sigma} .$$

From Figure 20 the mean values for $\Delta \ln \dot{\epsilon}$ and $\Delta \ln \sigma$ are respectively approximately 3 and 1, so that the mean probable error $dn/n \sim 15\%$. The n values over the grain size range 0.45 μm to 2.04 μm determined from the best fit lines varied from 3.1 to 3.3 and this variation (which may be due to grain size dependency of n) is within the limits of experimental error, and thus cannot be considered significant.

(f) Structure Factor Exponent

The dependency of strain rate on grain size is given by the following general equation,

$$\dot{\epsilon} = kd^{\alpha}$$

and α is thus the slope of the plot of $\ln \dot{\epsilon}_{0.004}$ vs ln d, i.e.,

$$\alpha = \frac{\Delta \ln \dot{\epsilon}}{\Delta \ln d} ,$$

from which,

$$\frac{d\sigma}{\sigma} = \frac{2d\dot{\epsilon}}{\dot{\epsilon}} \cdot \frac{1}{\Delta \ln \dot{\epsilon}} + \frac{2dd}{d} \cdot \frac{1}{\Delta \ln d} .$$

The grain sizes were determined using the intercept method on electron micrographs, for which the probable error was estimated at ±5%. The mean values for $\Delta \ln \dot{\epsilon}$ and $\Delta \ln d$ were respectively 1.6 and 1.6 (See Figure 27), which gives $d\sigma/\sigma \sim 15\%$. The values obtained for the structure factor exponent from the best fit curves for the various temperatures were all within ±10% of unity which is good agreement with the estimated probable error of ±15%.

In summary, the estimated probable errors in the values calculated for the stress factor (n) and the structure factor exponent are ±15%. The estimated probable error in the activation energy values is approximately ±12%, however, the mean standard deviation is approximately ±7%(±10 kcal/mole), which indicates that the temperature determinations were more precise than ±2°C.

V DISCUSSION OF RESULTS

The investigation of creep in $SrZrO_3$ consisted of examining the effects on creep rate of the creep variables: temperature, stress and grain size, for two levels of iron (Fe_2O_3) additions. The samples with the higher Fe_2O_3 content (1.35 wt. %, designated SZ-1.35-Fe) were dense and homogeneous (99% of theoretical density), and provided consistent and meaningful data. Consequently, most of the discussion will be directed to the creep results and mechanism related to this material. The samples with the lower concentration of Fe_2O_3 (0.85 wt. %, designated SZ-0.85-Fe) differed in porosity by as much as 10% for different grain sizes (firing times). The creep results for these samples showed considerable scatter (see Figure 19, Table VI), which is evidently related to the high porosity, and it was not possible to systematically characterize this material.

A. SZ-1.35-Fe

(1) Activation Energy (ΔH)

The activation energies obtained using the differential technique (Dorn)[63] did not vary significantly over the temperature range investigated, with the mean value at 169 $\pm$ 10 kcal/mole. Since the difference

in ΔH, when compared for two temperature ranges, is less than the sum of the standard deviations at these temperatures (see Table V), it may be assumed that the creep mechanism remained relatively unaltered over the entire temperature range. The activation energy is also relatively insensitive to grain size, and the stress level over the ranges these parameters were investigated (cf. Figures 18, 24, and 25), for the variations in slopes for each plot is not considered significant (the standard deviation for creep rate is indicated in Figure 18 by the vertical lines).

It is customary to compare the activation energy for creep against that reported for diffusion of the various ionic species in the ceramic, and if there is agreement this is taken as an indication that creep is a diffusion controlled process (viscous flow). To the author's knowledge there is no published diffusion data for $SrZrO_3$, and therefore the creep mechanism in this investigation must be inferred largely from the functional dependence of creep rate upon the variables of stress and structure factor (grain size). Hensler and Cullen[30] suggested that this functional dependence was a more reliable means of indicating creep mechanism than activation energy, due to large discrepencies in the activation energies reported by

various authors (for MgO). It is noteworthy that Tagai and Zisner[28] attempted to associate high activation energy (160-185 kcal/mole) creep in ceramics with nonviscous slip (dislocation) mechanisms, and low activation energy (90-130 kcal/mole) creep with diffusion mechanisms (viscous). For example, for creep in coarse grained alumina, ΔH = 185 kcal/mole[34] when $\dot{\epsilon} \propto \sigma^4$ (nonviscous creep). Also, Cummerow[26] states that slip occurs during creep in single crystal MgO for which the relatively high value of ΔH = 166 kcal/mole is observed. Thus, simply on the basis of the high activation energy of 169 kcal/mole obtained in the present investigation, it might be inferred that creep in $SrZrO_3$ is a nonviscous, dislocation-type process.

(2) Effect of Stress (σ)

The dependence of creep rate upon stress for the SZ-1.35-Fe specimens is of the form $\dot{\epsilon} \propto \sigma^n$, where $n \simeq 3$, and varies from the value of 3.1 for the 2.04 μm specimens increasing to 3.3 for the 0.45 μm specimens (cf Figures 20 and 21). A value of 3 for the stress factor is generally accepted as evidence that creep is a nonviscous process, with dislocation climb as the limiting stage[17]. Viscous creep (i.e. $\dot{\epsilon} \propto \sigma$) or deformation results from the stress directed diffusion

of vacancies, either through the crystal lattice (Nabarro-Herring[6,7]) or through grain boundaries (Coble[8]), and is generally accompanied by a change in grain size and shape. Although these diffusion processes may contribute to plastic or nonviscous deformation on · local scale as shown by Gifkins[12-14], the unequivocal value of 3 for the stress factor is strong evidence that creep occurs by a nonviscous, slip process[17].

(3) Effect of Grain Size (d)

In the various creep theories that have been developed, the grain size dependence of the creep rate may be one of the following: $\dot{\epsilon} \propto 1/d$, $\dot{\epsilon} \propto 1/d^2$, or $\dot{\epsilon} \propto 1/d^3$. The $1/d^2$ dependence of the creep rate is related to the stress directed volume diffusion of vacancies as shown by Nabarro and Herring. The $1/d^3$ dependence has been associated with a grain boundary diffusion mechanism (Coble). Both theories are based on viscous flow models, where creep rate is directly proportional to stress. A $1/d$ dependence of creep rate, when coupled with a $\dot{\epsilon} \propto \sigma^3$ relationship may be considered as further evidence that the deformation process is a nonviscous one, based on dislocation climb as the controlling stage (Weertman[17]). Garofalo[19],

in an attempt to account for grain size effects in the Weertman model, developed an expression for the creep rate which may be reduced to the form $\dot{\epsilon} \propto \sigma^n/d$. Gifkins[12], has shown that a 1/d dependence may also result from diffusion in local areas where stress during shear is increased due to protrusions in grain boundaries. However, in Gifkin's model a $\dot{\epsilon} \propto \sigma$ relationship is required.

For the SZ-1.35-Fe specimens a 1/d dependence of creep rate is obtained for the range of grain sizes studied. Figure 27 shows that the plot of log $\dot{\epsilon}_{0.004}$ (creep rate normalized to a strain level of 0.004) vs. log (d) for a 2000 psi stress level gives a slope of (-1) for four different temperatures over the grain size range of 0.45 μm to 1.83 μm. Figure 28 shows that the plot of log Z/σ^3 (i.e. creep rate normalized for temperature and stress) vs log (d) for all the data obtained over the ranges of temperature (1160°C-1275°C), and stress (1000 - 4000 psi) is a straight line, for which the slope is clearly (-1). Thus the relationship $\dot{\epsilon} \propto 1/d$ is definitely and conclusively established.

The rate dependence upon stress and grain size may be summarized in the relationship $\dot{\epsilon} \propto \sigma^3/d$, and

if this relationship is valid for the creep process in $SrZrO_3$, then an all inclusive plot of log (σ^3/d) vs log (Z) for the data should give a straight line for which the slope is (+1). This is indeed the case, as shown in Figure 29. The magnitude of the activation energy, plus the dependence of creep rate upon the stress cubed and the reciprocal of the grain size indicates that the creep process in $SrZrO_3$ is most probably a nonviscous one involving dislocation movement and climb.

(4) Effect of Strain Level (ϵ) upon Strain Rate ($\dot{\epsilon}$)

The continuous decay of creep rate with creep strain was observed in all test samples (SZ-1.35-Fe and SZ-0.85-Fe, cf. Figures 15, 16, and 17). This phenomenon has also been reported for creep in polycrystalline MgO, Al_2O_3, and BeO. Tagai and Zisner[28] proposed that the decrease in creep rate, which is time dependent, is due to grain growth during testing. For $SrZrO_3$, however, no significant grain growth is expected at the test temperatures (1160°C-1275°C) because the observed growth at the firing temperature was quite small (< 0.1 μm/hr. at 1600°C). Furthermore, electron micrographs of the creep specimens taken before and after creep testing show no significant change in grain

size (see Figures 2, 3, 4, and 5, Appendix A). Terwilliger et. al.[31] conclude that the decay of creep rate with time for refractory oxides is too great to be explained in terms of grain growth, and attribute it to some sort of inherent time-hardening mechanism, which still remains to be explained. For $SrZrO_3$ it is suggested that the decay phenomenon might be associated with the decrease in the number of grains favorably oriented for the deformation process. This point is discussed in more detail later, when a creep mechanism for $SrZrO_3$ is proposed.

B. SZ-0.85-Fe

The samples of $SrZrO_3$ with low iron content (0.85 wt. % Fe_2O_3) contained varying amounts of porosity depending upon the firing time (and hence the grain size) as shown in Table III. The 0.45 μm and 1.03 μm grain size specimens differed in open porosity by nearly 10%, and both contained about 2½% closed porosity. Both Table VI and Figure 19 show that activation energy for these samples varies with temperature, and Figure 22 shows that the stress effect also varied with temperature. The apparent activation energy for these specimens decreased from about 215 kcal/mole over the temperature range 1200°C - 1250°C, to about 115 kcal/mole at 1300°C

- 1350°C, while the stress factor (n) increased from 1.9 to 3.4 over the same temperature range. The transient behavior of the creep parameters and the large variation over the temperature intervals (particularly for samples with high pore content) renders any attempt to characterize the creep behavior of the SZ-0.85-Fe material impractical and of doubtful value. The 1.83 μm grain size specimens of SZ-0.85-Fe contained 6% open porosity and only 1½% closed porosity with the result that activation energy was relatively independent of temperature (158 ± 5 kcal/mole). However, even for these specimens the stress factor (n) varied from 0.55 to 1.88 over the temperature range investigated (Figure 23). Furthermore, Figure 26 shows the relatively large variation of activation energy with stress level for this material. Thus even though there appeared to be a stabilization in the activation energy, the creep rate dependence on stress and grain size was not constant, which must be attributed to the porosity factor.

In order to ascertain if densification was occurring in the SZ-0.85-Fe specimens during creep testing, the density of the samples was measured before and after testing. It was found that for the 0.45 μm sample creep tested for 5½ hours over the temperature range

1300°C -1350°C, the density increased from 85.9% to 88.5% of theoretical, and closed porosity decreased from 1.41% to 0.46%. In another specimen of the same grain size, tested for 40 hours over the temperature interval 1200°C - 1300°C, density increased from 88.0% to 89.1% of theoretical and closed porosity decreased by 50% (1.25% to 0.7%). No change in density was observed for the SZ-1.35-Fe specimens, which were all approximately 99% of theoretical. This supports the hypothesis that the transient behavior of the creep parameters for the SZ-0.85-Fe material is indeed due to the high porosity content, and agrees with the observation of Zisner and Tagai[29] that the effect of porosity upon rate is related to some thermally activated process. Thus the necessity for homogeneous specimens of high density for creep investigation is evident.

The results shown in Table B-III and B-IV (Appendix B) indicate higher creep rates for the dense SZ-1.35-Fe material compared to the less dense SZ-0.85-Fe material. Terwilliger et. al.[31] have also reported an increase in creep rate with increasing Fe_2O_3 content. Furthermore, the stress factor is generally less for the high porosity samples than for the denser materials (see Figures 20-23), which also suggests a higher creep rate for the higher

density specimens. It is suggested that the lower creep rates for the low density material arises from the densification process that is operating concurrently with the creep deformation, and which counteracts the creep extension of the specimen. It is clear that as densification is completed, the creep rate will increase. Furthermore, the very rapid decrease in the activation energy as temperature increases for the SZ-0.85-Fe specimens (215 kcal/mole to 115 kcal/mole) suggests that on the basis of activation energy alone, the lower density specimens will creep at a relatively higher rate than the higher density specimens above 1300°C.

C. CREEP MECHANISM IN $SrZrO_3$

It is suggested that the twinning mechanism, which has been shown to be operative in $SrZrO_3$ at room temperature[41-44] (and which accounts for its unusual mechanical properties), is also responsible for the observed creep characteristics of this ceramic. This is consistent with the high temperature x-ray diffraction results of this investigation, which shows that the mechanical twinning shear angle for $SrZrO_3$ remains nearly constant (0^o 34') from room temperature to 1300^oC. Hayden et. al.[51] also reported that twinning is generally less temperature dependent upon the stresses (and structure) propagating the mechanical deformation than is slip.

Mechanical twinning is generally defined as homogeneous shear in which all the atoms in the displaced region are moved through distances proportional to their distance from the mirror or twin plane. One difficulty with this concept is proposing a mechanism to account for the homogeneous and proportional movement of the atoms through the successive lattice planes, in contrast to slip which only requires movement on a single plane. In an attempt to solve this problem Cottrell and Bilby[65] proposed a dislocation mechanism for mechanical twinning. In twinning the following

points must be considered: firstly, it is highly unlikely that all atoms involved in twinning should move simultaneously, and secondly, twinning occurs at stresses far below the theoretical shear strength of a perfect lattice. Also, in contrast to simple slip, twinning produces a new atomic configuration and the dislocations causing it must be imperfect (the translation vector is not a period of the lattice). Now, homogeneous shear in twinning will require either an avalanche of dislocations, with one on every successive lattice plane without exception, or the more likely alternative of a single dislocation which moves successively from one plane to the next in a regular manner. The pole mechanism proposed by Cottrell and Bilby is based upon the latter concept, and is now generally accepted as a realistic model for dislocation movement during twinning.

THE POLE MECHANISM

Frank and Read[66] proposed the well known slip mechanism by which an unlimited amount of slip is produced by a single dislocation moving in a single slip plane. The dislocation process for twinning described by Cottrell and Bilby can be viewed in a similar way. Figure 30 shows three dislocation lines S_1, S_2 and S_3 meeting at a node point 0. The convention for defining

the Burgers vectors of dislocations at a node is to look outwards from the nodal point 0, and describe a closed clockwise circuit around each line. The same circuit repeated in the lattice as it existed before the dislocation was imposed will not be closed, and the displacement necessary to close the circuit is the Burgers vector. The Burgers vectors, b_1, b_2 and b_3 of the lines meeting at 0 must satisfy the relation

$$\sum_{n=1}^{3} b_n = 0 \qquad (33)$$

In the Frank-Read mechanism, S_3 is specified as a perfect dislocation (one whose Burgers vector is equivalant to the lattice parameter), and as the dislocation moves along its slip plane atoms are left behind in the positions originally occupied. For the Frank-Read source S_1 and S_2 (shown as S_1' and S_2' in Figure 30) are assumed to be rendered immobile when their intersection forms a dislocation line (the pole dislocation), and when they are perpendicular to the plane AOB in which S_3 lies. The part of the S_3 dislocation line that intersects the obstacle halts while the remainder of S_3 spirals around the obstacle (nodal point) forming a dislocation loop (when b_3 lies in AOB).

Cottrell and Bilby extended the above mechanism to the case where the Burgers vectors of S_1 and S_2

Figure 30

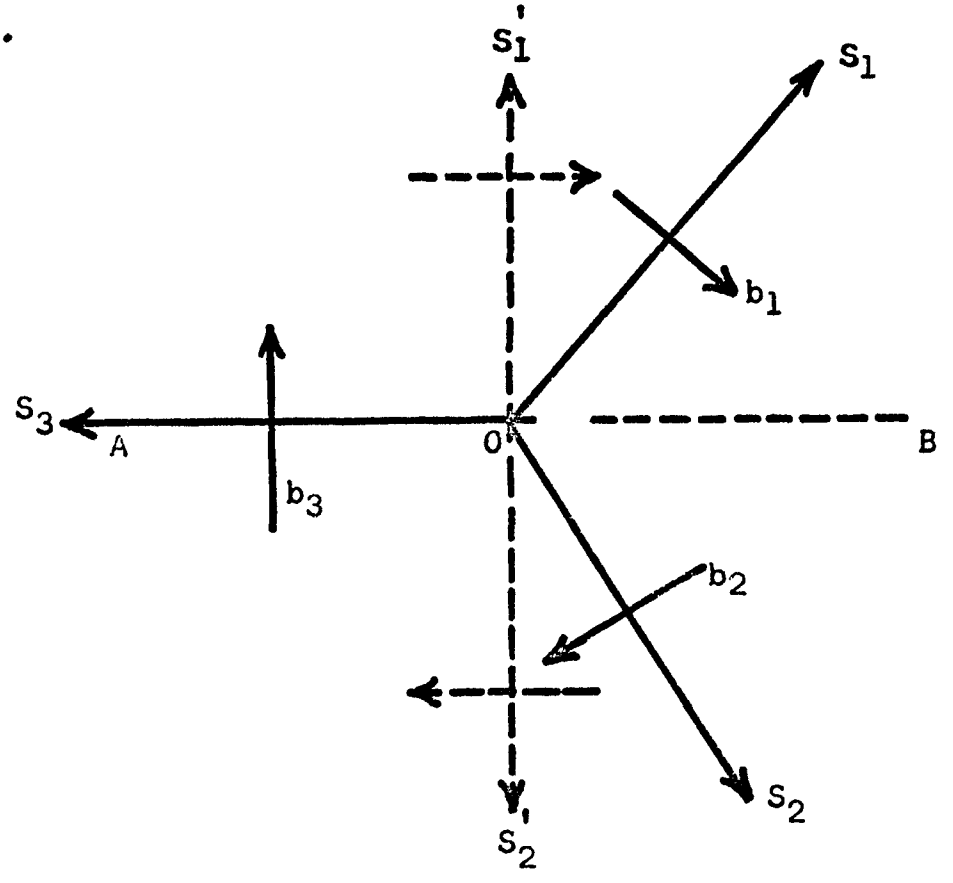

Three dislocation lines S_1, S_2 and S_3 meeting at a node, O. The dotted lines indicate the special case for the Frank-Read mechanism. The plane AOB is perpendicular to the page.

do not lie in a plane parallel to AOB which contains the spiraling dislocation line S_3 and its Burgers vector b_3. The mechanism is usually represented as shown in Figure 31. Three dislocations S_1, S_2, and S_3 again intersect at 0, however because S_1 and S_2 are not perpendicular to the twin plane, their Burgers vectors, b_1 and b_2, have a vertical component (which did not exist for the Frank-Read pole) when projected on a line perpendicular to the twin plane. Consequently, the "sweeping" dislocation S_3 is displaced by a positive vertical component for every complete revolution made around S_1, and a negative vertical component for each revolution made around S_2. The components of b_1 and b_2 perpendicular to the twin plane must be equal and opposite in sign, say +y for a complete revolution around S_1, and -y for a revolution around S_2 because Equation (33) is obeyed and the component of $b_3 = 0$. Weertman and Weertman[67] illustrate the pole mechanism as shown in Figure 32. A twin results as the partial dislocation crosses a pole dislocation (at 0) which possesses a Burgers vector component normal to the slip plane of the partial. As it spirals around the pole, the partial produces a deformation twin when the vertical component is equal to the distance between

Figure 31

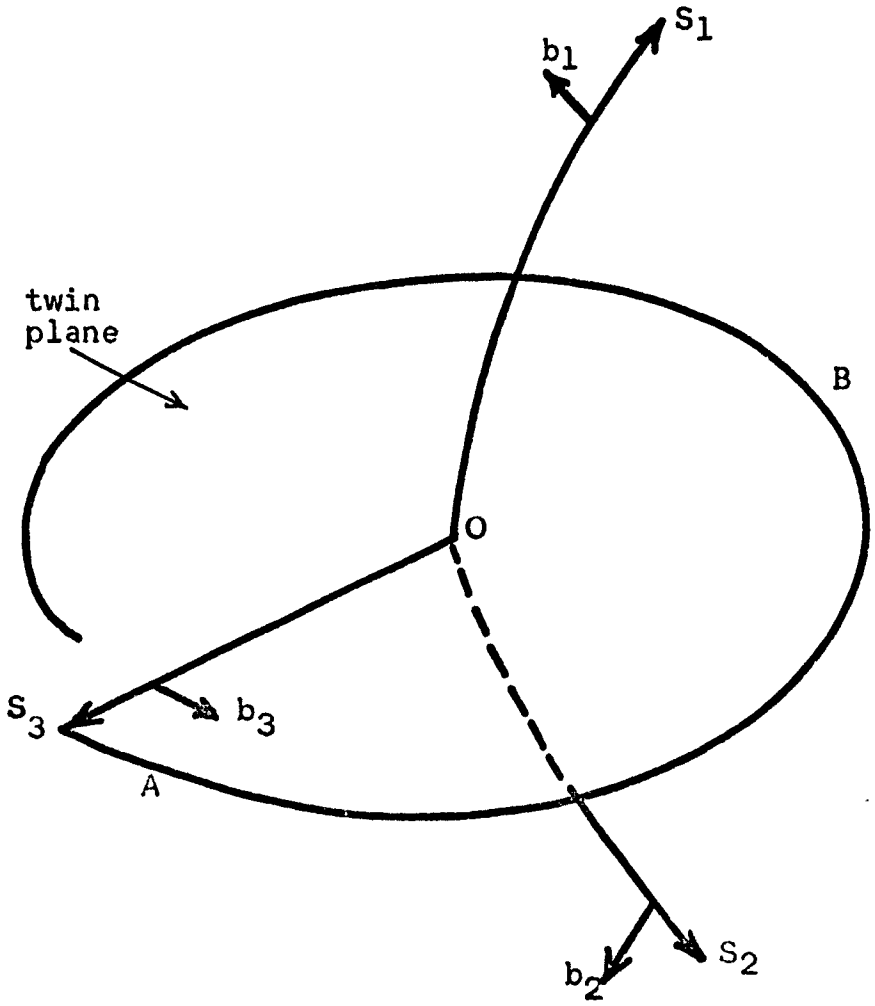

Schematic diagram for
pole mechanism illustrating growth
of a mechanical twin.

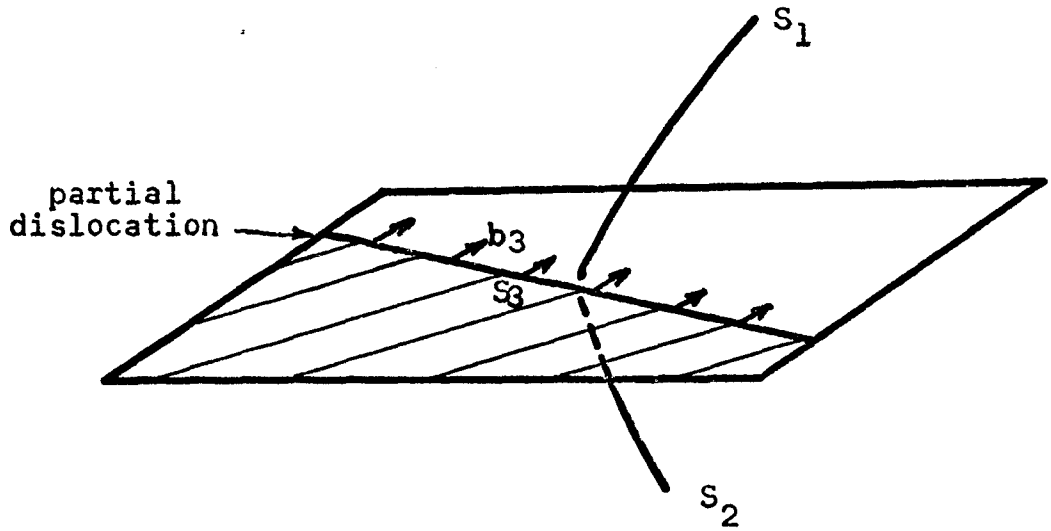

The "sweeping" dislocation intersects the pole (where two dislocations intersect, forming an immobile node).

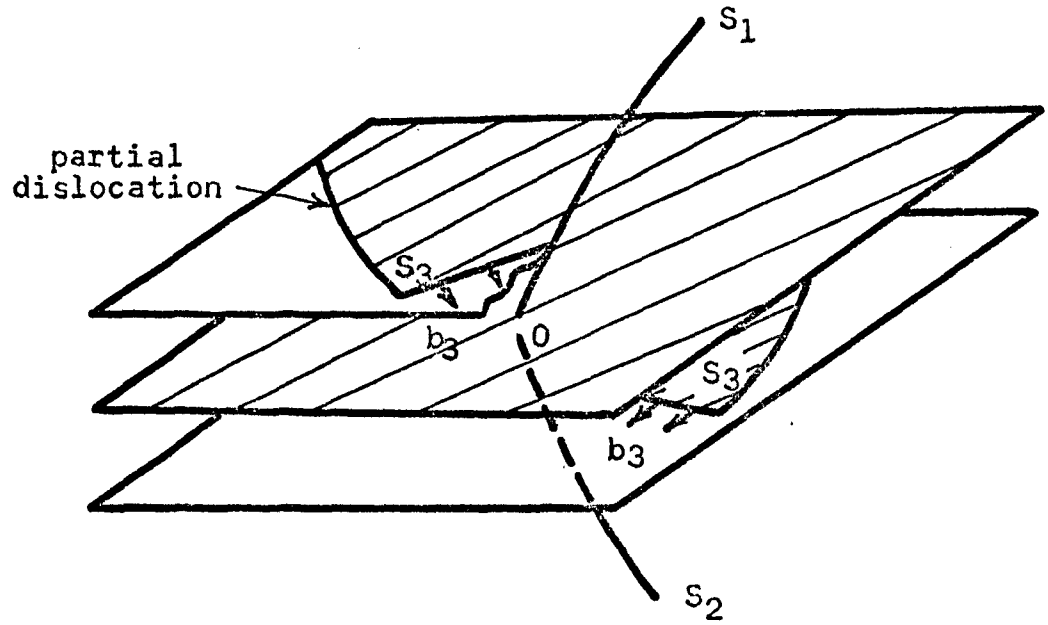

A twin is generated on successive lattice planes.

Figure 32

atomic planes. Under these conditions the sweeping dislocation produces a monolayer of twinned crystal for each revolution that it makes, and climbs one lattice spacing where the process is repeated to build a lamella of twinned crystal. The resulting shear deformation is homogeneous as observed for twinning.

The possibility of plastic deformation occurring in ceramics by a twinning mechanism has also been suggested by Kronberg[68,69], to account for deformation in sapphire. The deformation structure observed was found to be more consistent with a partial dislocation twinning mechanism than with conventional slip. Also, Williams[70] has suggested that creep in polycrystalline alumina may be a deformation twinning process.

Investigators have found that in general mechanical twins do not go through the whole of the specimen, but stop at obstacles such as boundaries or twins of another system. They have a lenticular shape whose boundaries must be analyzed in terms of dislocation loops[20,67,71]. The twins observed in single crystal $SrZrO_3$ were of this shape[41,42,44], indicating the above theory may be compatable with observations made on this perovskite-type material. Once twins have formed, they may propagate outward from the pole area in various ways.

Basinski and Christian[72] suggested that a specimen consisting of a series of fine parallel twin lamella may be continuously deformed by movement of existing twin boundaries. These boundaries, if sufficiently mobile, will move perpendicular to themselves, increasing or decreasing the proportion of the twinned orientation appropriate to the sign of the stress. The maximum strain possible will depend on the orientation of the stress axis and the relative amount of twinned crystal initially present. Hayden et. al.[51] suggested that the deformation that must accompany twinning causes slip and bending in the regions surrounding grains of a polycrystalline material, and causes twinning in neighboring grains. Thus once twinning has started, it can propagate through favorably oriented grains throughout the specimen.

Terwilliger et. al.[31] found that the addition of Fe^{+3} to polycrystalline MgO promoted viscous behavior, i.e., the stress factor (n) decreased as the Fe^{+3} concentration was increased. This behavior was attributed to the blocking of dislocation motion by the iron atoms, with the result that diffusion becomes the more significant mechanism for deformation through mass transfer. However, it is suggested that the plastic deformation in $SrZrO_3$ is related to mechanical twinning.

It has been shown that small additions of Fe_2O_3 do not affect the mechanical behavior of $SrZrO_3$ at room temperature[41-43]. X-ray studies in this investigation showed that an addition of 1.35 wt. % Fe_2O_3 produced no measurable shift for the $SrZrO_3$ slow scanned pattern (0.25 °/min.), even at high angles (up to 150°). Mori[73] noted that many alkaline earth perovskites form compounds over wide ranges with the transition metals where the structure is not disturbed. In these compounds (e.g. ferrates) iron is probably highly oxidized (to the Fe^{+4} state), in which case it is likely to occupy the octahedral position in the lattice. Evidence indicates that the perovskite structure is retained with small additions of iron and the twinning mechanism in $SrZrO_3$ is not disturbed.

As indicated earlier, a continuing decrease in creep rate is observed in all samples of $SrZrO_3$ as the strain level increases. These results may well be consistent with the proposed twinning mechanism. As creep proceeds there will be fewer grains properly oriented to the shear stress, so that fewer grains will be contributing to the deformation. Also the dislocation mechanism for twinning suggests that work hardening may occur as intersecting twins pin one another making propagation more difficult. Work hardening during twinning

has been reported by Yakovleva and Yakutovitch[74] for cadmium crystals. They observed that when the size difference in adjacent volumes increased the domains interacted to oppose extension. Either of the above mechanisms would require increasingly higher stresses to cause mechanical twinning to continue at a constant rate. Conversely, for a constant stress, creep rate would continuously decrease as creep testing continued and strain increases (which is in fact observed).

In conclusion, if the pole mechanism described above is operative in the mechanical twinning of $SrZrO_3$, the observed functional relationship $\dot{\varepsilon} \propto \sigma^3/d$ is consistent with the dislocation climb mechanism proposed by Weertman and modified by Garofalo to take account of grain size effects. In agreement with Weertman's theory, Friedel[20] noted that mechanical twinning results in the formation of voids and is subject to dislocation climb.

VI CONCLUSIONS

From the results of this investigation of the creep behavior of $SrZrO_3$ the following conclusions are presented:

1) The orthorhombic structure and the twinning shear angle (0° 34') of $SrZrO_3$ is invarient over the temperature range 25°C to 1300°C.

2) Fe_2O_3 additions to $SrZrO_3$ accelerate sintering and enhance densification. Powder compacts containing 1.35 wt. % Fe_2O_3 sintered to approximately 99% of theoretical density, while compacts containing 0.85 wt. % Fe_2O_3 showed considerable porosity (as low as 88% of theoretical density).

3) The creep results for dense $SrZrO_3$ (containing 1.35 wt. % Fe_2O_3) gave invarient creep parameters over the ranges of the variables investigated. No constant creep parameters were obtained for the specimens containing 0.85 wt. % Fe_2O_3, which is attributed to the porosity.

4) Creep in dense $SrZrO_3$ is a thermally activated process and is exponentially related to temperature by $\exp(-\Delta H/RT)$. The activation energy is 169 ± 10 kcal/mole and is relatively invarient with temperature over the range 1200°C - 1300°C.

5) The effect of stress on creep rate in dense

$SrZrO_3$ is essentially constant with temperature (1160°C-1275°C) and is described by the relation $\dot{\epsilon} \propto \sigma^n$, where n varies from 3.1±0.4 to 3.3±0.4 over the grain size range 0.45 μm to 2.04 μm respectively.

6) The effect of grain size on creep rate in dense $SrZrO_3$ is essentially constant with temperature (1160°C-1275°C) and stress (1000-4000 psi), and is described by the relation $\dot{\epsilon} \propto d^{\alpha}$, where $\alpha = -1.0 \pm 0.1$.

7) The function dependence $\dot{\epsilon} \propto \sigma^3/d$ is consistent with the nonviscous dislocation climb mechanism proposed by Weertman and modified by Garofalo to account for the effect of grain size.

8) Deformation in $SrZrO_3$ occurs by a twinning mechanism which may be described by the dislocation pole mechanism proposed by Cottrell and Bilby.

9) The creep rate decreases with strain (or time), indicating the presence of an inherent time-hardening mechanism as observed in the creep testing of other refractory oxides. The mechanism is probably one of work hardening accompanying the intersection of twins coupled with the decrease in the number of grains favorably oriented to the shear stress for twinning.

VII RECOMMENDATIONS FOR FURTHER STUDY

Much of the fundemental information which is of engineering significance is yet to be determined for ceramics of the perovskite-type family. As shown in this investigation the creep behavior is strongly dependent on density and grain size, so that a study of the sintering kinetics would provide valuable information relating to the optimum conditions and iron additions for maximizing the density and hence the creep resistance of $SrZrO_3$. The grain size and density will undoubtedly determine the room temperature "ductility" of $SrZrO_3$ as well, and an understanding of the effect of these parameters on the yield will be useful in controlling non-brittle fracture. A determination of the diffusion constants for the various ionic species, both for volume and grain boundary diffusion, is necessary if the creep process is to be unequivocally defined and thus permit maximum control or utilization of the deformation mechanisms.

$SrZrO_3$ is similar in structure to several piezoelectric and ferroelectric materials now in use. This group generally exhibits electrical aging which is probably related to some form of internal deformation or relaxation, so that an investigation of electrical

polarizability of $SrZrO_3$ may shed light on the deformation mechanisms.

Optical and Laue x-ray studies of single crystal $SrZrO_3$ would be useful to determine symmetry elements and identify the twin planes. A determination of the crystallographic directions in which the crystals are susceptible to deformation by mechanical stress and electric field would lead to a better understanding of the yielding process in the perovskite-type ceramics. The production of a high temperature ceramic which exhibits non-brittle behavior with a predictable yield at low temperatures, and retains high resistance to creep at elevated temperatures, would be an invaluable contribution to the materials field.

APPENDIX A

Electron Micrographs

of

SZ-1.35-Fe

and

SZ-0.85-Fe

Before Testing

Before Testing

SEM

Figure A-1
SZ-1.35-Fe
0.45 μm grain size

Before Testing

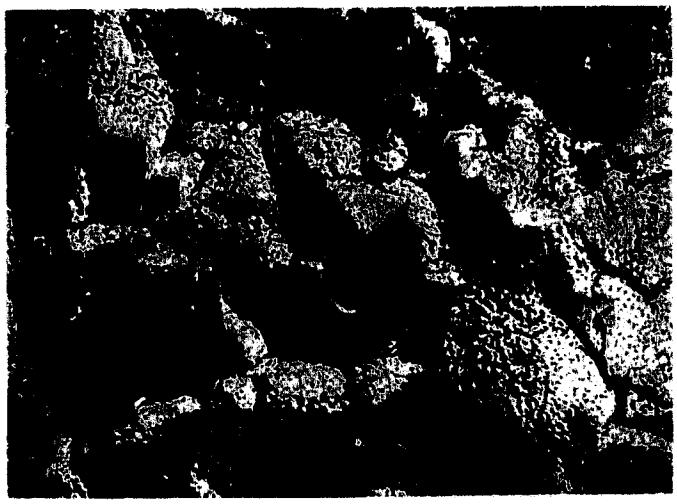

After Testing

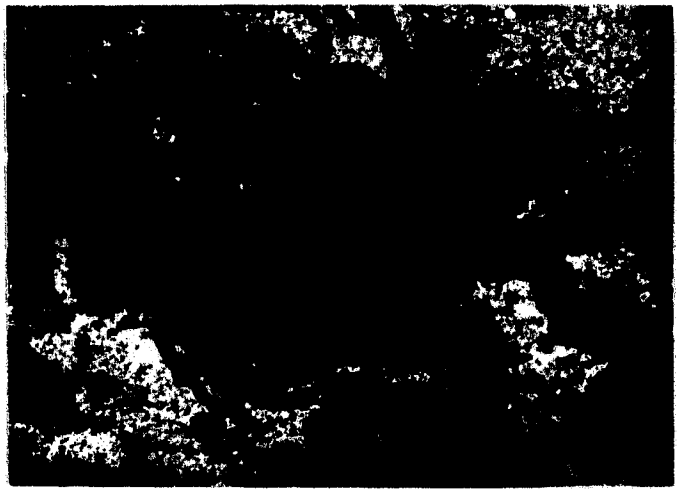

SEM

Figure A-2
SZ-1.35-Fe
1.06 μm grain size

Before Testing

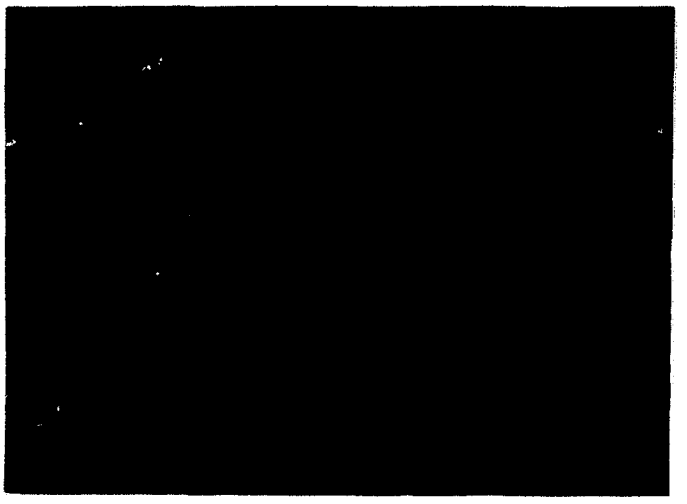

After Testing

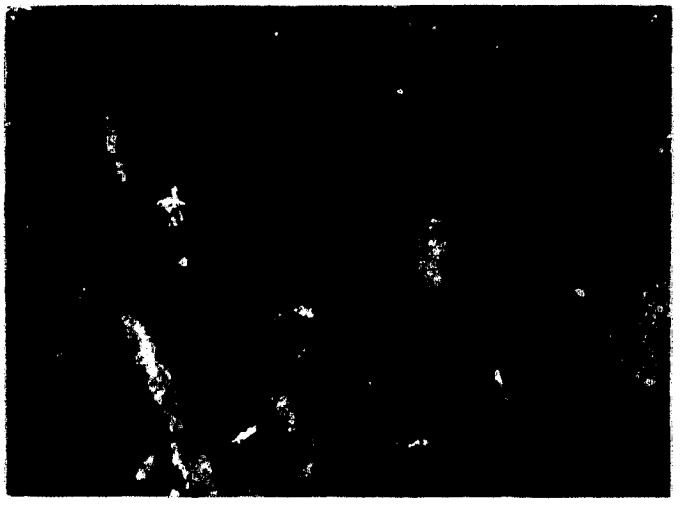

SEM

Figure A-3
SZ-1.35-Fe
2.04 μm grain size

Before Testing

After Testing

SEM

Figure A-4
SZ-0.85-Fe
0.45 μm grain size

Before Testing

After Testing

SEM

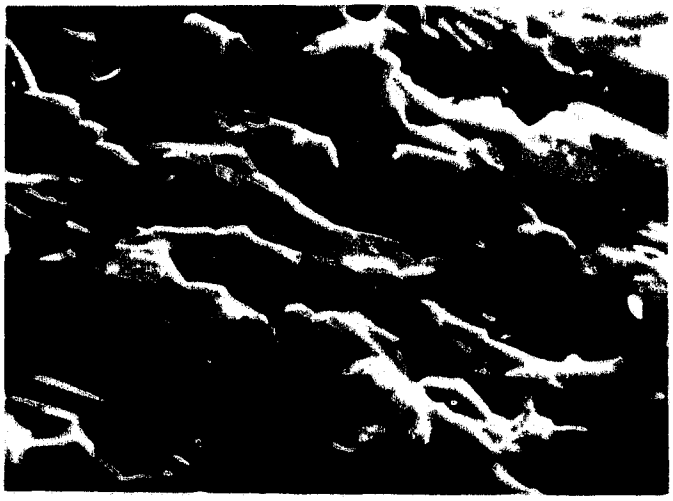

Figure A-5
SZ-0.85-Fe
1.03 μm grain size

After Testing

After Testing

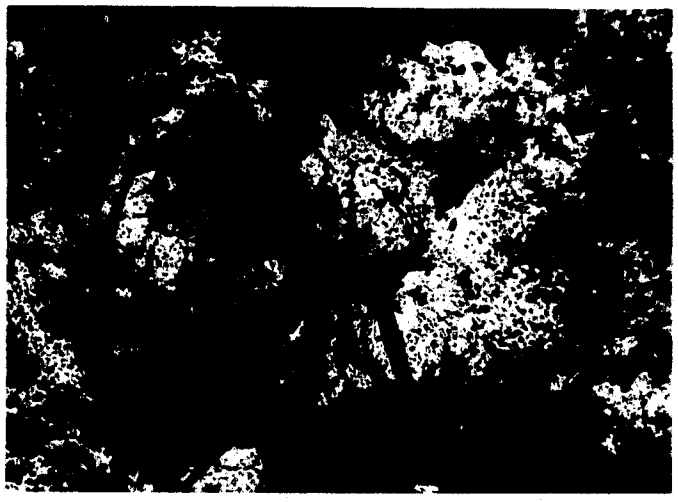

SEM

Figure A-6
SZ-0.85-Fe
1.83 μm grain size

APPENDIX B

Creep Rate Data
for
SZ-1.35-Fe
and
SZ-0.85-Fe

TABLE B-I

Creep Rate ($\dot{\epsilon}$) - Strain (ϵ) Data
For all SZ-1.35-Fe Samples
Obtained by Differential Method

Grain Size = 0.45 μm, dead load = 2000psi

Sample No.	Temp. °C	Creep Strain (ϵ) in/in	Creep Rate ($\dot{\epsilon}$) in/(in hr)
1	1200	0.77 x10^{-2}	1.74 x 10^{-3}
		0.90	1.68
		1.00	1.58
	1160	1.03 x10^{-2}	2.98 x 10^{-4}
		1.07	2.91
		1.10	2.86
	1200	1.13 x10^{-2}	1.40 x 10^{-3}
		1.17	1.33
		1.21	1.28
	1160	1.23 x10^{-2}	2.16 x 10^{-4}
		1.23	2.11
		1.24	2.07
	1200	1.26 x10^{-2}	1.05 x 10^{-3}
		1.28	1.00
		1.30	0.97
2	1200	0.42 x10^{-2}	1.20 x10^{-3}
		0.52	1.13
		0.62	1.05
	1160	0.64 x10^{-2}	1.62 x10^{-4}
		0.65	1.60
		0.66	1.54
1	1250	0.45 x10^{-2}	1.47 x10^{-2}
		0.50	1.41
		0.55	1.37
		0.60	1.33
		0.65	1.29
	1200	0.76 x10^{-2}	1.74 x10^{-3}
		0.82	1.69
		0.87	1.64
		0.92	1.61
		1.00	1.58

Sample No.	Temp. °C	Creep Strain (ϵ) in/in	Creep Rate ($\dot{\epsilon}$) in/(in hr)
3	1250	0.22×10^{-2}	7.11×10^{-3}
		0.28	7.00
		0.35	6.93
	1200	0.41×10^{-2}	1.11×10^{-3}
		0.52	1.08
		0.62	1.04
4	1200	1.25×10^{-2}	6.27×10^{-4}
		1.27	6.22
		1.30	6.16
	1250	1.35×10^{-2}	4.40×10^{-3}
		1.43	4.16
		1.52	4.02
5	1250	0.82×10^{-2}	9.69×10^{-3}
		0.90	9.32
		1.05	8.97
		1.15	8.72
		1.23	8.57
	1200	1.30×10^{-2}	1.26×10^{-3}
		1.35	1.23
		1.40	1.19
		1.45	1.16
		1.53	1.14
6	1250	0.33×10^{-2}	1.30×10^{-2}
		0.45	1.20
		0.58	1.14
	1275	0.79×10^{-2}	2.45×10^{-2}
		0.95	2.23
		1.08	2.03
	1250	1.21×10^{-2}	7.00×10^{-3}
		1.28	6.65
		1.32	6.35

Sample No.	Temp. °C	Creep Strain (ϵ) in/in	Creep Rate ($\dot{\epsilon}$) in/(in hr)
7	1250	0.34×10^{-2}	1.17×10^{-2}
		0.45	1.10
		0.56	1.05
	1275	0.81×10^{-2}	2.34×10^{-2}
		0.94	2.18
		1.07	2.02

Grain Size = 1.06 μm, dead load 2000 psi

Sample No.	Temp. °C	Creep Strain (ϵ) in/in	Creep Rate ($\dot{\epsilon}$) in/(in hr)
1	1200	0.90×10^{-2}	5.30×10^{-4}
		0.95	4.89
		0.97	4.46
		1.02	4.32
		1.06	4.09
	1160	1.06×10^{-2}	7.95×10^{-5}
		1.07	7.85
		1.09	7.69
		1.15	7.44
		1.12	7.40
	1200	1.14×10^{-2}	3.62×10^{-4}
		1.16	3.43
		1.18	3.26

Sample No.	Temp. °C	Creep Strain (ϵ) in/in	Creep Rate ($\dot{\epsilon}$) in/(in hr)
2	1200	0.25 x10^{-2}	3.47 x10^{-4}
		0.27	3.39
		0.30	3.17
	1160	0.30 x10^{-2}	5.92 x10^{-5}
		0.31	5.82
		0.32	5.80
	1200	0.35 x10^{-2}	3.05 x10^{-4}
		0.37	2.97
		0.38	2.94
3	1200	0.65 x10^{-2}	7.22 x10^{-4}
		0.73	6.09
		0.81	5.35
	1160	0.82 x10^{-2}	1.05 x10^{-4}
		0.85	1.02
		0.87	0.09
	1200	0.91 x10^{-2}	4.40 x10^{-4}
		0.95	4.16
		0.98	3.91
1	1250	0.55x10^{-2}	4.00 x10^{-3}
		0.70	3.55
		0.86	3.07
	1200	0.90x10^{-2}	5.30 x10^{-4}
		0.95	4.[illegible]
		1.00	4.32
2	1250	0.15x10^{-2}	3.87 x10^{-3}
		0.19	3.69
		0.23	3.51
	1200	0.26x10^{-2}	3.47 x10^{-4}
		0.28	3.37
		0.30	3.17

Sample No.	Temp. °C	Creep Strain (ϵ) in/in	Creep Rate ($\dot{\epsilon}$) in/(in hr)
2	1200	0.36×10^{-2}	3.03×10^{-4}
		0.37	2.97
		0.38	2.94
	1250	0.41×10^{-2}	2.21×10^{-3}
		0.45	2.08
		0.49	1.94
3	1250	0.40×10^{-2}	4.48×10^{-3}
		0.45	4.26
		0.54	4.08
	1200	0.63×10^{-2}	6.38×10^{-4}
		0.71	5.88
		0.80	5.55
4	1250	0.58×10^{-2}	4.44×10^{-3}
		0.70	4.00
		0.80	3.66
		0.90	3.33
		1.02	3.07
	1200	1.10×10^{-2}	4.47×10^{-4}
		1.14	4.33
		1.17	4.22
		1.20	4.05
		1.23	3.97
	1250	1.25×10^{-2}	2.17×10^{-3}
		1.30	1.96
		1.35	1.92
2	1250	0.42×10^{-2}	2.21×10^{-2}
		0.46	2.08
		0.50	1.94
	1275	0.56×10^{-2}	3.91×10^{-3}
		0.60	3.71
		0.64	3.39
	1250	0.65×10^{-2}	1.46×10^{-3}
		0.67	1.43
		0.68	1.42
	1275	0.70×10^{-2}	2.85×10^{-3}
		0.72	2.77
		0.73	2.70

Sample No.	Temp. °C	Creep Strain (ϵ) in/in	Creep Rate ($\dot{\epsilon}$) in/(in hr)
5	1250	0.20 x10^{-2}	5.73 x10^{-3}
		0.26	5.63
		0.32	5.53
	1275	0.43 x10^{-2}	1.40 x10^{-2}
		0.59	1.34
		0.75	1.28
	1250	0.97 x10^{-2}	4.96 x10^{-3}
		1.01	4.90
		1.05	4.86

Grain Size = 2.04 µm, dead load = 2000 psi

Sample No.	Temp. °C	Creep Strain (ϵ) in/in	Creep Rate ($\dot{\epsilon}$) in/(in hr)
1	1200	0.32 x10^{-2}	5.80 x10^{-4}
		0.36	5.03
		0.40	4.55
	1160	0.41 x10^{-2}	8.41 x10^{-5}
		0.42	8.00
		0.44	7.58
	1200	0.45 x10^{-2}	3.36 x10^{-4}
		0.47	3.11
		0.48	3.00
2	1200	0.30 x10^{-2}	2.88 x10^{-4}
		0.34	2.72
		0.38	2.62
	1160	0.43 x10^{-2}	5.20 x10^{-5}
		0.44	5.16
		0.45	5.12

Sample No.	Temp. °C	Creep Strain (ϵ) in/in	Creep Rate ($\dot{\epsilon}$) in/(in hr)
2	1200	0.46 x10^{-2}	2.90 x10^{-4}
		0.49	2.86
		0.51	2.84
3	1200	0.20 x10^{-2}	6.54 x10^{-4}
		0.25	6.25
		0.30	5.95
	1160	0.30 x10^{-2}	1.12 x10^{-4}
		0.31	1.11
		0.31	1.09
3	1160	0.39 x10^{-2}	1.09 x10^{-4}
		0.39	1.08
		0.40	1.06
	1200	0.44 x10^{-2}	5.58 x10^{-4}
		0.46	5.45
		0.48	5.41

Sample No.	Temp. °C	Creep Strain (ϵ) in/in	Creep Rate ($\dot{\epsilon}$) in/(in Hr)
2	1200	0.47 x10^{-2}	2.91 x10^{-4}
		0.48	2.87
		0.50	2.83
	1250	0.55 x10^{-2}	2.15 x10^{-3}
		0.59	2.13
		0.62	2.06
3	1200	0.44 x10^{-2}	5.58 x10^{-4}
		0.46	5.45
		0.48	5.41
	1250	0.51 x10^{-2}	3.49 x10^{-3}
		0.56	3.41
		0.60	3.36
	1200	0.62 x10^{-2}	5.41 x10^{-4}
		0.63	5.33
		0.64	5.29
	1250	0.67 x10^{-2}	3.30 x10^{-3}
		0.72	3.27
		0.75	3.21

Sample No.	Temp. °C	Creep Strain (ϵ) in/in	Creep Rate ($\dot{\epsilon}$) in/(in hr)
4	1200	0.31 x10^{-2}	2.68 x10^{-4}
		0.32	2.66
		0.33	2.62
	1250	0.36 x10^{-2}	1.84 x10^{-3}
		0.40	1.82
		0.43	1.79
5	1250	0.14 x10^{-2}	4.18 x10^{-3}
		0.18	4.00
		0.22	3.91
		0.26	3.83
		0.29	3.63
	1200	0.32 x10^{-2}	5.33 x10^{-4}
		0.34	5.29
		0.36	5.22
		0.38	5.18
		0.40	5.12

Sample No.	Temp. °C	Creep Strain (ϵ) in/in	Creep Rate ($\dot{\epsilon}$) in/(in hr)
2	1250	0.56x10^{-2}	2.15 x10^{-3}
		0.59	2.13
		0.62	2.06
	1275	0.64x10^{-2}	5.07 x10^{-3}
		0.70	4.83
		0.76	4.51
	1250	0.77 x10^{-2}	1.88 x10^{-3}
		0.79	1.85
		0.81	1.83
	1275	0.84 x10^{-2}	4.22 x10^{-3}
		0.88	4.17
		0.93	3.92

Sample No.	Temp. °C	Creep Strain (ϵ) in/in	Creep Rate ($\dot{\epsilon}$) in/(in hr)
6	1250	0.19×10^{-2}	4.44×10^{-3}
		0.26	4.30
		0.33	4.14
	1275	0.44×10^{-2}	9.11×10^{-3}
		0.53	8.88
		0.62	8.62
	1250	0.70×10^{-2}	3.51×10^{-3}
		0.71	3.49
		0.73	3.47

TABLE B-II

Creep Rate ($\dot{\epsilon}$) - Strain (ϵ) Data
For all SZ-0.85-Fe Samples
Obtained by Differential Method

Grain Size = 0.45 μm, dead load = 2000 psi

Sample No.	Temp. °C	Creep Strain (ϵ) in/in	Creep Rate ($\dot{\epsilon}$) in/(in hr)
1	1250	0.46 x10^{-2}	2.18 x10^{-4}
		0.48	1.92
		0.49	1.83
		0.51	1.72
	1200	0.51 x10^{-2}	1.84 x10^{-5}
		0.52	1.79
		0.52	1.74
	1250	0.54 x10^{-2}	1.51 x10^{-4}
		0.56	1.45
		0.58	1.37
		0.59	1.28
	1200	0.59 x10^{-2}	1.04 x10^{-5}
		0.59	1.01
		0.59	0.98
2	1200	0.52 x10^{-2}	2.58 x10^{-5}
		0.53	2.36
		0.53	2.27
	1250	0.54 x10^{-2}	3.33 x10^{-4}
		0.55	2.63
		0.57	2.22
1	1300	0.35 x10^{-2}	9.85 x10^{-4}
		0.40	9.34
		0.44	8.88
	1250	0.45 x10^{-2}	2.18 x10^{-4}
		0.47	1.93
		0.50	1.72

Sample No.	Temp. °C	Creep Strain (ϵ) in/in	Creep Rate ($\dot{\epsilon}$) in/(in hr)
3	1300	0.45 $\times 10^{-2}$	8.63 $\times 10^{-4}$
		0.49	8.50
		0.53	8.25
		0.57	7.50
	1250	0.61 $\times 10^{-2}$	1.18 $\times 10^{-4}$
		0.63	1.17
		0.64	1.15
		0.65	1.13
		0.66	1.10
3	1250	0.73 $\times 10^{-2}$	9.79 $\times 10^{-5}$
		0.74	9.68
		0.74	9.58
	1300	0.76 $\times 10^{-2}$	5.13 $\times 10^{-4}$
		0.77	4.76
		0.80	4.66

Sample No.	Temp. °C	Creep Strain (ϵ) in/in	Creep Rate ($\dot{\epsilon}$) in/(in hr)
1	1300	0.75 $\times 10^{-2}$	1.18 $\times 10^{-3}$
		0.80	1.04
		0.83	0.96
	1350	0.89 $\times 10^{-2}$	3.87 $\times 10^{-3}$
		1.00	3.10
		1.15	2.60
4	1300	0.44 $\times 10^{-2}$	7.00 $\times 10^{-4}$
		0.50	6.85
		0.55	6.74
	1350	0.70 $\times 10^{-2}$	2.90 $\times 10^{-3}$
		0.83	2.77
		0.94	2.68
	1300	0.97 $\times 10^{-2}$	5.17 $\times 10^{-4}$
		1.00	5.08
		1.03	4.97
	1350	1.08 $\times 10^{-2}$	1.93 $\times 10^{-3}$
		1.13	1.86
		1.18	1.79

Sample No.	Temp. °C	Creep Strain (ϵ) in/in	Creep Rate ($\dot{\epsilon}$) in/(in hr)
5	1300	0.45 x10^{-2}	1.50 x10^{-3}
		0.50	1.29
		0.55	1.17
		0.60	1.10
	1350	0.80 x10^{-2}	2.59 x10^{-3}
		0.85	2.43
		0.90	2.21
		0.95	2.01
	1300	1.04 x10^{-2}	7.05 x10^{-4}
		1.05	6.65
		1.07	6.50
	1350	1.15 x10^{-2}	1.90 x10^{-3}
		1.20	1.78
		1.22	1.62

Grain Size = 1.03 μ dead load = 2000psi

Sample No.	Temp. °C	Creep Strain (ϵ) in/in	Creep Rate ($\dot{\epsilon}$) in/(in hr
1	1250	0.70 x10^{-2}	5.88 x10^{-4}
		0.75	5.86
		0.80	5.85
		0.85	5.83
		0.90	5.82
	1200	0.91 x10^{-2}	4.79 x10^{-5}
		0.91	4.79
		0.92	4.79
	1250	0.95 x10^{-2}	5.82 x10^{-4}
		1.00	5.82
		1.05	5.79

Sample No.	Temp. °C	Creep Strain (ϵ) in/in	Creep Rate ($\dot{\epsilon}$) in/(in hr)
2	1250	0.75 x10^{-2}	6.15 x10^{-4}
		0.80	6.00
		0.85	5.71
		0.90	5.47
		0.95	5.24
	1200	0.96 x10^{-2}	5.00 x10^{-5}
		0.96	4.93
		0.97	4.86
	1250	0.99 x10^{-2}	5.15 x10^{-4}
		1.05	4.95
		1.17	4.85
3	1300	0.45 x10^{-2}	3.47 x10^{-3}
		0.55	3.33
		0.65	3.18
	1250	0.69 x10^{-2}	6.22 x10^{-4}
		0.75	6.05
		0.80	5.88
		0.90	5.55
		1.03	5.33

Sample No.	Temp. °C	Creep Strain (ϵ) in/in	Creep Rate ($\dot{\epsilon}$) in/(in hr)
	1300	1.08 x10^{-2}	2.50 x10^{-3}
		1.20	2.35
		1.30	2.27
2	1300	0.51 x10^{-2}	3.22 x10^{-3}
		0.60	3.12
		0.67	3.03
	1250	0.73 x10^{-2}	6.20 x10^{-4}
		0.77	5.05
		0.82	5.80
		0.92	5.32
4	1300	0.56 x10^{-2}	2.24 x10^{-3}
		0.65	2.15
		0.75	2.07
	1250	0.77 x10^{-2}	4.33 x10^{-4}
		0.81	4.27
		0.86	4.22

Sample No.	Temp. °C	Creep Strain (ϵ) in/in	Creep Rate ($\dot{\epsilon}$) in/(in hr)
4	1300	0.92 x10^{-2}	1.95 x10^{-3}
		0.97	1.87
		1.03	1.83
5	1300	0.91 x10^{-2}	1.71 x10^{-3}
		0.95	1.65
		0.98	1.60
	1350	1.15 x10^{-2}	4.65 x10^{-3}
		1.20	4.34
		1.25	4.08
		1.30	3.87
		1.35	3.65
6	1300	0.34 x10^{-2}	6.64 x10^{-3}
		0.40	6.32
		0.46	6.00
	1350	0.57 x10^{-2}	1.58 x10^{-2}
		0.63	1.45
		0.68	1.37
	1300	0.78 x10^{-2}	4.66 x10^{-3}
		0.81	4.54
		0.84	4.43
7	1300	0.21 x10^{-2}	4.20 x10^{-3}
		0.25	4.09
		0.30	3.98
	1350	0.45 x10^{-2}	1.21 x10^{-2}
		0.54	1.13
		0.62	1.05

Grain Size = 1.83 μ dead load = 2000psi

Sample No.	Temp. °C	Creep Strain (ε) in/in	Creep Rate ($\dot{\varepsilon}$) in/(in hr)
1	1250	0.61 x10^{-2}	2.51 x10^{-4}
		0.62	2.44
		0.63	2.36
		0.64	2.29
		0.65	2.24
	1200	0.67 x10^{-2}	3.55 x10^{-5}
		0.68	3.41
		0.68	3.22
	1250	0.69 x10^{-2}	1.91 x10^{-4}
		0.71	1.86
		0.72	1.81
		0.73	1.71
		0.74	1.73
2	1250	0.61 x10^{-2}	1.63 x10^{-4}
		0.63	1.58
		0.65	1.53
		0.67	1.50
		0.69	1.46
	1200	0.70 x10^{-2}	2.27 x10^{-5}
		0.71	2.19
		0.71	2.11
3	1300	0.50 x10^{-2}	1.16 x10^{-3}
		0.55	1.83
		0.60	1.02
		0.63	0.95
	1250	0.64 x10^{-2}	2.18 x10^{-4}
		0.66	2.07
		0.67	1.97
		0.68	1.86
1	1250	0.70 x10^{-2}	1.87 x10^{-4}
		0.72	1.81
		0.74	1.73
	1300	0.76 x10^{-2}	9.75 x10^{-4}
		0.77	9.51
		0.80	9.37
		0.82	9.21

Sample No.	Temp. °C	Creep Strain (ϵ) in/in	Creep Rate ($\dot{\epsilon}$) in/(in hr)
4	1250	0.61 $\times 10^{-2}$	2.76 $\times 10^{-4}$
		0.62	2.62
		0.63	2.58
	1300	0.66 $\times 10^{-2}$	1.16 $\times 10^{-3}$
		0.70	1.14
		0.72	1.11
4	1300	0.75 $\times 10^{-2}$	1.07 $\times 10^{-3}$
		0.80	1.03
	1250	0.81 $\times 10^{-2}$	2.14 $\times 10^{-4}$
		0.82	2.11
		0.83	2.09
5	1300	0.52 $\times 10^{-2}$	1.22 $\times 10^{-3}$
		0.55	1.15
		0.60	1.07
	1250	0.62 $\times 10^{-2}$	1.61 $\times 10^{-4}$
		0.63	1.59
		0.64	1.54
	1300	0.66 $\times 10^{-2}$	7.95 $\times 10^{-4}$
		0.70	7.51
		0.75	7.12
5	1300	0.68 $\times 10^{-2}$	7.94 $\times 10^{-4}$
		0.72	7.48
		0.75	7.12
	1350	0.84 $\times 10^{-2}$	1.98 $\times 10^{-3}$
		0.90	1.85
		0.95	1.65
		1.00	1.56

TABLE B-III

Normalized Creep Rate ($\dot{\epsilon}^{\circ}_{0.004}$)

for SZ-1.35-Fe

Grain Size of Sample	Temperature °C	0.004 hr^{-1}	
0.45μm	1160	4.453×10^{-4}	(3)*
	1200	2.006×10^{-3}	(5)
	1250	1.263×10^{-2}	(6)
	1275	3.936×10^{-2}	(2)
1.06μm	1160	1.704×10^{-4}	(3)
	1200	8.960×10^{-4}	(5)
	1250	5.137×10^{-3}	(5)
	1275	1.685×10^{-2}	(3)
2.04μm	1160	8.807×10^{-5}	(4)
	1200	4.775×10^{-4}	(5)
	1250	3.103×10^{-3}	(6)
	1275	8.448×10^{-3}	(3)

* The number in the ( ) indicates the number of determinations which were averaged to obtain the value of $\dot{\epsilon}_{0.004}$ shown.

TABLE B-IV

Normalized Creep Rate ($\dot{\epsilon}^{o}_{0.004}$)

For SZ-0.85-Fe

Grain Size of Sample	Temperature °C	$\dot{\epsilon}^{o}_{0.004}$ hr^{-1}	
0.45μm	1200	2.084×10^{-5}	(3)*
	1250	2.964×10^{-4}	(5)
	1300	1.373×10^{-3}	(6)
	1350	4.795×10^{-3}	(2)
1.03μm	1200	8.929×10^{-5}	(2)
	1250	6.849×10^{-4}	(5)
	1300	3.704×10^{-3}	(7)
	1350	1.424×10^{-2}	(3)
1.83μm	1200	4.100×10^{-5}	(2)
	1250	2.463×10^{-4}	(5)
	1300	1.235×10^{-3}	(5)
	1350	5.469×10^{-3}	(3)

* The number in the ( ) indicates the number of determinations which were averaged to obtain the value for $\dot{\epsilon}^{o}_{0.004}$ shown.

APPENDIX C

Constant Temperature,

Constant Load,

Creep Tests

for

1.83 μm SZ-0.85-Fe

Figure C-1

Creep strain vs. time
SZ-0.85-Fe
σ for each sample = 850 psi.

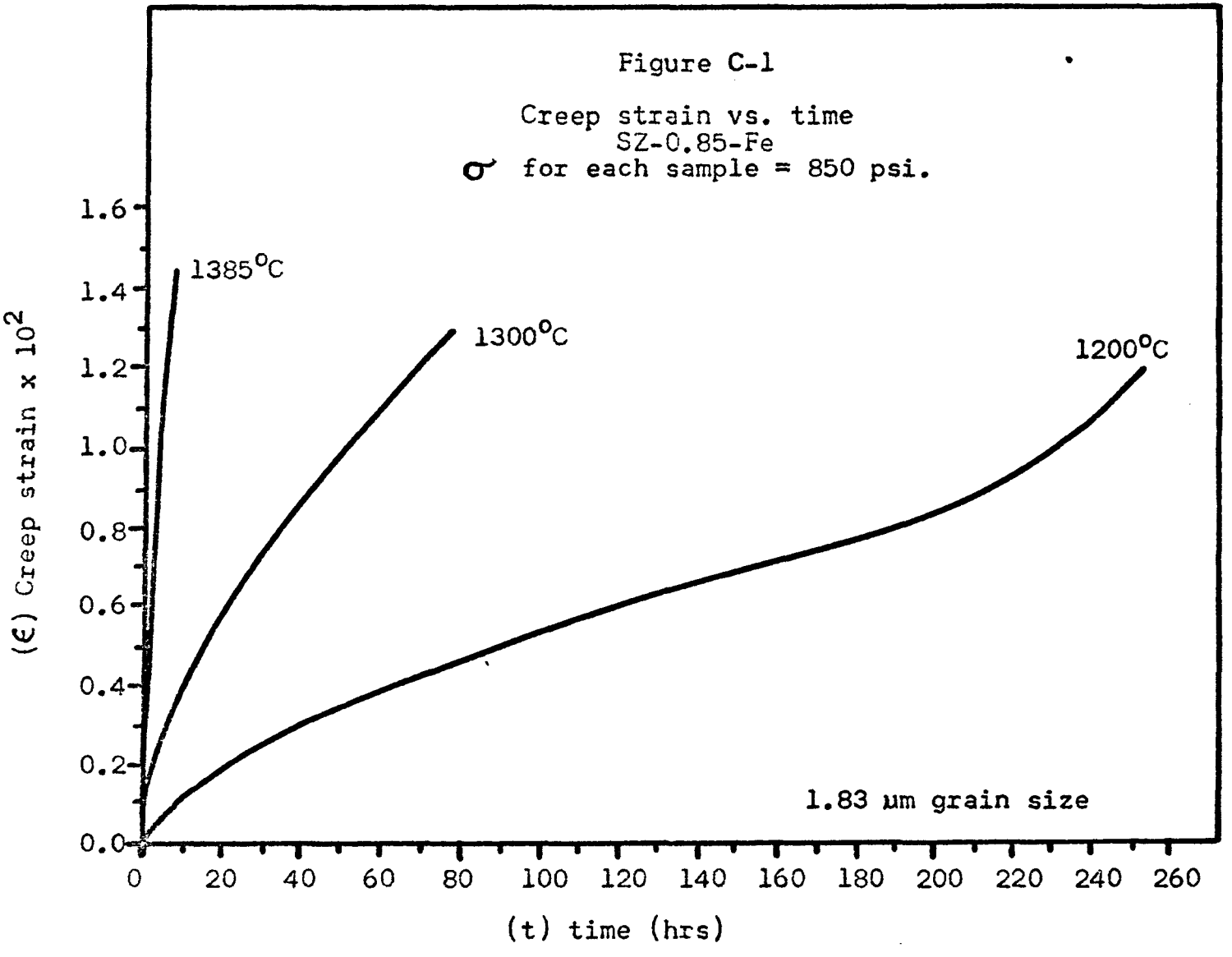

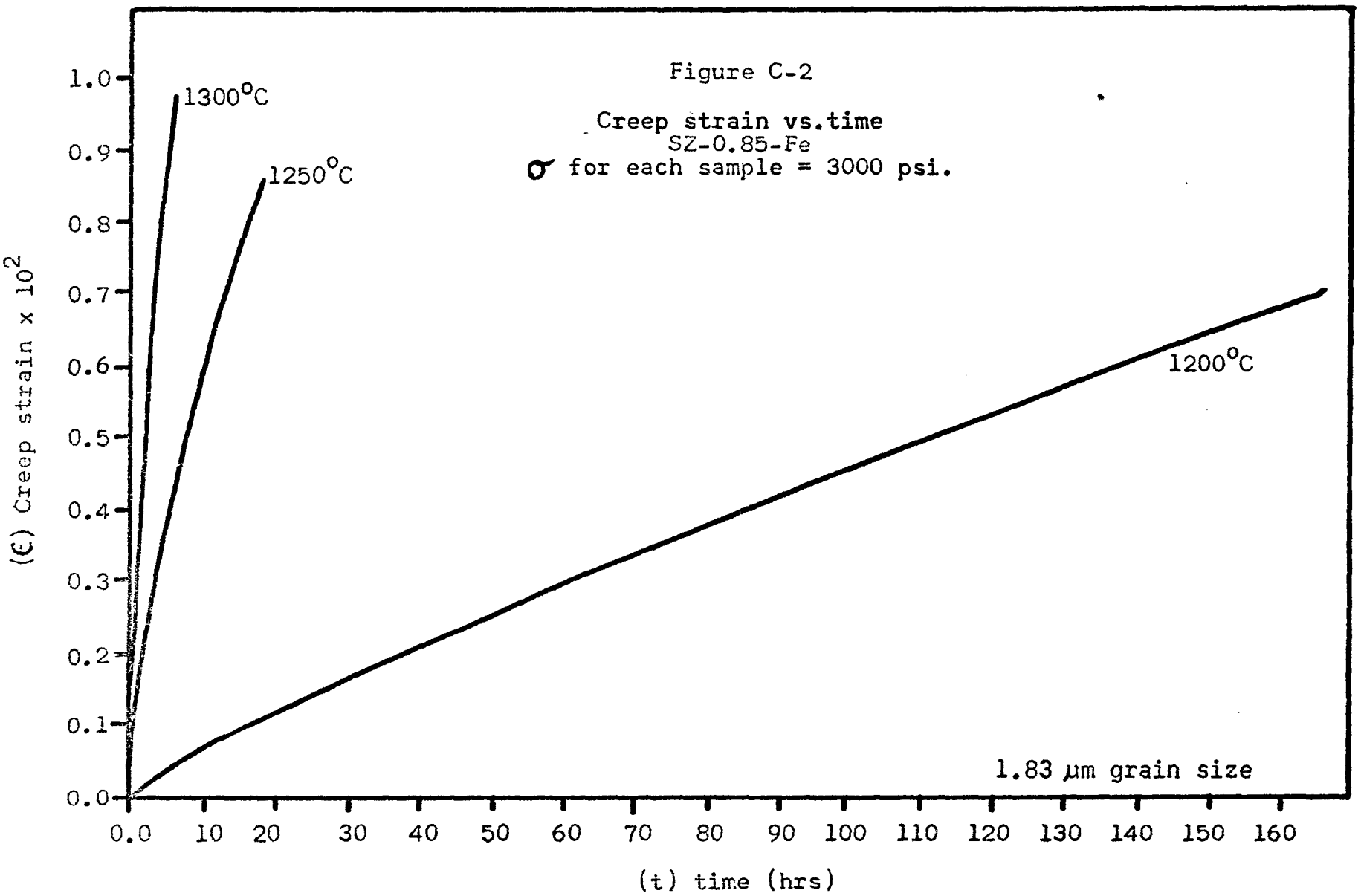

Figure C-2

Creep strain vs.time
SZ-0.85-Fe
σ for each sample = 3000 psi.

REFERENCES

1. Tinklepaugh, J.R., Funk, J.E., and Sullivan, R.M., "Metal Fiber Reinforced Composites for Extreme Temperature and Stress Applications" Final Report, Contract No. DA-30-069-ORD-3386, U.S. Army Ordnance Missle Command, State University of New York College of Ceramics at Alfred University, Sept. (1962).

2. Von Wartenburg, H., and Gurr, W., Phase Diagrams for Ceramists, ed. by Levin, E.M., McMurdie, H.F., and Hall, F.P., Am. Cer. Soc, Fig. 147 (1956).

3. Noguchi, T. Okubo, T. and Yonemochi, O.,"Reactions in the System ZrO_2-SrO" J. Am. Cer. Soc.,52(4) 178-181 (1969).

4. Glasstone, S., Laidler, K.J., and Eyring, H., The Theory of Rate Processes, McGraw-Hill Co., Reading Mass. (1941).

5. Kausman, W., "Flow of Metals from the standpoint of the Chemical Rate Theory" Trans. AIME,143 57-78 (1941).

6. Nabarro, F.R.N., Report of a Conference on Strength of Solids, University of Bristol, H. Wills Physical Laboratory, Bristol England, 75-90 (1947).

7. Herring, C., "Diffusional Viscosity of a Polycrystalline Solid" J. Appl. Phys., 21(5) 437-445 (1950).

8. Coble, R.L., "A Model for Boundary Diffusion Controlled Creep in Polycrystalline Materials" J. Appl. Phys., 34(6) 1679-1682 (1963).

9. Paladino, A.E., and Coble, R.L., "Effect of Grain Boundaries on Diffusion-Controlled Processes in Aluminum Oxide" J. Am. Cer. Soc., 46(3) 133-136 (1963).

10. Oishi, Y., and Kingery, W.D., "Self-Diffusion of Oxygen in Single Crystal and Polycrystalline Aluminum Oxide" J. Chem. Phys., 33, 480-486 (1960).

11. Laurent, J.F., and Bernard,J., "Determination of the Autodiffusion in Mono-and Polycrystalline Sodium Chloride" J. Phys. Chem. Solids, 7(2-3) 218-227 (1958).

12. Gifkins, R.C., and Snowden, K.U., "Mechanism for Viscous Grain Boundary Sliding" Nature, 212(5065) 916-917 (1966).

13. Gifkins, R.C., "Superplasticity during Creep," J. Inst. Metals, 95(12) 373-377 (1967).

14. Gifkins, R.C., "Diffusional Creep Mechanisms," J. Am. Cer. Soc., 51(2) 69-72 (1968).

15. Mott, N.F.,"A Theory of Work-Hardening of Metals," Phil. Mag., 44, 742-765 (1953).

16. Mott, N.F., "A Discussion of some Models of the Rate-Determining Process in Creep," Chapter in Creep and Fracture of Metals at High Temperatures, Her Majesties Stationery Office, London (1957).

17. Weertman. J.R., "Theory of Steady State Creep Based on Dislocation Climb," J. Appl. Phys., 26, 1213-1217 (1955).

18. Hull, D., Introduction to Dislocations. Pergamon Press, London (1965).

19. Garofalo, F., Fundementals of Creep and Creep-Rupture, MacMillan Co., New York (1965).

20. Friedel, J., Dislocations, Pergamon Press, London, (1964).

21. Cottrell, A.H., Dislocations and Plastic Flow in Crystals, Oxford Press, London, (1953).

22. Parker, E.R., "Ductility of Magnesium Oxide," Chapter in, Mechanical Properties of Engineering Ceramics, ed. by Kriegel, W.W., and Palmour, H., Interscience Pubs. New York, (1961).

23. Pask, J.A., "Mechanical Properties of Ceramic Materials," Chapter in, Mechanical Behavior of Materials at Elevated Temperatures, Ed. by Dorn, J.E., McGraw-Hill Inc., (1961).

24. Wygant, J.F., "Elastic and Flow Properties of Dense, Pure, Oxide Refractories," J. Am. Cer. Soc., 34(12) 374-380 (1951).

25. Vasilos, T., Mitchell, J.B., and Spriggs, R.M., "Creep of Polycrystalline Magnesia," J. Am. Cer. Soc., 47(4) 203-204 (1964).

26. Cummerow, R.L., "High-Temperature Steady-State Creep Rate in Single Crystal MgO," J. Appl. Phys., 34(6) 1724-1729 (1963).

27. Passmore, E.M., Duff, R.H., and Vasilos, T., "Creep of Dense, Polycrystalline Magnesium Oxide," J. Am. Cer. Soc., 49(11) 594-600 (1966).

28. Tagai, H. and Zisner, T., "High Temperature Creep of Polycrystalline Magnesia,I," J. Am. Cer. Soc., 51(6) 303-310 (1968).

29. Zisner, T., and Tagai, H., "High Temperature Creep of Polycrystalline Magnesia,II," Ibid, pp 310-314.

30. Hensler, J.H., and Cullen, G.V., "Stress, Temperature and Strain Rate in Creep of Magnesium Oxide," J. Am. Cer. Soc., 51(10) 557-559 (1968).

31. Terwilliger, G.R., Bowen, H.K., and Gordon, R.S., "Creep of Polycrystalline MgO and MgO-Fe_2O_3 Solid Solutions at High Temperatures," J. Am. Cer. Soc., 53(5) 241-251 (1970).

32. Langdon, T.G., and Pask, J.A., "Mechanism of Creep in Polycrystalline Magnesium Oxide", to be published in Acta. Met.

33. Groves, G.W., and Fine, M.E., "Solid Solution and Precipitation Hardening in Mg-Fe-O Alloys," J. Appl. Phys., 35(12) 3587-3593 (1964).

34. Warshaw, S.I., and Norton, F.H., "Deformation Behavior of Polycrystalline Aluminum Oxide," J. Am. Cer. Soc., 45(10) 479-486 (1962).

35. Scheuplein, R., and Gibbs, P., "Surface Structure in Corundum, I, Etching of Dislocations," J. Am. Cer. Soc., 43(9) 458-472 (1960).

36. Wachtman, J.B., and Maxwell, L.H., "Factors Controlling Resistance to Deformation and Mechanical Failure in Polycrystalline (Glassfree) Ceramics," Ceramics Abstracts, pp224h (1961).

37. Barmore, W.L., and Vandervoort, R.R., "High-Temperature Plastic Deformation of Polycrystalline Beryllium Oxide," J. Am. Cer. Soc., 48(10) 499-505 (1965).

38. Newkirk, H.W., and Cline, C.F., "Electrical Properties of Small Crystal and Polycrystalline BeO at High Temperatures," University of California, Lawrence Radiation Laboratory, Livermore, California, Report No. UCRL 7261-T.

39. Vandervoort, R.R., and Barmore, W.L., "Compressive Creep of Polycrystalline Beryllium Oxide," J. Am. Cer. Soc., 71(4) 180-184 (1963).

40. Fryxell, R.E., and Chandler, B.A., "Creep, Strength, Expansion, and Elastic Modulii of Sintered BeO as a Function of Grain Size, Porosity and Grain Orientation," J. Am. Cer. Soc., 47(6) 283-291 (1964).

41. Funk, J.E., Nemeth, J., and Tinklepaugh, J.R., "The Stress Strain Behavior of $SrZrO_3$," Final Rept., Contract NOw 64-0051-d, Bureau of Naval Weapons, State University of New York College of Ceramics at Alfred University, Alfred, New York (1964).

42. Funk, J.E., Nemeth, J., and Tinklepaugh, J.R., "The Thermal, Mechanical Behavior of $SrZrO_3$," Final Rept. Now 65-0131-d, Ibid (1965).

43. Funk, J.E., Nemeth, J., and Tinklepaugh, J.R., "The Mechanical Behavior of $SrZrO_3$," Final Rept. NOw 66-0191-d, Ibid (1966).

44. Nemeth, J., "Growth of Single Crystals of the Perovskite Material, $SrZrO_3$, and the Observation of Domain Structure and Motion in These Crystals," M.Sc. Thesis, College of Ceramics at Alfred University, Alfred, New York (1966).

45. Von Hippel, A., "Ferroelectricity, Domain Structure, and Phase Transitions in $BaTiO_3$," Tech. Rept. 27 and 28, Laboratory for Insulation Research, M.I.T. (1950).

46. Kay, H.F., and Vousden, P., "Symmetry Changes in $BaTiO_3$ at Low Temperatures and Their Relationship to its Ferroelectric Properties," Phil. Mag., 40 1019-1040 (1949).

47. Megaw, H.D., Ferroelectricity in Crystals, Methuen and Co. Ltd., London, (1957).

48. Forsbergh, P.W., Jr., "Domain Structures and Phase Transitions in $BaTiO_3$," Phys. Rev., 76 1187-1201 (1949).

49. Cameron, D.P., "Domain Orientation in $BaTiO_3$ Single Crystals," IBM J. of Research and Development, 1 2-7 (1957).

50. Roth, R.W., "Classification of Perovskites and Other ABO_3 Type Compounds," J. Res. Nat. Bur. Standards, 58 75-88 (1958).

51. Hayden, H.W., Moffatt, W.G., and Wulff, J., The Structure and Properties of Materials, Vol. III-Mechanical Behavior, J. Wiley and Sons Inc., New York (1965).

52. Keler, E.K., and Kuznetsov, A.K., "Synthesis and Physiotechnical Properties of Strontium and Barium Zirconate," J. Appl. Chem., U.S.S.R., 34 2044-2049 (1961).

53. Jorgensen, P.J., and Anderson, R.C., "Grain-Boundary Segregation and Final Stage Sintering of Y_2O_3," J. Am. Cer. Soc., 50(11) 553-558 (1967).

54. Kingery, W.D., Introduction to Ceramics, John Wiley and Sons Inc., New York (1960).

55. Lewis, D., and Lindley, M.W., "Enhanced Activity and the Characterization of Ball Milled Alumina," J. Am. Cer. Soc., 49(1) 49-50 (1966).

56. Lewis, D., and Lindley, M.W.,"X-Ray Line Broadening Study of the Introduction and Removal of Strain in some Refractory Oxides," J. Am. Cer. Soc., 47(12) 652-652 (1964).

57. Richards, B.P., and Greenham, A.C., "Strain Induced in Yttrium Iron Garnet by Various Milling Treatments," Brit. J. Appl. Phys., 1(2) 1297-1302 (1968).

58. Northwood, D.O., "The Effect of Mechanical Deformation on Selected Chemical and Physical Properties of Crystalline Solids," PhD Thesis, University of Surrey, England (1968).

59. Searle, A.B., and Grimshaw, R.W., The Chemistry and Physics of Clays, Interscience Publishers Inc., New York (1959).

60. Bush, E.A., and Hummel, F.A., "High Temperature Mechanical Properties of Ceramic Materials: I, Magnesium Dititanate," J. Am. Cer. Soc., 41(6) 189-195(1958).

61. Bush, E.A., and Hummel, F.A., "High Temperature Mechanical Properties of Ceramic Materials: II, Beta-Eucryptite," J. Am. Cer. Soc., 42(8) 388-391 (1959).

62. Timoshenko, S., Strength of Materials, Vol III, 3rd ed., D. Van Nostrand Co., New York, (1956).

63. Dorn, J.E., "The Spectrum of Activation Enerties for Creep," Chapt. in Creep and Recovery, Am. Soc. for Met., Cleveland (1957).

64. Zener. C., and Hollomon, J.H., "Effect of Strain Rate upon Plastic Flow of Steel," J. Appl. Phys. 15, 22-32(1944).

65. Cottrell, A.H., and Bilby, B.A., "A Mechanism for the Growth of Deformation Twins in Crystals," Phil. Mag., 42(329) 573-581(1951).

66. Frank, F.C. and Read, W.T., "Multiplication Processes for Slow Moving Dislocations," Phys. Rev., 79, 722-723(1950).

67. Weertman, J., and Weertman, J.R., Elementary Dislocation Theory, Macmillan Co., New York, (1964).

68. Kronberg, M.L., "Plastic Deformation of Single Crystals of Sapphire: Basal Slip and Twinning," Acta. Met., 5, 507-524(1957).

69. Kronberg, M.L., Discussion in Mechanical Properties of Engineering Ceramics, ed. by Kriegel, W.W., and Palmour, H., Interscience Pubs., New York, (1961).

70. Williams, L.S., "Fatigue and Ceramics," Chapt. in Mechanical Properties of Engineering Ceramics, Ibid.

71. Klassen-Neklyodova, M.V., Mechanical Twinning of Crystals, Consultants Bureau, New York, (1964).

72. Basinski, Z.S., and Christian, J.W., "Crystallography of Deformation by Twin Boundary Movements in Indium-Thallium Alloys," Acta. Met., 2, 101-116(1954).

73. Mori, S., "Phase Transformation in Barium Orthoferrate, $BaFeO_{3-x}$," J. Am. Cer. Soc., 49(11) 600-604(1966).

74. Yakovleva, E.S., and Yakutovitch, M.V., "Relation to Diameter of Critical Shearing Stress for Twinning and Slip for Cadmium Crystals," Zhur. Eksptl. Theoret. F.Z., 10, 1146-1150(1940).

VITA AUCTORIS

The author was born in Ithaca, New York, U.S.A. on December 29, 1940.

EDUCATION: B.Sc. and M.Sc., obtained at College of Ceramics, Alfred University, Alfred, N. Y.

PUBLICATIONS: "The Strength of Cobalt Wiskers", J. Nemeth, R. T. Hamilton and J. Gordon Parr, Cobalt, No. 45, Dec. 1969, pp. 177-179.

SOCIETIES: American Ceramics Society
American Society for Metals
American Institute of Metallurgical Engineers
Keramos (Honorary Ceramics Association)